

**ON THE IMPROVEMENT OF PERMEABILITY ASSESSMENT OF FIBROUS
MATERIALS**

A Dissertation by

Sanjay Sharma

MS Aerospace Engineering, Wichita State University, 2004

Submitted to the Department of Mechanical Engineering
and the faculty of the graduate school of
Wichita State University
in partial fulfillment of
the requirements for the degree of
Doctor of Philosophy

May 2010

© Copyright by Sanjay Sharma 2010
All Rights Reserved

**ON THE IMPROVEMENT OF PERMEABILITY ASSESSMENT OF FIBROUS
MATERIALS**

The following faculty members have examined the final copy of this dissertation for form and content, and recommend that it be accepted in partial fulfillment of the requirements for the degree of Doctor of Philosophy, with a major in Mechanical Engineering.

Dennis A. Siginer, Committee Chair

Mark S. Ewing, Committee Member

Hamid Lankarani, Committee Member

Brian Driessen, Committee Member

John S. Tomblin, Committee Member

Krishna Krishnan, Committee Member

Accepted for the College of Engineering

Zulma Toro-Romos, Dean
College of Engineering

J. David McDonald, Dean of Graduate School

ACKNOWLEDGEMENTS

I am grateful to my advisor and committee chair, Dr. Dennis Siginer, for his guidance and support. His insight in the subject coupled with an excellent research standard has kept me motivated throughout. I owe a special thanks to Dr. Mark Ewing for painstakingly reviewing the work and suggesting changes in the write up that have shaped the final form and content of the dissertation. I also express my appreciation and thanks to my other committee members, Dr. Hamid Lankarani, Dr. Brian Driessen, Dr. John Tomblin and Dr. Krishna Krishnan for going through the dissertation. I appreciate the helpful advice on validation experiments from Dr. John Tomblin which has resulted in a better correlation with the computed values. I am also grateful to NIS grants that have resulted in part of the acoustical study discussed in the work. I express my gratitude to Dr. Wenlung Liu for measuring samples for physical properties at such a short notice.

I express my thanks to late Dr. Kurt Soschinske, who lent me his RTM mold and related equipment to carry out the experiments. Throughout the duration of my research work, I have been helped by students and staff from National Institute for Aviation Research and the department of Mechanical Engineering. In particular, I would like to thank Chee Kuen Chan, Ian Goodman and Ravi Kiran for their support during experiments. Support from Dr. Indranil Dandaroy of Hawker Beechcraft has been very helpful in understanding the acoustical methods of passive noise reduction.

I thank my family members and friends for their encouragement and patience during the last few years.

ABSTRACT

The focus of this work is to understand the current state of permeability measurement and prediction methods for fibrous, porous media and to suggest improvements. For this purpose the most widely used and accepted measurement technique, the channel flow method, is used to experimentally investigate the effects of fiber sizing and fluid viscosity on the permeability of glass and carbon fibers.

Experiments have shown that the variation in permeability occurs due primarily to the fluid viscosity and not the nature of fluid, which other researchers have proposed. Studies were also carried out on both sized and unsized fibers to show that significant permeability variation occurs when fluids of different viscosity are used. Further, experimental studies on the effect of secondary flow have revealed that, for fiber products representative of the aerospace industry, secondary flow has little effect, which challenges models proposed by other researchers. Previous studies had shown a dual scale flow for fiber products with a significantly lower fiber volume fraction.

A novel acoustical method based on standardized impedance tube measurements has been developed to predict physical properties—both permeability and characteristic length—of the porous medium. The predicted permeability values from the acoustical method for the range of porosity studied in this work compare well enough with existing permeability models' predictions to warrant further study. The acoustical method is quick and repeatable, and when compared with the existing flow methods may provide a convenient alternative. It also provides a measure of fiber arrangement (via the “viscous characteristic length”) that should be studied further to explain variations in permeability measurements due to alternative fiber product architecture.

TABLE OF CONTENTS

Chapter	Page
1. INTRODUCTION	1
2. PERMEABILITY MEASUREMENT METHODS IN ANISOTROPIC MEDIA	5
2.1. Classification of Permeability Measurements	6
2.1.1. Radial Flow Methods	7
2.1.2. Channel Flow Methods	13
2.1.2.1. Set Up For Channel Flow Experiments	16
2.1.3. Mixed Methods of Permeability Measurements	20
2.1.4. Continuous Measurement Method	28
2.1.5. Predictive Methods of Permeability Measurement and Modeling	32
2.1.6. Measurement of 3D Permeability	37
2.2. Inconsistencies with Existing Measurement Methods and Models	38
2.3. Cross Transport Phenomena and Fluid Flow In Porous Media	45
2.4. Some Observations and Concluding Remarks on Permeability Measurement Methods	47
2.5. Motivation & Objectives	48
3. EFFECT OF FIBER SIZING - TEST FLUID INTERACTION ON THE UNSATURATED AND SATURATED FLOW IN THE VARTM PROCESS	51
3.1. Introduction	51
3.2. Experimental Set Up	52
3.2.1. Material Matrix	55
3.2.2. Data Reduction	58
3.3. Results and Discussion	59
3.4. Conclusions	66
4. DEVELOPMENT OF AN ACOUSTIC METHODOLOGY TO DETERMINE PHYSICAL PROPERTIES OF POROUS MATERIALS	67
4.1. Introduction	67
4.2. Background and Proposed Model	69
4.2.1. Impedance Tube Method	69
4.2.2. Proposed Model	70
4.3. Experimental Methodology	72
4.3.1. Experimental Apparatus and Setup for Direct Measurements	73

TABLE OF CONTENTS (Continued)

Chapter	Page
4.3.2 Validation Procedure	75
4.4 Discussion of Model Performance	77
4.5 Conclusions	81
5. EXPERIMENTAL VALIDATION OF INVERSLY CALCULATED FLOW RESISTIVITY	83
5.1 Introduction	83
5.2 Experimental setup for Measuring Physical Properties	84
5.2.1 Measurement of Porosity	84
5.2.2 Measurement of Tortuosity	85
5.2.3 Measurement of Flow Resistivity	86
5.3 Measurement Results	86
5.4 Comparison of measured results with analytically validated physical properties	87
6. PREDICTION OF PERMEABILITY OF ORTHOTROPIC COMPOSITE FIBERS USING THE ACOUSTICAL METHOD	91
6.1 Introduction	91
6.2.1 Experimental Constraints	92
6.2.2 Proposed Comparison of Acoustical Method with the Flow Method	95
6.3 Validation Procedure	96
6.4 Acoustical Methodology Results	97
6.5 Comparison of Acoustical with Existing Methods	101
6.6 Some Observations on Permeability Measurement and Modeling	105
6.7 Conclusion	107
7. CONCLUSION & RECOMMENDATION	108
7.1 Summary of Work	108
7.2 Conclusions	109
7.3 Original Contribution to Literature	110
7.3.1 Effects of Sizing on Permeability	110
7.3.2 Dual Scale vs. Single Scale Flow for VARTM	110
7.3.3 Acoustical Method of Permeability	111
7.4 Recommendations for Future Work	114
REFERENCES	116

TABLE OF CONTENTS (Continued)

Chapter	Page
APPENDICES	126
Appendix A: Fabric Constituents	127
Appendix B: Comparison of Predicted and Measured Absorption Coefficient Values for Orthotropic Fibers	128
Appendix C: Data for Figures 42 and 43.	130

LIST OF TABLES

Table	Page
1. A summary of some of the data collection methods used for permeability determination by various investigations	16
2. Fabric Characteristics	56
3. Fiber Porosity, Orientation, and Number of Layers Used	57
4. Test Fluid Characteristics	57
5. Material test configuration	76
6. Material elastic properties of foams	76
7. Physical properties of fibrous materials	77
8. Measured physical properties (Courtesy HBC co.)	87
9. Comparison of measured and predicted flow resistivity values	87
10. Physical properties of orthotropic fiber preforms	101

LIST OF FIGURES

Figure	Page
1. Radial flow pattern- Flow spreads in a circular or elliptical pattern	8
2. Channel flow method – top view	13
3. In-plane principal permeability direction determination experiments	14
4. An experimental set up for permeability measurement	17
5. 3D CAD drawing of the mold	17
6. Boundary Conditions for 1 D channel flow method	18
7. A Unified Approach to determine K	23
8. A micrograph of a transverse section of a fiber glass composite showing tow gaps (macro flow) and cross stitching (Uniaxial glass fiber- tow size -1200)	33
9. VARTM Setup	54
10. Different fiber reinforcements used in the experiments	56
11. Setup used for conducting flow and permeability experiments	58
12. Permeability comparison of Fiber glass Biax	60
13. Permeability comparison of Fiber glass UD	61
14. Permeability comparison of UD Carbon 1	62
15. Permeability comparison of UD Carbon 2	62
16. Saturated Flow behavior of Hercules AS 4 fibers with Vinyl Ester Process	63
17. UD Glass Saturated flow behavior	64

LIST OF FIGURES (Continued)

Figure	Page
18. UD Carbon Saturated flow behavior	65
19. A closed-loop validation process	68
20. An acoustic model in AutoSEA2 based on ASTM E90-02	72
21. Setup for impedance tube for absorption coefficient measurements	73
22. Setup for impedance measurement tube type 4206T for TL measurements	74
23. Schematic diagrams of large and small tube measurement systems	74
24. Comparison of predicted and measured absorption coefficients for 1-inch fiberglass	79
25. Comparison of predicted and measured absorption coefficients for 1.7-inch melamine foam	80
26. Comparison of predicted and measured TL for 1-inch fiberglass	80
27. Comparison of predicted and measured transmission loss for 0.9-inch melamine Foam	81
28. Tortuosity meter TOR 2008-1 (Courtesy Hawker Beechcraft Co.)	85
29. Bar chart of the predicted and measured flow resistivity values (ASTM C 522)	88
30: A comparison of measured and predicted absorption coefficient curves for PHM foam	89
31: A comparison of measured and predicted absorption coefficient curves for PHM ULfoam	89

LIST OF FIGURES (Continued)

Figure	Page
32: A comparison of measured and predicted absorption coefficient curves for Soundcoat	90
33. A comparison of measured and predicted absorption coefficient curves for UAI	90
34. UD Glass fabric cut in 50.4 mm width strips to roll into samples with the Desired tows	94
35. UD Glass fiber strips rolled into 29 mm diameter sample for measurement in The Impedance tube	94
36. A comparison of acoustical method with the channel flow technique	95
37. UD Carbon 135 tows sized- Comparison of measured and predicted absorption coefficient curves based on the computed physical properties	99
38. UD Carbon 135 tows Unsized- Comparison of measured and predicted absorption coefficient curves based on the computed physical properties	99
39. UD Glass 200 tows Sized- Comparison of measured and predicted absorption coefficient curves based on the computed physical properties	100
40. UD Glass 200 tows Unsized- Comparison of measured and predicted absorption coefficient curves based on the computed physical properties	100
41. Figure 41. Various models for permeability vs. porosity relationship [120]	102
42. A comparison of permeability measured by acoustical method with existing models and methods for glass fibers (r is the fiber diameter).	103

LIST OF FIGURES (Continued)

Figure	Page
43. A comparison of permeability measured by acoustical method with existing models and methods for carbon fibers (r is the fiber diameter).	104

NOMENCLATURE

β = Shearing angle of deformation of the medium

γ_{SV} = Surface Energy between solid and vapor

γ_{SL} = Surface Energy between solid and liquid

γ_{LV} = Surface Energy between liquid and vapor

λ = Pore Size

μ = Dynamic fluid viscosity

η = Porosity

ξ = Drag tensor

A = Pore volume to surface ratio (characteristic length)

σ = Effective flow resistivity

b = Parameter based upon Poisson's ratio of zero porosity material

d = diameter

h = preform thickness

h_0 = Original preform thickness (before compression)

\dot{h} = Rate of change of preform thickness during compression

k_0 = shape factor

(l_e/l) = Tortuosity of the medium

m = slope of the curve

q = Flow rate inside the medium

q_o = Flow rate through the outlet tube

r_i = inlet port radius (radius of the tube supplying the fluid)

NOMENCLATURE (Continued)

r_f = flow front radius at time t

r_o = Total preform radius

t = time of flow

x_f = Flow front position from origin

v_f = Fiber Volume fraction

v_l = Longitudinal wave velocity

v_t = Shear wave velocity

B = Conductance of a channel (function of the shape of channel cross section)

C_w = Channel width

C_h = Channel height

D_f = Pore area fractal dimension

D_T = Tortuosity fractal dimension

$E(r)$ = local electrical field

F = Formation factor

\mathbf{K} = Permeability tensor of the porous medium

K_1 = Principal Permeability

$K_I = K_{II} = K_{III}$ = permeability measured in three different orientations

$K_e = K_{\text{eff}}$ = Effective Permeability

K_{hex} = Permeability for hexagonal packing

K_{sq} = Permeability for square packing

L = Total length of fibers per unit length

NOMENCLATURE (Continued)

∇P = Pressure gradient in the direction of the flow

P_i = inlet pressure

R = Fiber Radius

$S_0 = \Sigma$ = Specific surface

S_p = Pore surface

T = Tortuosity tensor

V = Flow velocity vector

V_x = Flow velocity vector in x direction

V_y = Flow velocity vector in y direction

V_p = Pore volume

W_s = Work of Spreading

CHAPTER 1

INTRODUCTION

The characterization and modeling of the flow of fluids through any porous medium has been a subject of extensive research for more than a century. This phenomenon, which is governed by the Generalized Porous Medium Equation (GPME) occurs in aquifers, earthen dams, petroleum bearing rocks and composite manufacturing processes to name a few. To suit the various naturally occurring or man-made processes the GPME is modified, sometimes slightly to explain the flow behavior of fluids. These models are then used in ground water exploration, engineering hydrology and secondary oil recovery etc. The GPME when applied to composites manufacturing processes gives rise to a different set of problems. Some of these problems are highlighted during permeability measurement processes. Measurement methods of the phenomenological coefficient (permeability) of the GPME are many and the results from different types of experiments usually do not agree well. The correlation between experimental results and models are reviewed as well. Difficulties and inconsistencies in characterizing permeability of porous medium are highlighted. Since it is not possible to discuss the permeability measurement methods without their associated models, a brief summary of some models is included. The difficulties involved in solving such problems are detailed. Finally, some alternative methods of characterizing permeability are presented.

The first attempt at explaining the fluid behavior in a porous medium was done by Henri Darcy in 1856. He conducted an experiment to determine the flow velocity of water through a vertical column of sand with known pressure gradient. Based on observation he derived an empirical formula that has come to be known as Darcy's law [1]. He introduced the parameter called permeability that characterizes a porous medium. This relation is given in equation (1),

$$V = -\left(\frac{K}{\mu}\right)\nabla P \quad (1)$$

The porous medium used in this case is homogeneous and isotropic. The fluid used in the experiment (water) obeys Newton's law of viscosity. All models based upon this law use chemically inert fluids. The solid matrix of the porous medium should be rigid and stationary for Darcy's law to remain valid. The flow should be laminar and the Reynolds's number, $0 < R_e < 10$ for the equation to be valid. Effect of gravity is not included in this relation. Further, no cross transport phenomena or coupled effect on the flow due to a non conjugated force is considered here. For instance Soret effect i.e. mass flux caused by temperature gradient and its reverse i.e. Dufour effect is not considered here. In other words, the flow behavior is studied under isothermal conditions without being affected by a non conjugated force field. Equation (1) in conjunction with the continuity equation for incompressible flow yields the Laplacian,

$$\nabla \cdot V = 0, \quad \nabla \cdot V = -\left(\frac{K}{\mu}\right)\nabla^2 P, \quad \nabla^2 P = 0 \quad (2)$$

Since it is assumed that the porous medium is homogeneous and isotropic K is taken as a constant.

Further, the viscosity of the fluid is taken as constant with respect to space and time coordinates. Various boundary conditions according to the physical nature of the phenomenon at hand are employed to solve this equation. If the medium is anisotropic the introduction of the permeability tensor $\mathbf{K}(\mathbf{x})$ requires substantial modification of equation (2)₃.

If the permeability tensor is not a point function such as in an orthotropic medium like fiber reinforced composites, K takes the form of a symmetric second order tensor and (2)₃ reads in Cartesian coordinates,

$$K_{xx} \frac{\partial^2 P}{\partial x^2} + K_{yy} \frac{\partial^2 P}{\partial y^2} + K_{zz} \frac{\partial^2 P}{\partial z^2} + 2K_{xy} \frac{\partial^2 P}{\partial x \partial y} + 2K_{xz} \frac{\partial^2 P}{\partial x \partial z} + 2K_{yz} \frac{\partial^2 P}{\partial y \partial z} = 0 \quad (3)$$

$$K = \begin{bmatrix} K_{xx} & K_{xy} & K_{xz} \\ K_{yx} & K_{yy} & K_{yz} \\ K_{zx} & K_{zy} & K_{zz} \end{bmatrix} \quad (4)$$

Darcy's law is a macroscopic law and as is evident does not contain any term for porosity, tortuosity and capillary effect etc. These microscopic physical properties of the matrix ultimately determine the permeability. Permeability is akin to conductivity in electrical flow through wires. The dimensions of permeability are L^2 and represents the averaged cross sectional area of the medium allowing fluid flow. Most of the subsequent models based upon Darcy's law utilize the continuum approach. The continuum approach ignores all the microscopic details while taking an average representation of the matrix characteristics. A Representative Volume Element (RVE) large enough to capture the microscopic parameters and/or the flow characteristics in the matrix is used for various types of matrices. Several types of RVE are developed for different types of porous medium as detailed by Du Plessis and Diedericks [2].

Boussinesq has successfully carried out the application of Darcy's law to ground water infiltration, Vasquez [3]. Mathematically the problem governed by this equation is well posed i.e. has existence of unique solution and is stable. Variations in the porous medium equations have been introduced by many researchers to suit different applications. Some variations of the GPME however have been shown not to be well posed [4]. Isakov et al. [4] introduce a saturation parameter in the equation to explain the degree of saturation in secondary oil recovery methods. Various models based upon capillary tube, averaging the Navier-Stokes equations, Fissure models, Hydraulic radius models, resistance to flow models etc. are derivations of Darcy's law. However these models also do not relate all of the microscopic physical properties

of the matrix to the governing equation. A different approach to modeling flow in the porous medium is taken by Kozeny and later modified by Carman. The resulting equation is called the Kozeny-Carman equation and includes porosity as a factor in the model, Collines [5]. Permeability is defined as a purely material characteristic based upon specific surface, tortuosity and porosity of the medium as given in (5) where c is a dimensionless constant which depends on the geometry of capillary tube cross-section, for instance $c= 0.5$ for circle and $c= 0.5619$ for square cross-section.

$$K=c\eta^3/\Sigma^2 \quad (5)$$

Porosity η and specific surface Σ are defined as the ratio of volume of pores to the bulk volume of the material and as the interstitial surface area of the pores per unit bulk volume of porous material, respectively. In all the models Permeability K is the most critical parameter characterizing the porous medium.

In an orthotropic medium like fiber reinforced composites the principal directions of the permeability tensor with constant direction dependent components are determined through the eigenvalues and eigenvectors \mathbf{K} , Jacob Bear [6]. Once the principal directions are determined it is possible to design experiments such that the flow direction is aligned with the principal direction for which the permeability value needs to be determined.

If the principal permeability values for a given porous medium are known, flow prediction critical in measuring ground water level, seepage and saturation in soil, port location and tool design in composites manufacturing among a plethora of other applications becomes possible based upon any of the numerous available models.

CHAPTER 2

PERMEABILITY MEASUREMENT METHODS IN ANISOTROPIC MEDIA

The governing equations describing any phenomenon in poro-elastic materials pertain to macroscopic level. For instance, thermal flow, fluid flow or acoustical phenomenon is explained by the respective macroscopic Partial Differential Equations (PDE). The phenomenological coefficient in each case is usually a function of microscopic parameters that are difficult to relate to the macroscopic governing PDE. In case of fluid flow through porous medium, this coefficient is termed permeability and defined in the previous section. As is evident from Darcy's law it is related to the macroscopic fluid flow velocity. The measurement of permeability through experiments is crucial to accurately model flow fronts and pressure profiles in porous medium. In an anisotropic medium like fiber-reinforced composites, the three principal permeability values are required to model the three-dimensional flow, Weitzenbock et al. [7]. In this section developments related to permeability measurement are detailed further. Difficulties associated with such measurements and their validity on modeling is also considered. Much of the following discussion is restricted to Newtonian fluid flow in porous media.

This chapter is organized into the following sections:

1. Classification of permeability measurements-
 - a) Radial flow methods
 - b) Channel flow methods
 - c) Mixed methods of permeability measurement or flow characterization
 - d) Predictive methods of permeability measurement and modeling
 - e) Continuous measurement methods
 - f) Measurement of 3D permeability

2. Inconsistencies in the methods characterizing permeability
3. Cross Transport phenomenon related to fluid flow in porous medium
4. Observations and concluding remarks on permeability measurement methods

2.1. Classification of Permeability Measurements

In general all the flow based permeability measurement methods can be classified on the basis of type of flow (unidirectional or radial), discrete or continuous (measurement for one value of porosity or a series of values), type of fluid used (gas or liquid) and in-plane or out of plane measurements. These techniques of permeability measurement require controlling either the fluid velocity or the fluid pressure. These two broad data gathering techniques can be used in any experimental set up. The four most common types of permeability measurement techniques for fiber-reinforced composites that exist in the literature are,

1. Radial flow –constant pressure or constant velocity
2. Channel flow – constant pressure or constant velocity.

There are also various predictive methods that are based upon flow past regularly arranged cylinders or other concepts. Techniques such as Lubrication model, cell models and Karman-Cozeny equation are not dependent upon fluid flow rate through the medium. Some of these are empirical relationships determined with the help of some material parameters. These will be discussed later in the report. In the following section, a general method of permeability measurement is explained. This method is used with minor variations in determining permeability characteristics of porous medium.

The experimental set up remains similar regardless radial or channel flow method is used. Only the mold and port location is changed. A list of these similar methods is presented classified into all the categories.

2.1.1. Radial Flow Methods

A large number of methods utilize the radial flow method as detailed in Table 1. It should be noted that one of the main drawbacks of this method is that only in-plane permeability values can be measured. As the name suggests, radial flow measurements pertain to the experiments with fluid inlet ports placed on top of the porous medium. When actual flow occurs through the medium, it follows a radial pattern of fluid distribution as shown in Figure 1. This experiment is either conducted by maintaining a constant flow velocity through the medium (thereby varying the injection pressure required to overcome the frictional forces in the medium) or by maintaining constant injection pressure at the inlet. This is desired as Darcy's law includes both velocity and pressure gradient as variables. By keeping one parameter constant and of known value, the other is experimentally measured. Details of both types of measurements and their comparisons are given by Cai [8] and Chan et al [9]. If the experiment involves constant pressure flow then the flow front location is measured at regular intervals. Usually the flow front pattern is elliptical and the major and minor axis lengths are measured at those intervals.

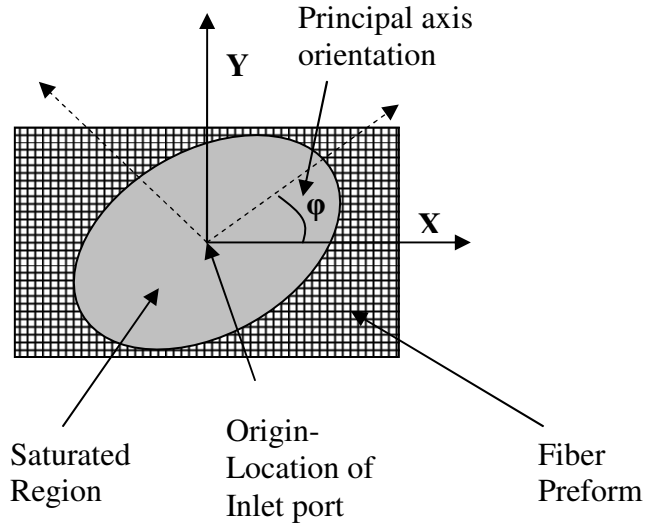


Figure 1. Radial flow pattern- Flow spreads in a circular or elliptical pattern

The governing equation i.e. Darcy's law is converted in polar coordinates and the permeability in the thickness direction is ignored therefore the medium is assumed isotropic. The following derivation is suggested by Chan et al. [9]. The governing equation (2)₃ in polar coordinates and the boundary conditions are,

$$\frac{d^2 P}{dr^2} + \frac{1}{r} \frac{dP}{dr} = 0, \quad P|_{r=r_i} = P_i, \quad P|_{r=r_f} = P_{fi} \quad . \quad (6)$$

P_i is the constant inlet pressure, r_i is the inlet port radius (radius of the tube supplying the fluid) and r_f is the flow front radius. Since the medium is isotropic, the flow front shape is circular. Thus the θ and z terms in the PDE could be neglected. The solution of this equation gives pressure and pressure gradient at any point in the preform. Equation (6) can be solved for constant flow experiment as well with different boundary conditions. A relationship between initial pressure, superficial velocity and porosity as given by (7)₁ is used in determining the boundary condition (7)₂ and obtaining the solution (8) ,

$$\frac{dr_f}{dt} = \frac{V}{\eta} = \frac{KP_i}{\eta\mu r_f \ln\left(\frac{r_f}{r_i}\right)} \quad \frac{dP}{dr}\bigg|_{r_i} = -\frac{q\mu}{2\pi r_i hK}, \quad P|_{r_f} = 0, \quad (7)$$

$$P = \frac{q\mu}{2\pi hK} \ln\left(\frac{r_f}{r}\right) \quad . \quad (8)$$

A plot of P versus $\ln(r_f/r)$ is used to calculate the slope ‘m’. The slope value is used in (9) to obtain permeability,

$$K = \frac{q\mu}{2\pi hm} \quad . \quad (9)$$

The flow front position with respect to time is given by

$$\left(\frac{r_f}{r_i}\right)^2 \left[2 \ln\left(\frac{r_f}{r_i}\right) - 1 \right] + 1 = \frac{4K\Delta Pt}{\eta\mu r_i^2} \quad (10)$$

For orthotropic porous media the flow front takes an elliptical shape and the orthotropic form of the governing equation is transformed into an “Equivalent Isotropic System – EIS”. To implement EIS, a point (x,y) is transformed into (x_e,y_e) ,

$$K = \begin{bmatrix} K_x & 0 \\ 0 & K_y \end{bmatrix} \quad x_e = \left(\frac{K_y}{K_x}\right)^{1/4} x \quad y_e = \left(\frac{K_x}{K_y}\right)^{1/4} y \quad y = \left(\frac{K_y}{K_x}\right)^{1/2} x \quad (11)$$

The plot of flow front positions along the x and y axes (denoted as R_x and R_y) against time shows a linear relationship. The slope ‘m’ is then given as,

$$m = \left(\frac{K_y}{K_x}\right)^{1/2} \quad (12)$$

In the equivalent system eq. (10) takes the following form,

$$\left(\frac{r_x}{r_i}\right)^2 \left[2 \ln\left(\frac{r_x}{r_i}\right) - 1 \right] + 1 = \frac{4K_e \Delta P t}{\eta \mu r_{xi,e}^2} \quad (13)$$

$$K_e = K_x K_y \quad , \quad r_{xi,e} = \left(\frac{K_y}{K_x}\right)^{1/4} r_i \quad (14)$$

A noteworthy feature of the radial flow methods is that it does not require separate determination of principal directions in an anisotropic medium. That is due to the fact that the principal directions coincide with the major and minor axes of the elliptical flow front. Equation (9)₄ governs the relationship between principal permeabilities and the ellipse axes. Hence measuring the orientation of the ellipse with respect to the lab coordinates yields the desired values.

The above equation is solved for pressure gradient dP/dr and pressure field P/P_i . The lab coordinates are assumed at an angle θ with respect to the principal permeability directions as shown in Figure 1. The initial radius r_i of the inlet tube expands to r_f in time. The flow front location denoted by r_f is noted. The pressure at inlet port is also measured and recorded as well as the history of flow front and pressure drop versus time. Clearly for radial flow experiments, constant velocity measurements are better suited and more accurate. Interestingly, however the permeability values for the same medium changes when a higher flow velocity is used. The Reynolds number remains less than 10 and hence the applicability of Darcy's law is not in question. The possible explanation may be that to maintain higher flow velocity pressure is constantly increased perhaps adversely affecting the deformation of the porous medium.

A large number of methods utilize the radial flow method as detailed in Table 1. One of the main drawbacks of this method is that it measures in-plane permeability only. However it is in extensive use. Cai [8] details the differences in fill time and inlet pressure required for various gate locations simulating actual trials in industry for complex geometries or different preforms.

Gauvin et al. [10] conduct bidirectional flow measurements for both constant pressure and constant flow rate. Different inlet tube radii are chosen for the same fabric keeping all other parameters constant. It is observed that the principal permeability values decrease as the inlet radii is increased. Lai et al. [11] conduct transient and steady state flow experiments for 1D and 2D permeability characterization of the porous medium. Constant flow rate and constant pressure conditions are chosen to run various experiments for channel flow and radial flow methods. The objective of their study is to assess the variations measured in permeability by different techniques. To solve for the radial flow permeability measurements, equations developed by Chan et al. [9] are used. A variation of less than 10% in the permeability values is observed between different techniques. The experiments are run for dry and saturated fibers. The main reason for excellent agreement between the 1D channel flow and 2D radial flow method is the inclusion of capillary pressure in the permeability equation. Young and Wu [12] develop an expression based on the fiber mat geometry, principal direction angle and the permeability for steady state flow conditions. This expression given in Eq. (15) is verified by numerical simulation then utilized for permeability measurements.

$$q = \frac{2\pi h K_r}{\mu} \frac{P_{in}}{\ln\left(\frac{d_{out}}{d_{in}}\right)} \quad (15)$$

Constant flow rate is maintained to wet the unsaturated fibers. For different values of porosity, pressure drop is plotted against the flow rate to yield permeability values.

For higher flow rates it is observed that the pressure/flow rate relationship becomes non-linear and hence Darcy's law is not applicable. The method developed uses a specified size of fiber preform and a variation in this size leads to changes in geometry. Hence this method cannot be used with preforms of different sizes. Hammami et al. [13] utilize a radial flow technique to

account for principal permeability variations induced due to fabric deformation. Layers of woven fabric are sheared at an angle to simulate deformation induced in complex shaped parts in an RTM mold. The study concludes that principal permeability in one direction increase while the value for its orthogonal counterpart decreases with shearing angle. Han et al. [14] use the radial flow technique to measure permeability for higher FV fibers accounting for capillary effect. The technique uses measurement of pressure at four points of the preform for saturated flow conditions under steady state. Permeability measured for the highest FV is 53%, which is higher than the values measured in previous studies. Comparisons with channel flow measurements are made and found to be in good agreement. Liu et al. [15] develop an extensive sensor system for use in radial flow measurement of permeability. Electrical sensors embedded into the top and bottom mold in a radial pattern provide information about the flow front progress and its orientation. This determines the principal axes and the radius of the flow front. Constant flow rate experiment is used and the injection pressure at the inlet is monitored with respect to time. A new relationship that takes into account the non ideal entrance effects in radial flow experiments is developed.

$$P_{in} = \frac{\mu q}{4\pi h K_{rr}} \ln \left(1 + \frac{qt}{\eta \pi h r_i^2} + \frac{c}{r_i^2} \right) K_{rr} = \sqrt{K_{xx} K_{yy}} \quad (16)$$

The two sets of same sensors on top and bottom molds provide very close in-plane permeability values indicating that the fluid flows uniformly in different layers of the preform. The tests are conducted for a FV of 35.8% for glass fibers. This sensor system however cannot be used against carbon fibers, as they are electrically conductive.

2.1.2. Channel Flow Methods

A permeameter is very similar in set up to that of the actual apparatus used by Darcy for measurement. It has the added advantage of measuring permeability as a function of FV by varying the compaction pressure. Hence a comparison of permeability values for a particular medium by both methods lends validity to the new technique of channel flow. Channel flow injection mold permeability measurements compare well with permeameter measurements, Verheus and Peeters [16]. Figure 2 displays a channel flow method employed to measure permeability. In the channel flow method both types of measurements, constant pressure and constant flow rate, can be conducted. For constant pressure method, flow front location is noted with respect to the specified time intervals. The flow front is usually a straight line in channel flow measurements. Both constant flow rate and constant pressure methods are used to measure permeability by Weitzenbock et al. [7]. Their study also details the determination of principal directions of permeability when the medium is anisotropic.

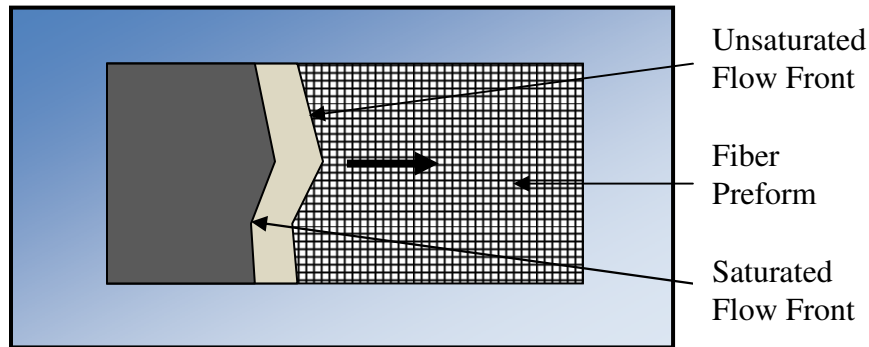


Figure 2. Channel flow method – top view

In order to determine principal permeability values in 2 dimensions for a given preform, three measurements of effective permeability at different orientations are needed. The three measurements of effective permeability given as K_I , K_{II} and K_{III} are shown in Figure 3 and given in equations (17 & 18). From the measurements, angle φ is calculated first. This angle determines the orientation of the principal axes w.r.t the measurement axes. Next, the principal values (K_1 & K_2) in both the directions are determined. Using the two principal values and the angle so determined permeability tensor is fully defined.

$$K_1 = K_I \frac{(A-D)}{(A-D / \cos 2\varphi)}, \quad K_2 = K_{III} \frac{(A+D)}{(A+D / \cos 2\varphi)} \quad (17)$$

$$\varphi = \frac{1}{2} \tan^{-1} \left\{ \frac{A}{D} - \frac{A^2 - D^2}{K_{II} D} \right\}, \quad A = \frac{(K_I + K_{III})}{2}, \quad D = \frac{(K_I - K_{III})}{2} \quad (18)$$

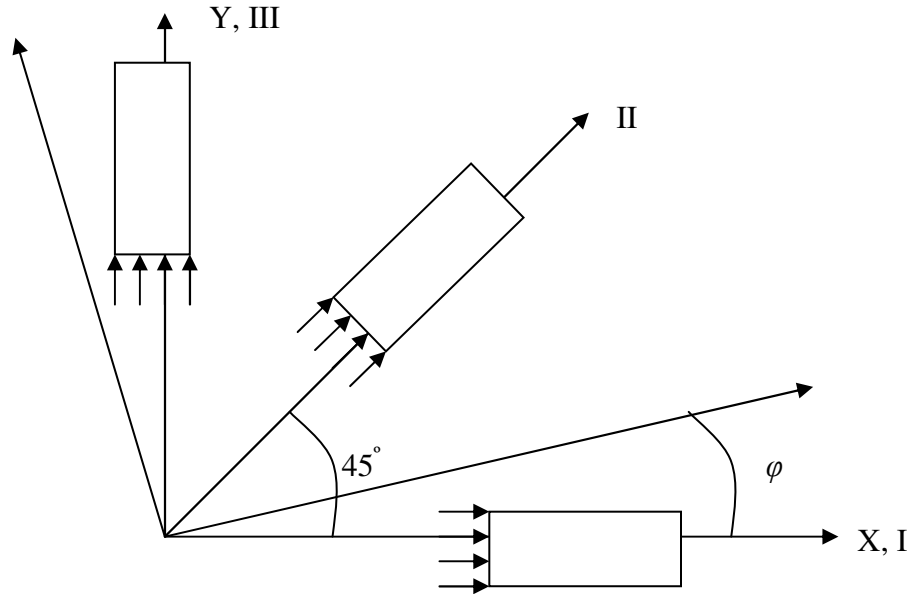


Figure 3. In-plane principal permeability direction determination experiments

Various formulae based upon Darcy's law have been derived for both constant flow rate and constant inlet pressure conditions. These formulae are specifically suited for rectangular molds with associated boundary conditions and relate the effective permeability of the medium to the pressure or flow rate in the experiment. The most common relation for constant flow rate and for constant pressure is of the following form, respectively, Weitzenbock et al. [7],

$$K_{eff} = \frac{\mu q}{A} \frac{x_f}{\Delta P} \quad , \quad K_{eff} = \frac{\mu \eta}{2\Delta P} \frac{x_f^2}{t} \quad (19)$$

Lee et al. [17] develop as well a predictive method based on channel flow. The flow front is measured in channel flow and plugged in the following relation derived on the assumption that pressure gradient remains linear in the preform to obtain the principal permeability,

$$K_l = \frac{\mu \eta}{2\Delta P} \frac{x_f^2}{t} \quad (20)$$

Values of x_f^2 are plotted against t and a linear relation is observed. Lee et al [17] determine the permeability for different values of porosity in this way. Gauvin et al. [18] use the channel flow method to determine effective permeability along the continuous fiber direction. The same study also uses radial flow method with constant pressure and constant flow rate techniques to determine bidirectional permeabilities. Minor variations in these formulae have been suggested by various investigators conducting channel flow measurements. Some of the methods developed to measure permeability using either of these methods are detailed in Table 1.

Table 1. A summary of some of the data collection methods used for permeability determination by various investigations.

Constant flow rate	Constant pressure	Predictive method
Gauvin & Chibani [88]	Cai [8]	Gebart [52]
Weitzenbock et al. [7]	Ferland et al. [91]	Astroem et al. [89]
Gauvin et al. [18]		Young [54]
Kim and Daniel [65]	Gebart and Lidstrom [24]	Van der Westhuizen and Prieur du Plessis [90]
Ferland et al. [91]	Sun et al. [23]	Cai & Berdichevsky [55]
Verheus & Peeters [16]	Verheus & Peeters [16]	Bruschke & Advani [51]
	Weitzenbock et al. [7]	Bielefield [93]
Um and Lee [92]	Um and Lee [92]	Choi et al. [94]
Stadtfeld et al. [46]	Wu et al. [67]	Yu and Lee [57]
Chan et al. [9]	Lee et al [17]	
Um, Daniel & Childs [28]	Bickerton and Abdullah [39]	
Bickerton and Abdullah [39]	Heardman et al. [33]	
Heardman et al. [33]		

2.1.2.1. Set up for Channel Flow Experiments

A typical RTM set up for the measurement of permeability is shown in Figure 4. Usually a flat metal tool with holes for pressure gage is used. An inlet and outlet port from where the liquid flows are chosen depending upon the method used. The layers of fabric supposed to be measured are laid flat on the metal plate. A transparent glass plate is clamped on top of this fabric. The mold is sealed on all sides. In order to force the fluid flow through the medium a potential due to pressure difference is created by the injection pressure of the fluid. As the fluid passes through the medium, the flow front location is noted at regular time intervals. Similarly pressure values at different points can also be noted. A 3D CAD drawing of the mold used in permeability measurement is shown in Figure 5. The channel inlet along the width ensures a uniform flow in one dimension.

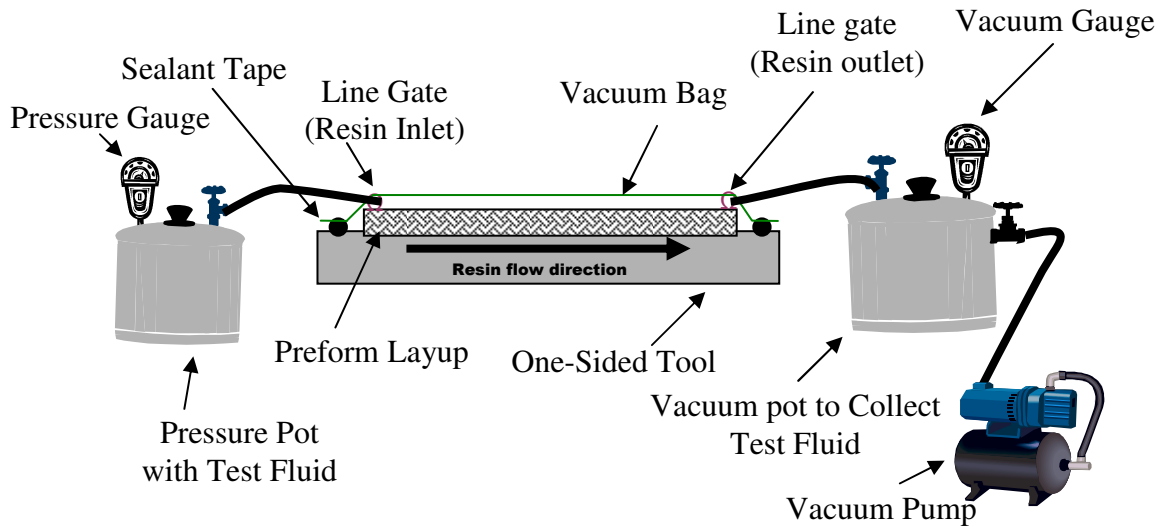


Figure 4. An experimental set up for permeability measurement [19]

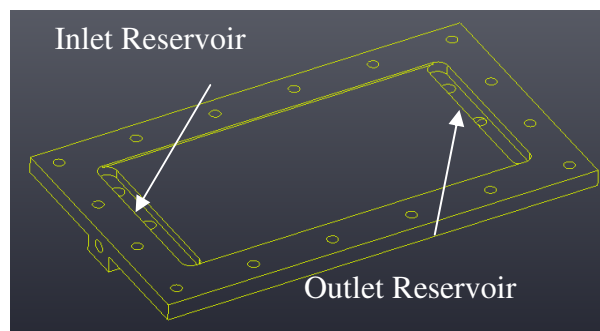


Figure 5. 3D CAD drawing of the mold [20]

For radial flow experiments, the experimental set up is similar to the one explained above. The only difference in the set up is the location of inlet port. In all radial flow methods, the inlet port is located on top and center of the preform (porous medium). The flow front then takes the shape of a circle or ellipse as shown in Figure 1. The boundary conditions for the

channel flow experiment valid for both constant flow rate and constant pressure cases are shown in Figure 6.

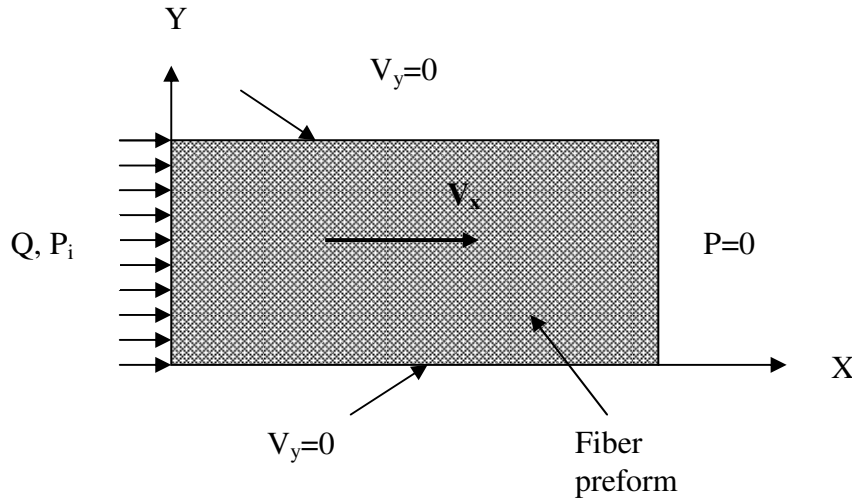


Figure 6. Boundary Conditions for 1 D channel flow method

It is observed that constant pressure experiments are easier to conduct as pressure transducers are not required at various locations. Further, a real time control system is required that can adjust the drop in inlet pressure by increasing the injection pressure to maintain a constant flow rate.

Demaria et al. [21] derive a relationship between effective permeability obtained by channel flow method and principal in-plane permeability. Constant injection pressure is used in this study. The method used is called an iterative ellipse method. By measuring effective permeabilities in 0° , 45° and 90° orientations, principal in-plane permeability values and the orientation angle is determined. The orientation angle ' β ' here refers to the shear deformation angle of the fabric in the mold. The shearing angle is supposed to simulate the conditions of the deformed fabrics in the RTM mold. The drawback of this method is that it can only be used to

determine permeability values for increments of 45° . The relation between effective and principal permeability is given by,

$$\begin{bmatrix} K_e^0 \cos^2 \beta & K_e^0 \sin^2 \beta & 0 \\ \frac{K_e^{45}}{2} & \frac{K_e^{45}}{2} & \frac{K_e^{45}}{2} \sin 2\beta \\ K_e^{90} \sin^2 \beta & K_e^{90} \cos^2 \beta & 0 \end{bmatrix} \begin{bmatrix} \frac{1}{K_1} \\ \frac{1}{K_2} \\ \frac{1}{K_2} - \frac{1}{K_1} \end{bmatrix} = \begin{bmatrix} 1 \\ 1 \\ 1 \end{bmatrix} \quad (21)$$

The change in ellipse orientations due to the shear deformation is verified by radial flow measurements. A good agreement between the iterative ellipse method and principal flow orientation is observed. A variation of less than 6% is observed for all the cases. Principal permeability decreases with increase in shear angle for 0 and 45° .

In order to visualize flow occurring through the thickness of the preform, electrical wires are placed between various layers of glass fibers in the study done by Diallo et al. [22]. Channel flow methods are usually inspected for flow front progression by a camera. By having conductive wires within the thickness direction, the flow front progression in the thickness direction is also captured. The calculation of permeability is done using Darcy's law and compared with a numerical solution. Sun et al. [23] carry out channel flow experiments to determine in plane permeabilities of preform with a highly permeable medium placed on top. The highly permeable medium (also called flow media) and the peel ply are used in Seemann Composites Resin Infusion Molding Process (SCRIMP). The SCRIMP process is the same as VARTM except that the highly permeable medium (flow media) is placed on top of the fiber perform, such that it forces the flow of resin in the transverse direction as well. Thus the flow of resin in the SCRIMP process is a combination of in-plane and out of plane directions. Hence determining 3D permeability of performs for SCRIMP becomes necessary. Due to the presence

of a flow media the flow front in the fabric preform lags behind the flow front in the flow media. Flow visualization of the highly permeable medium and peel ply is done separately to measure their respective in-plane permeability. Based on the 3D CV/FEM and the experimental results, a leakage flow model is developed. Gebart and Lidstrom [24] develop a “multicavity” method of determining permeability of preforms. Instead of using permeability expressions for the measurement, they use flow resistance tensor in 2D and determine permeability from that. Flow resistance is the inverse of permeability. Before testing this method, permeability measurements based upon channel flow with moving flow front, channel flow with pressure drop and radial flow with moving flow front are conducted and the results compared. It is observed that permeability values obtained from radial flow method versus channel flow method differed by more than 25%. Mold deflection due to high injection pressure is conjectured to be the cause of the variation between the two measurements. The study details experiments on two cavities being infused simultaneously to validate the approach. The cavities have the same preform at different angles for the measurement of effective permeability. When extended to four cavities, the same method is purported to measure the permeability tensor for a given FV in one step without measuring fluid viscosity. It is required to have a reference fabric with known permeability value in one of the cavities.

2.1.3. Mixed Methods of Permeability Measurements

Some of the methods discussed here are no different than the channel flow or radial flow techniques. However, the associated models used in measurements have some added parameters that were not discussed previously.

The influence of fiber distribution on transverse permeability was examined on a microscopic scale by Bechtold et al. [25]. Morishita algorithm is applied in this study to quantify fiber distribution across the width of the preform. A relationship between disorder in fiber arrangement and permeability is presented. A lower Morishita index (more regular arrangement of fiber cross section) leads to higher permeability. This study was done on a single layer of preform. Hence it needs to be extended to a more usual scenario of a number of layers in the preform. Natural fiber mats like Sisal and jute are measured in channel flow experiments for unsaturated permeability by Rodriguez et al. [26]. Due to the isotropic and homogeneous nature of these mats no difference between unsaturated and saturated permeability is observed. Permeability is measured using Darcy's law for various values of porosity. The measured results are compared with predictions based on Carman-Kozeny and Gauvin's methods. It is found that the best fit of the experimental results is obtained by modifying Carman-Kozeny model. Since the Carman-Kozeny constant is related to the tortuosity and specific surface of the porous medium, the final expression fitting the measured permeability results appears in Eq. (22).

$$K = \frac{\eta^{n+1}}{(1-\eta)^n} \frac{1}{k_0} \left(\frac{l_e}{l} \right)^2 \frac{1}{S_0^2} \quad (22)$$

Where, n is determined using Carman-kozeny equation, k_0 is the shape factor, l_e/l is the tortuosity and S_0 is the specific surface.

Ding et al. [27] utilize the in situ measurement and monitoring technique to determine the permeability field of a preform by using gas flow. The method depends upon the correlation between the resin permeability and air permeability for the same fiber preform with well controlled gas flow. Measurement of permeability is done using Darcy's relation by substituting for the measured pressure at various places in a preform. Um et al. [28] use a gas flow method with radial flow technique without factoring for differences between gas and liquid based

permeability. Cairns [29] cites a limitation of Darcy's law for being over-predictive of permeability for gas flow as opposed to liquid flow. This had been previously studied by Bear [30] in highly random porous materials. He suggests a relationship between permeability values derived from gas flow and that of liquid flow.

Weitzenbock et al. [31] develop a Unified Approach (UA) of permeability measurement by combining radial and channel flow measurement techniques. All the existing formulations based upon various boundary conditions for channel flow and radial flow methods are discussed as shown in Figure 7. Four new data collection methods using the above two techniques are developed in this study. A procedure to determine principal permeability using the UA method is presented. The UA method is based upon identifying and separating all the constants in the effective permeability formulations based upon different methods and data collection techniques. Details concerning the variation in permeability values obtained from different approaches for the same porous medium are discussed. Radial flow with constant flow rate experiments results in large scatter in permeability values when pressure difference is measured and used in the formulation. The same experiment using pressure measurement at a point yields permeability values that are off by a factor of 2 to 3.

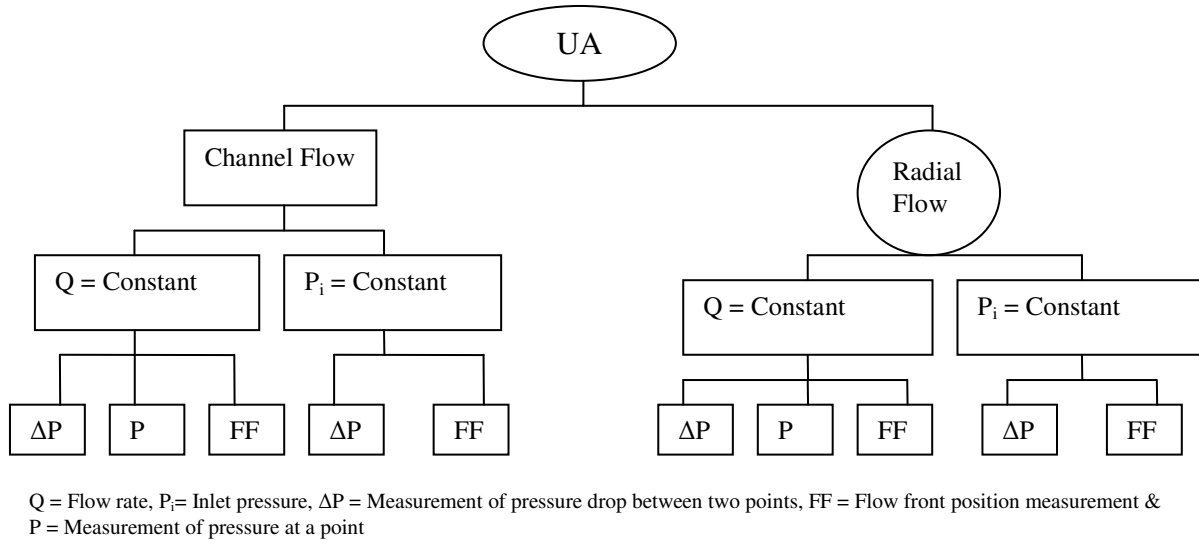


Figure 7. A Unified Approach to determine K [31]

The permeability measurement techniques so far consider preform composed of layers of the same fiber and architecture. Hence the flow front in individual layers in the in-plane direction is uniform. Seong et al. [32] study permeability of preform composed of different layers of fibers. The study uses combinations of glass, carbon and aramid fiber layers to create the hybrid preforms. A model to predict effective average permeability for such hybrid preforms is developed and its results compared with the weighted averaged permeability. When preforms are composed of different types of layers, the flow front progression is no longer uniform through the thickness. The effective average permeability of hybrid preforms is based upon the assumption that significant transverse flow takes place between individual layers of different fiber types or orientations. The calculation of effective average permeability needs transverse and both in-plane permeability values as input. Permeability of individual layers of fibers is calculated separately.

Heardmen et al. [33] develop numerical methods for the determination of principal in-plane permeabilities for the radial flow technique. The set up uses constant injection pressure under transient conditions to measure pressure values. The values measured using variable pressure method for the same fabric preform is compared with the previous method. The merits of differential versus integral methods of data collection using transient radial flow technique are discussed. Silicon oil is used as the injection fluid in all the experiments. For the same mold spacing however an actual resin is also used to make a laminate and its thickness measured. It is observed that the actual laminate thickness is 10% higher than the mold spacing gap. The actual thickness is used in permeability calculations thus reducing the measurement error substantially. It is worth noting here that no study has employed actual measurement of FV and Void Content (VC) using established ASTM standard testing. For RTM process the accurate measurement of FV and VC will give the correct value of porosity to be used in permeability formulations. The methods used that take into account the real weight and density of the fabrics to calculate the porosity should be replaced by actual FV and VC testing. Weitzenbock et al. [31] observe that the velocity used by some authors is different than others,

$$v = \frac{dx_f}{dt} \quad , \quad v = \eta \frac{dx_f}{dt} \quad (23)$$

At the same time however, the FV and VC testing results should be taken into account with care for SCRIMP or VARTM to determine porosity values. This is due to the spring up effect of the fiber preform induced by the resin at higher pressure than the preform. The flow front of the resin at atmospheric pressure inside the preform cancels out the compaction pressure on the plastic bag due to the atmosphere.

This results in an increase in the fiber spacing and hence amounting to the spring up effect. Investigation focusing on the increase in permeability due to the spring up effect of a fiber preform can quantify this effect in VARTM or SCRIMP.

Simacek and Advani [34] develop an algorithm within the framework of Liquid Injection Molding Software (LIMS) to model and predict fiber tow saturation during Liquid Composite molding (LCM). Standard CVFEM is used to model the influence of saturation on filling or flow rate within a preform. Mathur et al. [35] develop a model for 3D flow in a VARTM process and validate the same by measuring flow fronts using SMART weave system. Sensors Mounted As Roving Threads (SMART) weave is a non-destructive way of measuring the flow of resin through the fiber bed in 3D. Permeability of flow media is separately measured using a 1D channel flow method. As defined earlier, flow media is a highly permeable medium that forces the resin to flow in the transverse direction of the fiber perform. Fill time for a particular length, flow front region length and shape of the flow front are determined in the experiment. The model predicts the flow front shape and length of flow front as a function of through thickness permeability, porosity and Darcy velocity. Belov et al. [36] model the permeability of woven textile reinforcements using the Lattice Boltzmann Method (LBM). This technique utilizes an integrated design tool composed of a generic description of a wide variety of textile reinforcements. The complexity of flow in the textile is determined using a numerical approach based upon LBM. WiseTex software [36] which captures the geometrical aspects of the textile is interfaced with LBM to simulate flow through the preform. This method is computationally intensive and as per the author “is extremely CPU time consuming”.

An optimization approach to simulate multiphase flow has been presented by Kearsley et al. [37]. The flow of two immiscible fluids through pores is modeled by considering two phases

as wetting and non-wetting. The governing equations of the fluid motion are taken as Darcy's law and mass conservation law. These two equations are coupled with the volume balance equation for wetting and non-wetting saturation. Assuming that one of the saturation phases is known, these equations are decoupled. These linear elliptic equations considered as equations of phase pressures are then solved using appropriate boundary and initial condition. A non-linear operator is created based on the solution of these two equations and the capillary pressure for the given saturation value. An unconstrained minimization of the non-linear functional based on the non-linear operator is formulated using these equations. Methods to solve such an unconstrained optimization problem are presented.

Optimization of the VARTM process for increasing devolatilization has been presented by Grujicic et al. [38]. Process parameters are scrutinized using an optimization approach to study the gas phase contents in VARTM. Vacuum pressure and tool plate heating rate are identified as the key to lower gas phase content. A lower tool plate heating rate promotes devolatilization of the solvent inside the part being infused. Variation of pressure at the tool-plate preform interface is a function of tool-plate temperature under a constant heating rate of the tool plate. The study shows that lower heating rates are preferred in order to achieve a more thorough removal of the gas phase in the VARTM process. On the other hand, lowering of the heating rate increases the manufacturing time and hence cost. Higher vacuum pressure decreases the gas-phase linearly for a given tool-plate heating rate.

A methodology to control the curing of composite materials based on an inverse algorithm for optimal processing is presented by Bailleul et al. [39]. During the cure cycle of composite fabrication, chemical reactions taking place in the resin system are highly exothermic. The fiber material, especially glass, has low thermal conductivity resulting in temperature and

state of cure gradients through the thickness of the part. These gradients in turn create non-uniform stresses that could result in defects. A method to control the thermoset by monitoring the temperature of the mold walls has been proposed. A comparison of fill times for RTM and Injection Compression Molding (I/CM) is done by Bickerton and Abdullah [40]. The effects of process design parameters on the resulting fill times and clamping force for both methods are presented. A tradeoff between reductions in fill time and an increase in clamping force is discussed. Mastbergen and Cairns [41] create and validate a two dimensional (2D) simulation model for fluid infusion in preform made with glass fibers. Diluted corn syrup as a test fluid is used in the experimental validation. The experiment is conducted under constant injection pressure. Fluid is infused via a pressure-bag molding and distributed using a channel that covers the whole surface of the fabric. Fabric is infused with the fluid by applying pressure on the vacuum bag. The effect of fiber architecture and compaction pressure on permeability is observed in the measured results.

It is worth noting that most of the fiber preform used in composite manufacturing is heterogeneous. Parnas and Phelan [42] detail the effects of heterogeneous medium on flow modeling. Due to the presence of large tows (each tow is a bundle of fibers usually ranging from 1000 to even 80000 in number) stitched or woven together, two distinct flow regimes exist.

Flow in macro pores (gap between the tows) and micro pores (flow within a tow) are distinct. The continuity equation is modified by including a sink factor. Unsaturated permeability is measured and a model based upon the sink term in continuity equation is analyzed for 1D channel flow by Slade et al. [43]. The medium is conceived as dual scale based upon two distinct regions of pores. One region is represented by unsteady state flow through the gap between the tows and the other region characterized by slower flow inside the tow. The sink term is

introduced to account for variations in flow rate due to delayed infusion of fibers inside the tow. This sink term is shown to be dependent upon the capillary number. A dimensionless number called the sink effect index that represents the liquid absorption by the tows is defined. This index is dependent upon the tow ratio and channel permeability values.

Flow of Newtonian, viscoelastic and viscoinelastic fluids through porous media with variable permeability is investigated by Siginer and Bakhtiyarov [44]. The heterogeneous porous medium in the experiments is composed of isotropic media in series of equal length made of randomly packed glass spheres in a cylindrical tube. The porosity remains the same but permeability values differ abruptly in the series of media in the tube. Permeability is determined with the help of Darcy's law. The experiments are conducted at constant flow rate. Expressions for superficial velocity and pressure drop as function of the resistance coefficient and Reynolds number for viscoinelastic fluids is derived from linear momentum balance equation. Oldroyd-B constitutive structure is used to model the elongational flows of viscoelastic fluids in porous media, and tortuosity is found to be a function of the properties of porous medium and fluid elastic properties.

It is shown for the first time that elastic (polymeric) fluids flowing through lower permeability medium first followed by higher permeability loose more energy when compared with the flow in the opposite direction.

2.1.4 Continuous Measurement Methods

All the flow methods based on channel flow or radial flow usually measure permeability values for a given fiber volume fraction. In order to measure permeability for a range of FV, a number of experiments need to be carried out. A continuous technique based on compression

driven flow developed by Buntain and Bickerton [45] requires a single measurement to determine permeability for a range of fiber volume fractions. The model in this study uses FV as a parameter in the governing equation. The samples are cut in a circular shape to fit in an aluminum mold of 300 mm diameter. Compression of fiber preform is carried out by an Instron machine with a 200 KN load cell. The dimensionless governing Poisson equation for fluid pressure in the preform reads as,

$$\frac{1}{\hat{r}} \frac{\partial}{\partial \hat{r}} \left(\hat{r} \frac{\partial \hat{P}}{\partial \hat{r}} \right) + m \frac{\partial^2 \hat{P}}{\partial \hat{z}^2} = 1 \quad \hat{r} = \frac{r}{R} \quad \hat{z} = \frac{z}{h} \quad ,$$

$$\hat{P} = P \left(\frac{\mu \dot{h} r_o^2}{hK} \right)^{-1} \quad m = \left(\frac{K_{zz}}{K} \right) \left(\frac{h_o^2 r_o^2}{h^4} \right) \quad (24)$$

Its solution in dimensional variables is given by,

$$P(r) = \frac{\mu \dot{h}}{4Kh} (r^2 - r_o^2) \quad (25)$$

Radial flow experiments for three different fiber volume fraction values are carried out and the permeability values noted. The compression flow method yields permeability as a function of fiber volume fraction in a single experiment. The results from radial flow method and compression flow method for permeability values agree well for fiber volume fractions of up to 30%. Beyond 30% FV there is a significant departure in permeability values from the two experiments. This deviation is explained on the basis of fabric deformation due to higher compaction.

Stadtfeld et al. [46] develop a work cell to determine unsaturated and saturated in-plane permeability values using 1D channel flow under constant flow rate conditions. The expression

used in permeability calculation based on Darcy's law needs only the slope from the pressure history determined from the experiment. Pressure history for unsaturated and saturated flow is recorded to yield the permeability values. Unsaturated permeability is given by,

$$K_{xx} = \frac{\mu}{\frac{dP_i}{dt} \eta} \left(\frac{q}{C_w C_h} \right) \quad (26)$$

The final expression for saturated permeability is given by considering the pressure difference between the inlet and vent location once the preform is completely wetted out.

$$K_{xx} = \frac{\mu q l_{preform}}{C_w C_h \eta \Delta P} \quad (27)$$

C_w and C_h represent the width and height of the channel mold. The work cell consists of one movable mold plate that can compress the fabric layers to the desired thickness during the experiment. Hence saturated permeability can be measured for various values of FV. The results detailed are for FV ranging from 45% to 63%.

For unsaturated permeability, however, only one set of permeability value for a given FV is obtained. The results showed good agreement with independent measurements of permeability at selected FV values. Permeability of CFM is measured using saturated radial airflow for a range of values of FV from 10% to 35% by Pomeroy et al. [47]. This continuous technique uses low flow rates to maintain laminar flow and avoid compressibility effects. Flow rates used in these experiments correspond to Reynolds numbers less than 0.1. The results compare fairly well with liquid flow measurement methods. Using air as permeating fluid is a lot cleaner and easier for maintenance of equipment. The dependence of the permeability values on the inlet radius used in the experiments is mentioned. Feser et al. [48] use compressed air flow to determine in-plane permeability for gas diffusion layers of Proton Exchange Membrane (PEM)

fuel cells. Measurements are taken for a range of flow rates using radial flow technique. Darcy's law in polar co-ordinates in conjunction with the ideal gas law in continuity equation is solved to give equation (28) for compressible flow.

$$q_{out} = \frac{\pi K_i h}{\mu \ln\left(\frac{r_o}{r_i}\right)} \frac{(P_i^2 - P_o^2)}{P_o} \quad (28)$$

The difference between inlet and outlet pressure is small compared to the absolute pressure employed in the experiment thereby allowing further reduction of (28) to (29) on the basis of incompressible flow.

$$q_{out} = \frac{2\pi K_i h}{\mu \ln\left(\frac{r_o}{r_i}\right)} (P_i - P_o) \quad (29)$$

Radial flow experiments are conducted using air and permeability values are computed via the equation for compressible flow.

Similarly water and the equation for incompressible flow are used for permeability measurement in the same medium. Both sets of results agree very well. However if the equation for incompressible flow is used to compute the permeability using airflow, the values differ substantially.

Pettersson et al. [49]. verify whether the equipment used for gas flow saturated permeability measurement gives reliable results for various flow rates and porosity conditions. The study measures the permeability of medium density fibers (used to make MDF boards) and expandable polystyrene spheres (EPS) used as reference material. The need for sensitive pressure transducers is highlighted and non-Darcian flow is observed even at low Reynolds number for EPS. Darcy's law is shown to be valid for the range of Reynolds numbers between 3 and 12 for EPS. At low flow rates, the non-Darcian behavior is explained on the basis of the Knudsen effect

or some erroneous values obtained from sensors. However for the medium density fibers, Darcy's law remained valid for the complete range of Reynolds number used in the experiments.

2.1.5. Predictive Methods of Permeability Measurement and Modeling

All the measurement methods and modeling discussed so far have been based upon either liquid or gas flow techniques. All of these methods use either radial or channel flow methods. Yet no standardized method exists for the measurement of this most critical porous medium property. No two methods result in same permeability values for a given porous medium. Chappell and Lancaster [50] researched the uncertainties in permeability measurement induced by different methodologies. Although soil samples are tested in their study, the same can be extended to composite fibers.

The first method developed independent of the flow characteristics in a porous medium is due to Cozeny-Karman, Vazquez [3]. The method of flow past cylinders based upon fiber volume fraction is introduced by Bruschke and Advani [51]. Lubrication model is used for permeability determination by Gebart [52]. This is extended by Bruschke and Advani [51] to include cell model that predicts permeability for lower fiber volume fraction composites. The explicit formula derived by Gebart [52] using lubrication approach assumes a certain packing arrangement of the fiber bed. Based upon either square or hexagonal packing of the fibers the model proposes that transverse permeability can be computed as

$$K_{sq.} = \frac{16}{9\sqrt{2}\pi} \left(\sqrt{\frac{\pi}{4v_f}} - 1 \right)^{2.5} R^2, \quad K_{hex.} = \frac{16}{9\sqrt{6}\pi} \left(\sqrt{\frac{\pi}{2\sqrt{3}v_f}} - 1 \right)^{2.5} R^2 \quad (30)$$

In practice however, the fiber distribution is irregular and the packing density falls somewhere in between the square and hexagonal arrangement as shown in the micrograph in Figure 8 taken from [53].

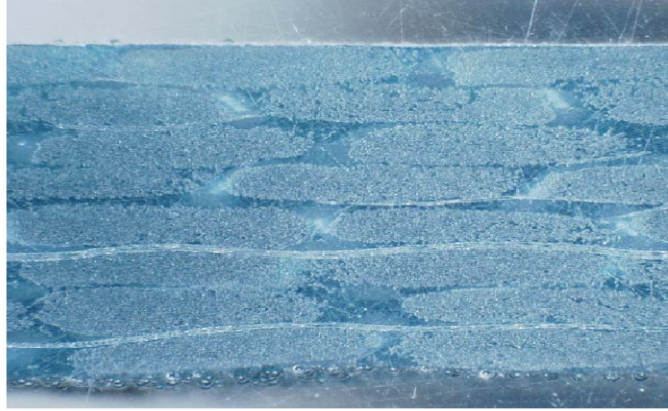


Figure 8. A micrograph of a transverse section of a fiber glass composite showing tow gaps (macro flow) and cross stitching (Uniaxial glass fiber- tow size -1200)

Similarly, Young [54] derived an expression for calculating transverse permeability given by equation (31) with the fiber volume fraction v_f . The radius of the fibers is denoted R .

$$K = \frac{R^2}{0.8} \left(\sqrt{\frac{0.82}{v_f}} - 1 \right)^3 \left(\frac{0.82}{v_f} - 1 \right)^{-1} \quad (31)$$

Longitudinal and transverse permeability expressions have been derived by Cai and Berdichevsky [55].

These expressions too are dependent upon fiber volume fraction and fiber diameter with a certain packing arrangement. All of the above predictive methods yield longitudinal and transverse permeability values. These are different from the permeability tensor components in principal directions. Hakanson et al. [56] develop a model for non-aligned fibers i.e. nonwovens, felts and paper webs etc. for higher FV. The model is based on the drag force experienced by a

volume averaged fiber length. When combined with Darcy's law, equivalence between permeability and drag tensor is established as given by

$$\mathbf{K}^{-1} = L\langle \xi \rangle \quad (32)$$

L is the total length of fibers per unit length, ξ is the drag tensor and the angle brackets represent average over the length of all fibers. Based on the assumption that the drag force depends on the fiber orientation, porosity and diameter a relationship between K_L and K_T and principal permeability values is established for planar random and isotropic cases. The results developed are for square arrangement of fibers. The respective representations for planar random and isotropic fiber distribution are given below.

$$K = \begin{bmatrix} \frac{2K_T K_L}{K_T + K_L} & 0 & 0 \\ 0 & \frac{2K_T K_L}{K_T + K_L} & 0 \\ 0 & 0 & K_T \end{bmatrix} \quad (33)$$

$$K = \begin{bmatrix} \frac{3K_T K_L}{K_T + 2K_L} & 0 & 0 \\ 0 & \frac{3K_T K_L}{K_T + 2K_L} & 0 \\ 0 & 0 & \frac{3K_T K_L}{K_T + 2K_L} \end{bmatrix} \quad (34)$$

Experimental validation of the generalized model is done using radial flow technique under saturated conditions using water as the test fluid. Values of K_L and K_T are calculated using previously existing models. It is found that Gebart's predictive model for higher FV agrees best with the experimental results.

Yu and Lee [57] develop a predictive method based on a unit cell representation of the woven fabrics. The model is developed based upon Navier-Stokes equations with appropriate

boundary conditions. An algorithm to measure the permeability based on this model is presented. It requires the measurement of fiber architecture details, weight and an initial porosity estimate to start the computations. The unit cell is broken into weft, channel and warp sections each of which represent the fiber architecture details. An averaged effective permeability is calculated using this model. The results for three values of porosity are compared with actual radial flow experiments under steady state. The measurements agree well with the predictive model. A fractal in-plane permeability model is developed by Yu and Lee [58] that considers a unit cell representation of the preform under compression.

The well-known Hagen-Poiseuille equation for determining flow rate through a single pore channel is integrated over the range of pore sizes. The total flow rate q is used in conjunction with Darcy's law to compute the permeability. The generalized expression for permeability has pore area fractal dimension D_f and tortuosity fractal dimension D_T as the defining parameters,

$$K = \frac{\mu L_0 q}{\Delta PA} = \frac{\pi}{128} \frac{L_0^{1-D_T}}{A} \frac{D_f}{3 + D_T - D_f} \lambda_{\max}^{3+D_T} \quad (35)$$

The determination of pore area fractal dimension is approximate and can lead to errors in the permeability prediction. Experimental results agree well with predictions. However effective or principal permeability values are not compared with experimental results.

Noting the wide variety of measurement methods and their differences in predictions Parnas et al. [59] propose a database of Standard Reference Materials (SRM) for permeability characterization. Radial flow, 1D channel flow for saturated and unsaturated permeability in both in-plane and through thickness direction is conducted for a SRM and random mat material. The SRM is a 3D woven glass fabric representative of the fabrics used in the actual manufacturing industry. The values of unsaturated permeability in 1D channel flow is 3.7 times the saturated

permeability value while the flow front is advancing to fill the mold. Variation in permeability values is observed for radial flow when the inlet flow rate is changed. Better agreement is obtained in permeability values by these methods when steady state is reached in both radial and channel flow experiments. In the second part of the study completed by Luce et al. [60] two layers of preform are compacted at various pressure values and their effective permeability determined. The in-plane unsaturated permeability values deviated from the saturated values again.

The study used an architecturally complex fabric common in industry and applied Darcy's law for 3D flow prediction. Some flow behavior could not be accounted by Darcy's law.

Optical Coherence Tomographic (OCT) imaging is used to capture details of microstructure of a preform and its influence on permeability by Dunkers et al. [61]. Images of glass fiber/ epoxy composite are converted to binary images for input into Lattice-Boltzmann flow code. The LB method determines the permeability based directly on the microstructure. The results of this prediction are compared with saturated radial flow method. The computed values from OCT are in good agreement with the measured values.

The results detail the effect of Brinkman fraction, tow surface area and the average mean free channel path on permeability computation. The Brinkman fraction is defined as the area occupied by the tows in an image. It varies from image to image for the same sample and hence can indicate permeability variations within a preform.

X-Ray imaging technique is used to determine real time saturation of core sample. The images are then used for the determination of unsaturated relative permeability, Maloney [62]. The X-Ray images capture unsteady state of flow between two fluids. Permeability using these two fluids, oil and brine, are calculated. Two phase relative permeability is measured by

Schembre and Kavscek [63] using X-Ray CT scanner. The scanner captures saturation of the core sample along the length as a function of time. The computed relative permeability in this method accounts for capillary pressure of the sample as well. The combinations of two fluids used in the study for unsteady state calculations are water-oil and water-air.

The relative permeability profiles are used to compute saturation history in either case. This computed saturation history matches well with the observed saturation history of the samples.

2.1.6. Measurement of 3D Permeability

So far the discussion of permeability measurement was restricted to in-plane directions of the medium only. A few methods have been developed to measure 3D preform permeability. Strictly speaking these would also fall either in channel flow or radial flow categories.

Weitzenbock et al. [64] conduct radial flow experiments to determine 3D permeability. Limits of this method to measure 3D permeability are discussed.

The determination of flow fronts in the thickness direction is done using thermistors. The impact of capillary force in the 3D flow is explained as the basis of increasing inlet pressure. The increased inlet pressure leads to flow induced compaction. It is concluded by the authors that measurement of 3D permeability should not be done by monitoring the flow front in unsaturated conditions. Instead, it is suggested to use steady state stationary flow front method for 3D measurements.

Kim and Daniel [65] determine the three dimensional permeability of fiber preforms by the inverse parameter estimation technique. The experimental set up uses two transparent mold plates so that flow front positions on both sides can be observed. Radial flow technique is used

and flow fronts are measured on top and bottom of the preform. A Control Volume Finite Element Model (CVFEM) is used to simulate flow through a preform.

The difference between observed and computed times of flow front position is minimized by using an optimization technique. The observed time of arrival of flow fronts at various locations in a preform is compared with the computed time of arrival using CVFEM. Scholz et al. [66] use both gas and water flow to determine transverse permeability as a function of FV continuously in one experiment. The experimental set up uses flow rates that result in Reynolds numbers less than one. Some difference in permeability values is observed when the same material in its non-precompacted stage is tested by air and liquid. Wu et al. [67] propose a radial method of transverse permeability measurement. The use of a typical radial set up is accomplished by the unique placement of fiber rolls. The fiber rolls are wound in a circular pattern around the inlet such that the flow is forced in the transverse direction. Glass woven fabric and fiber rovings are measured for four values of FV.

To determine the transverse permeability of a given preform Stoven et al. [68] have developed a continuous monitoring system for three-dimensional flow through a fiber preform. Flow front propagation is monitored using ultrasound transmission.

2.2. Inconsistencies with Existing Measurement Methods and Models

As observed by Chan et al. [9], the permeability values change as the flow rate is increased while keeping all other parameters constant for the same porous medium. Some studies have used test fluids to measure permeability. Steenkamer et al. [69] study the role of different test fluids in determining permeability. To separate the effect of test fluid on fibers, three test fluids and two fibers are chosen. Three test fluids are: diluted corn syrup, motor oil, and vinyl

ester resin. Two types of fabric are; a continuous strand mat and a biaxial fabric. Each fabric is tested for permeability at two values of FV by these test fluids. The total number of permeability tests conducted is twelve.

Radial flow technique is used for the experiments. Constant flow rate is maintained by a pressure regulator and pressure transducers record the values at various positions. Darcy's Law in polar co-ordinates is used to determine principal permeability. Continuous strand mat shows higher permeability in weft than the warp direction for all three test fluids. The converse is true for the biaxial ($\pm 45^\circ$) knitted fabric i.e. warp direction permeability is more than weft direction permeability. This contrast is thought to be due to the presence of chain stitches that hold the $+45^\circ$ and -45° layers together and are parallel to the warp direction. Comparing the results on the basis of test fluids, the highest permeability values are obtained using motor oil and the lowest permeability values using diluted corn syrup for both types of fabrics. Vinyl ester resin gives values between those obtained by motor oil and corn syrup for both the weft and warp direction. This is explained on the basis of a favorable contact angle for wetting out of glass fibers by motor oil as compared with vinyl ester.

Variations in the permeability of fiber preform due to the fiber architecture are investigated by Shih and Lee [70]. Radial flow tests with constant flow rate on four types of glass fiber reinforcements are done. Permeability measurements are done for different FV fractions. FV is changed by altering the number of fiber layers inside the mold. The test fluid used in these experiments is DOP oil. The results show that permeability values for three types of fabrics with different tow sizes and construction are the same. Higher permeability values are observed for biaxial fiber mats.

Steenkamer et al. [71] conduct permeability measurements for five types of glass fibers with three resin systems. The objective of the study is to determine fiber wetting and its effect on permeability measurement. The five preforms for permeability measurements are: Continuous strand mat, bi-axial (0°/90°) knitted fabric, bi-axial knitted fabric with a chopped strand mat (0°/90°/C), bi-axial (±45°) knitted fabric, and unidirectional woven fabric. The three test fluids are Vinyl ester, diluted corn syrup and motor oil. Radial flow method with constant flow rate is employed to determine the desired parameters. Permeability measurements are carried out at different FV values using vinyl ester as the test fluid. The range of FV in the experiments for various preforms is between 28% and 16%. Lower FV is chosen so that the required injection pressure does not increase to the extent that fiber rearrangement takes place. Higher in-plane permeability value is observed for continuous strand mat as compared with the other mats. It is conjectured that it is due to higher porosity of continuous strand mat relative to the directional fabrics. The second principal in-plane permeability values, K_2 of bi-axial (0°/90°) and bi-axial (±45°) knitted fabrics are similar, but their K_1 values differ significantly.

When the same preforms are tested using diluted corn syrup and motor oil, the permeability values obtained differ from that of vinyl ester measurements. Once again measurements done using motor oil display the highest permeability values while corn syrup shows lower values. This dependence of permeability values on the type of fluid used is explained on the basis of fiber surface wetting governed by three-phase thermodynamic equilibrium between solid, liquid, and vapor phases. The corresponding interfacial forces between these phases is governed by the Young-Duprè equation [71],

$$\gamma_{SV} = \gamma_{SL} + \gamma_{LV} \cos \theta \quad (36)$$

γ_{SV} , γ_{SL} , and γ_{LV} are surface energies between solid, liquid, and vapor phases and θ is the equilibrium contact angle. The contact angle $\theta > 0^\circ$, $\theta = 0^\circ$ and $\theta < 0^\circ$ describe the affinity of the fluid with respect to the fiber surface. The contact angle also determines whether external force is required to wet out the fiber surface as given by eq. 37.

The wetting is measured by the work of spreading W_S where W_{LL} is the work of cohesion of the fluid and W_{SL} is the work of adhesion.

$$W_S = W_{SL} - W_{LL} = \gamma_{SV} - \gamma_{SL} - \gamma_{LV} \quad (37)$$

Polar, dispersive and total surface free energies of the three test fluids and the fibers are measured. Based on that and the dynamic contact angle analyzer, work of spreading is calculated for all the test fluids. Motor oil results in higher permeability and is attracted towards the glass fiber as compared to the vinyl ester and diluted corn syrup. Vinyl ester and diluted corn syrup have a negative work of spread W_s . A negative work of spread indicates that there is a need for external pressure on these test fluids to wet the fibers.

Until a complete understanding of test fluid-fiber interaction is developed, Steenkamer et al. [71] recommend that the fibers should be characterized with the actual liquid composite resin for a given application. Sizing (chemical coating) on the fiber surface bonds the matrix and reinforcement and helps wettability during a manufacturing process, in addition to protecting the fiber surface from damage. It is worth noting that radial flow methods employed by Steenkamer suffer from the entrance effect as reported later in some studies. The entrance effect is not considered in these studies.

The effect of fiber sizing on the behavior of fluid flow is investigated by Karbhari and Palmese [72]. They conduct experiments using glass fibers with different sizings. Except for one sizing that contains condensed silane all the other fiber sizings contain some hydrolyzed

material. Experiments are conducted by letting uncatalyzed resin as a test fluid to flow over these fibers with different sizings at room temperature.

The test set up has a vertical stainless tube with known diameter. Resin is infused through the fiber bundles of equal FV in this stainless steel tube. The resin-sizing compatibility for manufacturing is validated by the experiments. The fiber (specifically sized for vinyl ester and polyester) shows the highest steady-state flow rate. The second fiber formulated for high temperature resins displays the highest initial flow rate and longest transient flow period. Steady state flow rates for these fibers are measured and compared. It is observed that the sizing-resin compatibility plays an important role in the flow rate and fiber wetting. It is inferred that permeability is altered due to sizing –resin interaction.

To separate the effect of sizing on microscopic flow from that of macroscopic flow, Palmese and Karbhari [73] conduct experiments on sized and unsized carbon fibers. The resin transfer molding process is used to run the experiments in a stainless steel tube that is similar to the one used in the previous study [72]. Uncatalyzed vinyl ester is injected through the axially oriented fibers in the tube at constant pressure. FV of the fiber preforms is varied by increasing the number of tows. After saturation, resin is collected in a pot that is kept on a weighing scale. Cumulative weight with respect to time is measured. Cumulative flow results with respect to time, display two flow regimes. There is an initial transient region characterized by a rapid flow rate, followed by a steady-state region with a significantly lower flow rate. For lower FV the initial rapid flow regime is more pronounced. When the fiber sizing is removed, the shape of the curve remains the same, but the overall flow rate is reduced, thereby indicating the influence of sizing on flow behavior.

The explanation provided for this flow behavior is based upon capillary forces and the difference between macro and micro flow. Macro flow occurs between the tows and is characterized by a rapid flow rate due to large available space. Micro flow takes place, as the flow from macro pores slowly seep in the micro channels due to capillary forces. Hence the cumulative weight plot displays the rapid regime due to macro flow and a gradual change to steady state region as the fluid enters the micro pores. When the FV is increased due to higher number of tows inside the tube, it increases the capillary pressure resulting in shorter transient regime. This non-linear curve forms the basis of sink term in the continuity equation. The sink term is then based upon the capillary forces in the micropores. This type of flow behavior is termed as dual scale flow as it shows macro and micro scales of flow in the fiber performs. A sink term based on capillary forces has been introduced to explain the dual scale flow and the eventual loss of flow due to micro pores.

Steady state flow is reached only after the tows are wetted inside as well. At lower FV, the tows spread out enlarging the micro pores in the process. Once, the macro flow has been completely absorbed in the micro pores, a steady state between the dual scale flow is reached.

The issue of the permeability dependence on test fluids is discussed by Abrate [74]. All the test fluid – sizing interaction studies have been conducted using fluids of different viscosities. Experiments conducted with fluids of different viscosity for the same fiber preform have resulted in varying permeability values. The investigation points to fluid sizing interaction altering permeability values.

Variations in permeability values for the same medium using two or more different measurement techniques are studied by Chan [9]. Pillai [75] reviews the confusion surrounding the applicability of Darcy's law for some experiments. According to Pillai [75] it has been

reported that Darcy's law holds good only for radial flow measurements. The same review mentions that the pressure gradient which should remain linear for experiments in fact depends upon the type of medium used. A non-linear pressure gradient is observed for continuous fiber bed that is characterized by a highly ordered porosity. A linear pressure gradient is observed for random fiber beds. It is worth noting here that Darcy's relation is also derived from a random porosity medium i.e. sand.

Breard et al. [76] also measure the pressure profile and observe that there is a non-linear pressure gradient. This is in contrast to the linear pressure gradient used in the Darcy relation. Schoelkopf et al. [77] report non-linear pressure relation while using Darcy's law to determine permeability in fine pigment structures. No linear permeability-porosity relationship is observed in the same experiments. A hysteresis in permeability is observed after saturation. No mention of steady state or unsteady state measurement is indicated in the experiments.

Kaynak and Kas [78] study and explain the effects of injection pressure in RTM composite manufacturing. Five different injection pressures are chosen for the RTM process. Fill time, edge effects and FV of the finished carbon/epoxy composite are noted. Injection pressures above 2 atm. results in distinct separation of macro versus micro flow. This dual scale flow results in higher void content in the composite. Kim and Daniel [79] investigate the effect of flow rate on fluid flow through the fiber preform. The fiber roving chosen for this experiment has minimal dual scale flow properties i.e. the difference between tow and channel flow is minimal. Both saturated and unsaturated experiments using radial flow method with constant injection pressure are conducted. Saturated and unsaturated permeability are plotted versus flow rate. As the flow rate is increased permeability increases until a certain point after which it begins to level off. Non-Darcian flow characteristics are observed for saturated flow conditions.

A model for saturated permeability based on geometry dependent coefficients and Reynolds number is created. Permeability for a range of Reynolds number ($10^{-7} < R_e < 2 \times 10^{-6}$) is calculated based on the model. Viscoelastic deformation of fiber preforms is observed when compressive forces are applied prior to infusion.

The investigation carried out by Bickerton et al. [80] highlights the time dependence of such compression and the resulting stress in fibers inside the mold. Effects of deformation impact flow characteristics in the preform.

2.3. Cross Transport Phenomena and Fluid Flow in Porous Media

Prasad [81] identifies the cross transport phenomenon of seismic wave velocity and permeability in rocks. A strong correlation of 0.65 -0.87 is established between wave velocity and permeability for various values of porosity. Johnson et al. [82] propose a relationship between electrical field, permeability and diffusion parameters.

The relationship is governed by the following equations where Λ is the pore volume to surface ratio (characteristic length), $E(r)$ is the local electrical field, V_p is the pore volume, S_p is the pore surface and F is the formation factor,

$$K = \Lambda^2 \frac{1}{8F}, \quad \Lambda = 2 \frac{\int |E(r)|^2 dV_p}{\int |E(r)|^2 dS_p} \quad (38)$$

Combining the Johnson et al. [82] expression with the random walk simulation approach, Tomadakis and Robertson [83] propose a permeability expression for flow parallel to unidirectional fibers,

$$\frac{K}{r^2} = \frac{\eta}{8 \ln^2 \eta} \quad (39)$$

An approximate predictive relationship for permeability of array of spherical particles is also given in the study. The results from previous predictive methods are compared with the approximate formulation and a good agreement is found.

The behavior of porous materials under an acoustical force field that is related to permeability has been observed by some investigators. A relationship between pore anisotropy and Anisotropy of Magnetic Susceptibility (AMS) is established by Benson et al. [84] for samples of sandstone. The same study also experimentally establishes a correlation between the porous medium permeability anisotropy and acoustic wave velocity. The samples used in this study are cylindrical with 38.1 mm diameter and 40 mm length. The acoustic wave velocity measurements are made radially for every 10 degree orientation using a pulse transmission method. Permeability is measured using distilled water at 5 MPa via Darcy's law. Acoustical wave velocity distribution coincides well with the permeability anisotropy directions.

Lafhaj et al. [85] detail a relationship between porosity and permeability of cement mortar mixture with Ultrasonic Pulse Velocity attenuation and velocity. The frequency range of UPV is 0.5 to 1.5 MHz. Permeability is measured using gas flow method at constant injection pressure. Porosity is measured by the gravity method using vacuum saturation. Longitudinal and shear wave velocities are respectively related to porosity by the following relationships,

$$v_l = v_{l0}(1 - b\eta) \quad , \quad v_t = v_{t0}(1 - b\eta) \quad (40)$$

These relationships are linearized considering very low porosity values. The parameter 'b' is determined based upon the Poisson's ratio of the material of zero porosity. Permeability is related to porosity through a very simple model of porous medium approximated as an assembly of regular circular channels,

$$K = \frac{\eta d^2}{32} \quad (41)$$

A relationship between longitudinal and shear wave velocities with permeability is then developed based upon the above equations,

$$K = \frac{d^2}{32b} \frac{\Delta v_{l,t}}{v_{l,to}}, \quad (42)$$

$\frac{\Delta v_{l,t}}{v_{l,to}}$ = Variation of UPV of longitudinal or shear wave for zero porosity value.

It is unclear whether this permeability calculated refers to unsaturated, saturated or effective value. Further, the use of UPV and the testing technique is not a standardized method of acoustically characterizing the material. The permeability porosity relation used in this study is based upon regular square arrangement of grains.

2.4. Some Observations and Concluding Remarks on Permeability Measurement Methods

A mathematical relationship between permeability as a function of porosity and tortuosity has been well established by Bear [86],

$$\eta B T_{ij} = K_{ij} \quad (43)$$

In related physical phenomenon like heat flow and acoustical wave propagation in a medium, the PDE is related to the microscopic physical properties of the medium. As an example, Biot's theory [87] provides the governing differential equation formulated in terms of characteristic lengths (viscous and thermal), porosity and flow resistivity of the porous medium. Such a relationship is desirable for flow in porous medium. But perhaps using an empirical equation (Darcy's law) to develop a generalized exact formulation for characterizing fluid flow in porous medium may be very difficult.

It is worth asking if permeability as a parameter is necessary and sufficient to characterize fluid flow through a porous medium in all the situations. A second theoretical

observation relates to the use of Laplace equation in determining unsteady state flow characteristics. The unsaturated permeability determined by the Laplace equation may not be entirely accurate. Laplace equation should be used for steady state experiments only. Use of Darcy's law in heterogeneous porous media for RTM (especially fabrics with large tow sizes) has been studied and a new sink term for continuity equation introduced. VARTM or RTM for high FV induce nesting effects on tows that minimize the heterogeneous nature of composite materials. Separate efforts should be directed towards such investigations as it has a direct bearing on industrial applications. Further in industrial applications, composite parts usually made with carbon fiber require higher than 60% FV. RTM usually produces parts with higher than 60% FV. The vast majority of studies detailed in this review investigate permeability measurement and flow characteristics for a FV in the range 20% to 40%. The relevance of these investigations to industrial operations hence becomes doubtful.

To reduce uncertainties in permeability measurement, FV should be measured using ASTM or its equivalent method. Use of areal weight and fiber density for FV calculation if done should be verified by actual measurements. Finally, alternative methods of permeability measurements related to electrical, thermal or acoustical cross transport phenomenon should be explored more. The flow based experiments do not correlate well with each other in all the cases.

2.5. Motivation & Objectives

As no standardized or accepted permeability measurement exists in the literature or the industry, it is imperative that the widely used flow based methods be investigated for some of the fundamental aspects of variability. One of the main flaws of Darcy's model as applied to composites manufacturing is the assumption that there is complete saturation of the preform

behind the flow front. Several researchers have shown that the perform acts as a heterogeneous medium and hence shows dual scale flow characteristics necessitating the use of sink term in the continuity equation. Hence, the measurement of flow front velocity and its use in Darcy's law results in the calculation of unsaturated permeability. Once the fluid completely saturates the medium, measurement based on pressure difference yields saturated permeability value. Saturated permeability for a given medium is always lower than the unsaturated permeability value. As detailed by some studies, the use of different fluids alters the permeability value of the given perform for the same experimental method. The variation in permeability values is explained on the basis of fluid –sizing interaction. But the experiments conducted so far have used fluids of different viscosity values. Thus the first objective of this study is to investigate the variability of permeability values due to different fluids having the same viscosity using channel flow technique. This will separate the fluid-sizing effect from the effect of viscous forces on the permeability value if any. The second objective is to determine the saturated flow characteristics of the fiber perform in order to capture the dual scale flow behavior. Both of these objectives will be investigated specifically for VARTM processes employing 1D channel flow method.

Since the wide variety of results reported in the literature about flow based methods have yielded little common agreement, cross transport methods are gaining interest. Knowing the relationship between physical properties of porous materials and wave propagation through it, absorption coefficient, reflection coefficient and the impedance ratio is determined using analytical techniques. However, using the absorption coefficient and impedance ratio of any porous material to conduct inverse parameter estimation to determine the physical properties is challenging. Research devoted to finding out the physical properties like flow resistivity, thermal and viscous characteristic lengths, porosity and tortuosity using the inverse techniques employ

optimization methods or search algorithms. The third objective of this study is to develop a validated acoustical methodology to inverse calculate physical properties of poro-elastic materials. This validated methodology is sought to be established based upon standardized acoustical measurement methods and analytical tools.

Flow resistivity is the inverse of permeability. The last objective of this investigation is to utilize the validated acoustical method of determining the physical properties to predict permeability of orthotropic materials used in composites manufacturing.

CHAPTER 3

EFFECT OF FIBER SIZING - TEST FLUID INTERACTION ON THE UNSATURATED AND SATURATED FLOW IN THE VARTM PROCESS

3.1. Introduction

Darcy's law is extensively used for flow modeling and permeability measurement of porous media. This empirical relation uses fluid viscosity, pressure gradient and flow rate as inputs to determine permeability of the medium. The fluid used in these experiments should be Newtonian, incompressible and be chemically inert. As long as these conditions are met fluids of different viscosities should yield the same permeability value for a given porous medium. However, it has been shown that the measurement of unsaturated permeability is dependent upon the type of fluid used in the experiment. The saturated flow characteristics through porous media are also affected by fiber sizing as indicated by several studies to characterize porous materials [1,68,89,93-95]. A review of these experiments is given by Abrate [74]. Examples of test fluids used are water, corn syrup, motor oil and silicone oil.

Studies carried out by Karbhari and Palmese [72] have shown that the type of resin used in fiber bundles in an RTM process results in different flow behavior. The three types of test fluids with different viscosities used by Steenkamer et al. [71] in RTM experiments yield varying in-plane permeability values for the same reinforcement. This hints at test fluid interaction with fiber sizing to cause the observed permeability variations. However, the saturated flow behavior of test fluids through a porous medium in the VARTM process has not been investigated thus far.

Further, the sizing–test fluid interaction cannot be captured accurately unless two or more types of test fluids with the same viscosity are used to measure the permeability variations. These thoughts molded the objectives of the present study.

Investigations are carried out as well to determine the saturated flow characteristics of test fluids using VARTM. The saturated flow characteristics provide an insight into the dual scale flow characteristics in heterogeneous media. Dual scale flow characteristics observed in some studies has led to a modification in the continuity equation as detailed by Pillai [75] in his review. The sink term introduced in the continuity equation accounts for the delayed impregnation of the tows. The modified continuity equation is now used in modeling of heterogeneous porous media. The saturated flow characteristics of test fluids as determined in VARTM are compared with similar results obtained using Resin Transfer Molding (RTM), Palmese and Karbhari [73].

3.2. Experimental Set Up

The objectives of this study are to determine if variations in permeability values can be attributed to the type of fluid used and to develop a saturated flow behavior model for VARTM to investigate the dual scale flow behavior in heterogeneous media. To this end a total of fifty eight in-plane unsaturated permeability measurements are conducted with all permutations for both sized and un-sized fibers using channel flow technique with four types of fiber reinforcements and three types of test fluids. The four types of fiber reinforcements have different sizings, tow sizes and material types. Two types of uni-axial carbon fibers with different sizing and tow sizes are chosen.

The V2[®] Fortafil carbon fiber has epoxy sizing, while the Saertex[®] uni-axial carbon has polyurethane sizing. Two glass fibers are also chosen with Silane as sizing. The three types of test fluids are high viscosity corn syrup (HVCS), low viscosity corn syrup (LVCS) and silicone oil (SO). Corn syrup is diluted to give HVCS that has nearly the same viscosity i.e. 0.045 Pa-Sec as SO. All experiments conducted are using 1D channel flow method at constant pressure. The fibers are stripped of their sizing using acetone and dried for twelve hours before conducting the experiment.

A rectangular mold with cavity dimensions 216 mm by 112 mm by 3 mm is used, Figure 9. Uniform one dimensional flow through the fiber preform is ensured by rectangular cavities on both ends of the mold. At the widthwise center of each rectangular cavity, slots for pressure transducers allow the monitoring of pressure during the experiment. The mold with aluminum has a matching transparent top for RTM based experiments. The vacuum bag for the VARTM process on the upper side of the tool is sealed with sealant tapes. Thin strips of flow media as seen in Figure 9 are placed in these reservoirs to allow the fluid to enter the fiber preform. Without the flow media strips, vacuum bag would obstruct the flow from reservoir to the preform. Matching outlet reservoir at the other end of the fiber preform allows a rectilinear and smooth flow front during experimentation. Out of plane flow in the preform is assumed negligible. The sides of the mold cavity along the mold length are filled with small amount of wax. This ensures no race tracking along the sides occur during experiments.

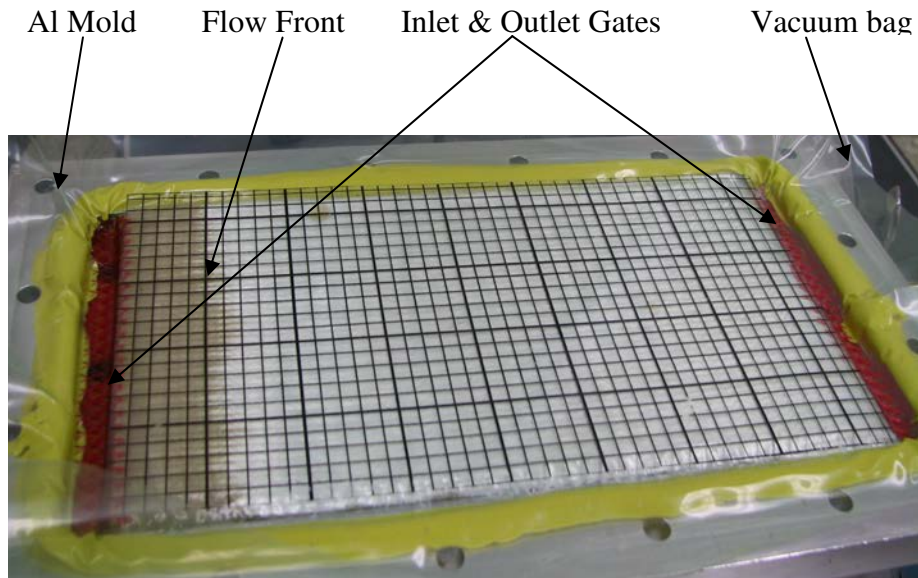


Figure 9. VARTM Setup [19]

The experimental set up is shown in Figure 4 in the previous chapter. The aluminum mold has an injection line gate and a vent line gate the size of the width of the mold. Both, the inlet gate and outlet gate are connected with clear plastic tubes of 0.635 cm inner diameter. These tubes are attached to plastic valves to control the flow. The outlet tube is connected to a vacuum chamber which in turn is connected to the vacuum pump. The inlet tube is connected to a fluid tank with pressure gage.

Prior to fluid injection, vacuum integrity of the system is checked. The mold is first brought to the desired vacuum level and the pump is then switched off. Vacuum pressure is monitored for about 20 minutes. Experiment is carried out only if there is no drop in the vacuum level in those 20 minutes (indicating very slow leak). Fluid is injected under constant pressure and the flow front is monitored using a motion camera. Pressure at the inlet and outlet is also monitored throughout the experiment. After saturation of the pre-form, fluid is collected in the resin trap.

The resin trap is placed on top of a weighing scale and the rate of change of mass is observed using a second motion camera. This way saturated flow rate is measured for all the experiments.

Darcy's Law, Darcy [1], is used to measure the unsaturated permeability of the preform,

$$V = -\frac{K}{\mu} \frac{dP}{dx} \quad , \quad L^2 = \frac{2K\Delta P}{\phi\mu} t \quad (44)$$

Where L , ΔP , t , and ϕ represent the length of the flow front, the pressure difference, the mold fill time and the porosity of the reinforcement, respectively, Lee et al [17]. Pressure difference of the fluid is noted with the help of pressure transducers located at each vent gate. Video camera is used to capture flow front data with respect to time. Based on the observed length of flow front with respect to the injection line gate as origin, an L^2/t graph is plotted. The slope of L^2/t is used in the above equation to obtain the permeability values of the tested fiber preform. Porosity ϕ is derived from the actual measurement of fiber volume fraction from test data. The FV fraction is measured using ASTM D792-91, ASTM D3171-90, and ASTM D2734-91 standards that utilize ignition burn and acid wash techniques. Since the effect of bubbling becomes noticeable at vacuum levels of 28.5" Hg, a vacuum regulator is used to control the pressure at 28" Hg. A slightly higher vacuum pressure is chosen to ensure continuous saturated flow without bubble formation. Sizing on the fiber preform is removed by washing them in a tray filled with acetone. The preform is then dried for at least two hours at room temperature condition.

3.2.1. Material Matrix

In plane permeability measurements are carried out for four fabrics with different sizings and tow sizes. Each fabric is tested by three test fluids with the sizing and without sizing on them. The physical details of these fiber materials are given in Table 2. Twenty four experiments

are conducted on all four fiber preforms with and without sizing by infusing the three test fluids. Additional experiments are carried out to study the saturated flow behavior. Figure 10 shows the fiber preforms and Tables 2 & 3 lists the fiber preform characteristics like, sizing, tow size, porosity, orientation and number of layers used in the experiments. Fiber samples used in the experiment include a unidirectional (UD) stitch bonded carbon fabric manufactured by Saertex, unidirectional glass fabric manufactured by Saertex, biaxial glass fabric by Saertex and unidirectional carbon fabric by V2.

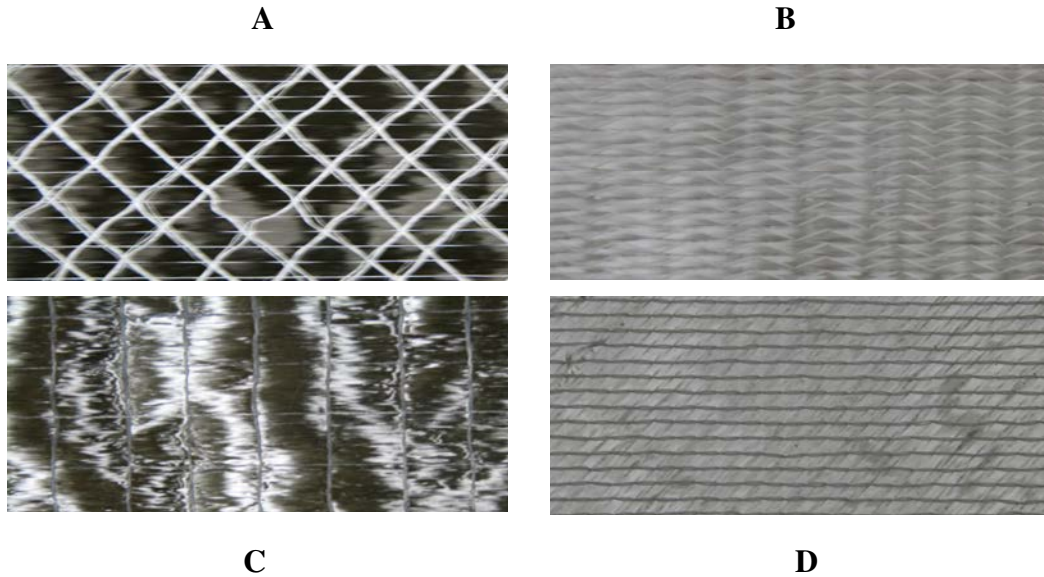


Figure 10. Different fiber reinforcements used in the experiments:
 (A) UD Carbon Fiber 1 (B) UD Glass Fiber
 (C) UD Carbon Fiber 2 (D) Biaxial Glass Fiber

Table 2. Fabric Characteristics

Fibers	Filament Diameter (μm)	Sizing	Tow Size (K)	Fiber Manufacturer
UD Carbon Fiber 1	7	Polyurethane	24	Saertex
UD Glass Fiber	17	Silane	1.2	Saertex
Biaxial Glass Fiber	17	Silane	1.2	Saertex
UD Carbon Fiber 2	7	Epoxy	68	V2

Table 3. Fiber Porosity, Orientation, and Number of Layers Used

Fiber Preform	Porosity (ϕ)	Number of Layers	Orientation
UD Carbon Fiber 1	0.4	6	0° Uniaxial
UD Glass Fiber	0.517	8	0° Uniaxial
Biaxial Glass Fiber	0.525	12	±45° Biaxial
UD Carbon Fiber 2	0.4	6	0° Uniaxial

Corn syrup and silicon oil are chosen because they have been used in previously reported investigations [1,70,74,91,95-99]. These fluids offer an ease of clean up after the experiments that is contrast to the epoxy resins. Further, the National Institute of Standards and Technology (NIST) database on fabric permeability cites diluted corn syrup as the test fluid to evaluate permeability [100]. Corn syrup is easily available and conforms to the properties of a Newtonian fluid. A ball and drop viscosimeter is used to measure dynamic viscosity of the test fluids before and after the experiments. Density of fluids is calculated using a high precision weight scale. The viscosities and densities of the test fluids used are shown in Table 4. Corn syrup is mixed just prior to the experiment to ensure the physical properties do not change with respect to temperature and time. All the experiments are conducted at room temperature. Viscosity values remained stable during all the experiments.

Table 4. Test Fluid Characteristics

Test Fluid	Mixture Ratio	Viscosity (Pa-Sec)	Density (gm/ml)
Low-Viscosity Corn Syrup	3 parts water : 1 part syrup	3.24×10^{-3}	1.10
High-Viscosity Corn Syrup	1 part water : 2 parts syrup	44.25×10^{-3}	1.27
Silicon Oil	As is	45.60×10^{-3}	0.97

Two video cameras are used to capture the readings from pressure transducers, flow front positions of the fluid through the fibers, and cumulative flow rate from the outlet. To determine the saturated flow rate, mass of the fluid being collected in the resin trap is measured with respect to time. The resin trap is placed on top of a weighing scale. A digital vacuum regulator (DVR 200 from J-KEM Scientific Inc.) is used to maintain a constant vacuum of 27.5” Hg for saturated flow studies. This vacuum level is required to avoid bubbling of test fluid that can result in intermittent flow. The complete experimental setup is shown in Figure 11.

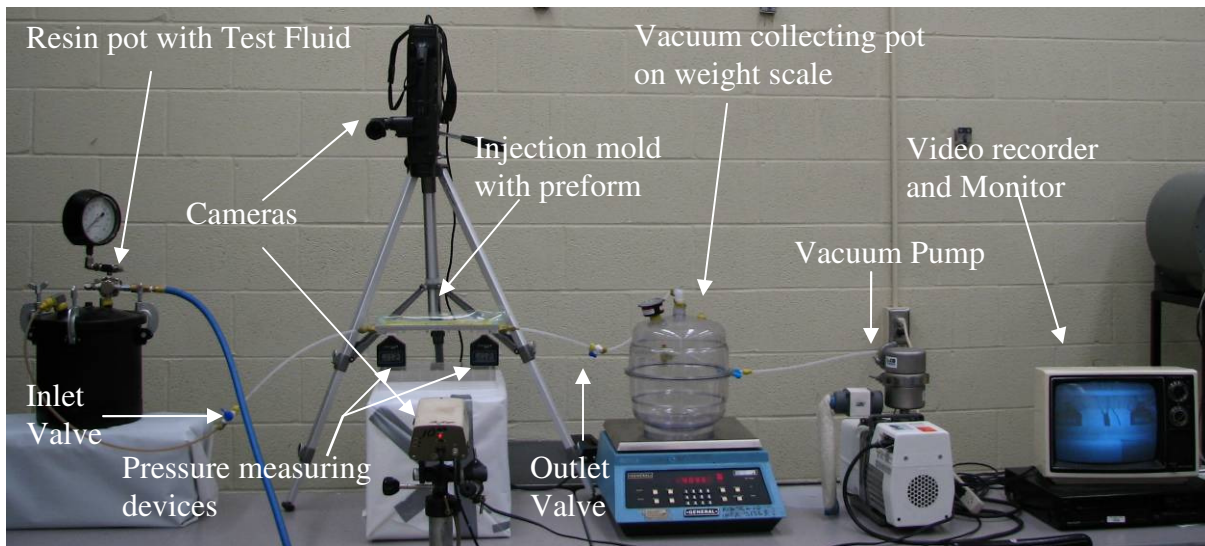


Figure 11. Setup used for conducting flow and permeability experiments [19].

3.2.2. Data Reduction

Pressure difference ΔP is constantly observed and its average value is used in the permeability calculations. Flow front position with respect to time is tracked by the video camera. The position of flow front with respect to the inlet gate is plotted to obtain the slope, L^2/t in m^2/sec . These values of L^2/t are used as input in the equation by Lee et al [17] for calculating permeability in units of Darcy ($1 \text{ Darcy} = 9.8697e-9 \text{ cm}^2$). For saturated calculations, flow rate is

measured by weight (mass in grams) with respect to time of the fluid flowing out of the mold under constant vacuum.

3.3. Results and Discussion

A comparison of permeability values for a given fabric system using different fluids is shown in Figures 12 to 15. For a given fiber system, the experiments are run using all three test fluids and the principal permeability values are noted. The same experiment is repeated with all three test fluids after stripping the fiber of the sizing. Permeability values obtained for various glass fibers in this study confirm the trend observed by Palmese and Karbhari [73] as well as Steenkamer et al [71]. It is observed that for all fibers except uni-directional carbon 2, the permeability values of sized fibers are lower than the unsized fibers. Further, the tow size of UD carbon 2 is 68 K and yet it displays higher permeability values than the UD carbon 1 that has a tow size of 24 K.

The conclusion derived by previous studies [69, 71, 72 & 73] postulated that the sizing of the fiber interacted with the test fluid because of the specific surface energy. The contact angle varied from one fluid to another for the same fiber surface and hence altered the flow behavior.

In this study, two fluids of different chemical composition but with similar viscosity values result in the same permeability value for a given fiber. This result demands a more comprehensive explanation than the specific surface energy as the cause for variation in flow behavior and hence permeability values. As observed in Figures 12 to 15, the last two permeability values are for HVCS and SO that have approximately the same viscosity viz. 0.045 Pa-Sec. The two glass fibers have silane as sizing. Permeability values measured using HVCS and SO for these sized glass fibers are nearly identical as shown in Figures 12 and 13 (21 & 20

for biax & 36 & 35.5 for UD) Permeability values show a significant variation when the fibers are stripped of their sizing. The unsized fibers display higher permeability values for both types of glass fibers. This could be due to the increase in fiber surface friction resulting in clustering of the fiber tows. It is observed that the unsized fibers stick together tightly and hence allow mostly inter tow fluid flow. The resulting permeability values are thus higher for unsized fibers. For LVCS the permeability values show a 213% jump from sized to unsized biaxial glass fibers. However, the values for UD glass with the same sizing as the biax glass is nearly the same for sized and unsized fibers.

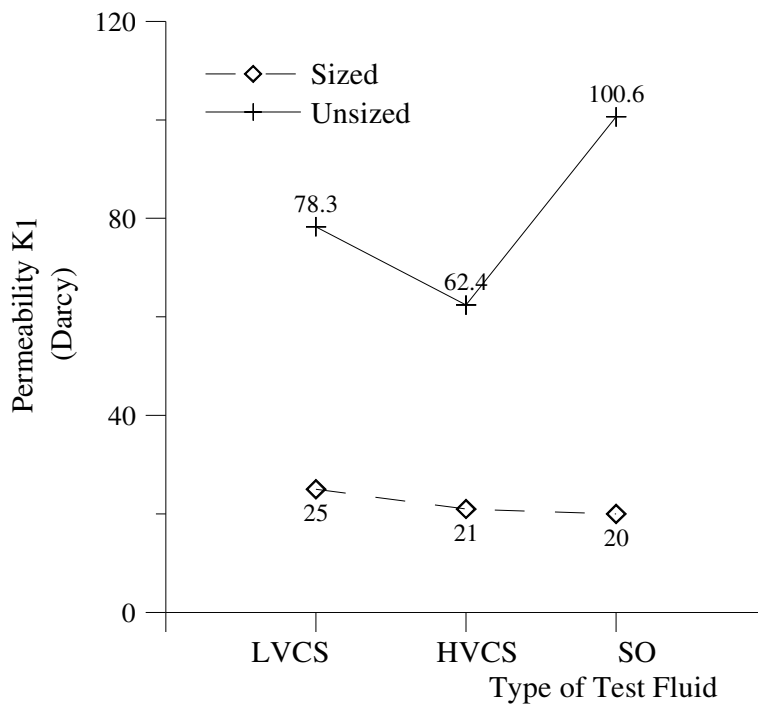


Figure 12. Permeability comparison of Fiber glass Biax (1 Darcy = $9.87 \times 10^{-13} \text{ m}^2$)

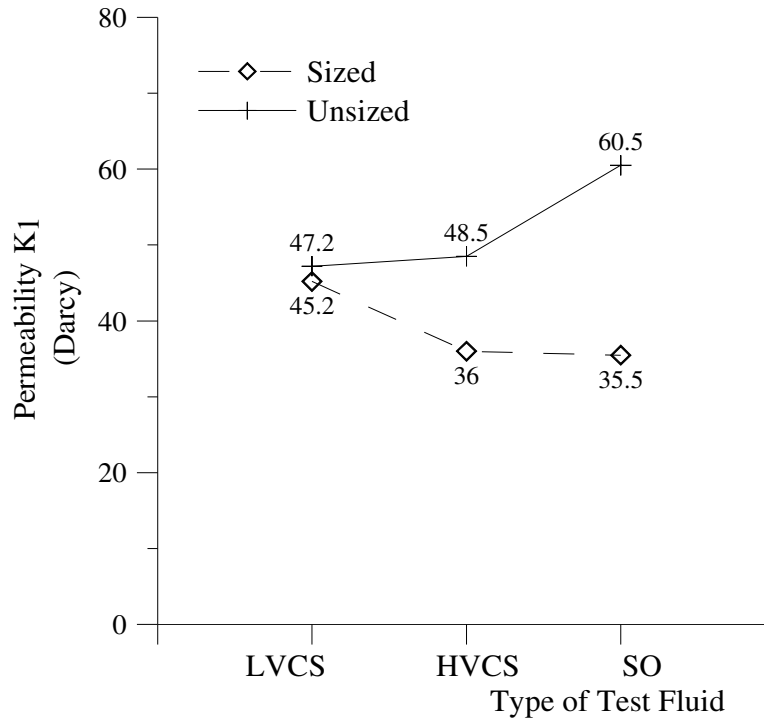


Figure 13. Permeability comparison of Fiber glass UD (1 Darcy = $9.87 \times 10^{-13} \text{ m}^2$)

When these experiments are repeated for carbon fibers 1 and 2 that have polyurethane and epoxy as sizings respectively, the results are similar to the glass fiber system. Figures 14 and 15 display principal permeability values obtained for both types of carbon fibers. The variation in permeability values due to two different test fluids is confirmed for these cases as well. Remarkably, the UD carbon 2 displays higher permeability values when it is sized in reverse trend as compared with other fibers. The possible reason for this is the very large tow size of UD carbon 2, which shows no tow gaps, Figure 10. Once the sizing is removed, the tows cluster together increasing the gaps between them and hence increasing the permeability. The variation in permeability values for both sized and unsized fibers measured with HVCS and SO (of similar viscosity) is nearly the same. This trend once again negates the previously held view of fluid-sizing interaction resulting in permeability variations.

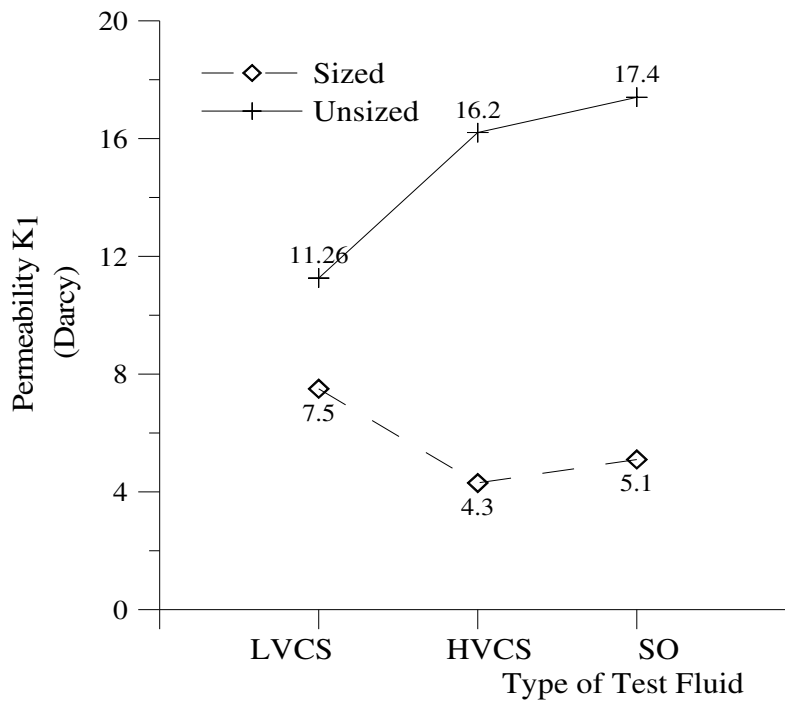


Figure 14. Permeability comparison of UD Carbon 1 (1 Darcy = $9.87 \times 10^{-13} \text{ m}^2$)

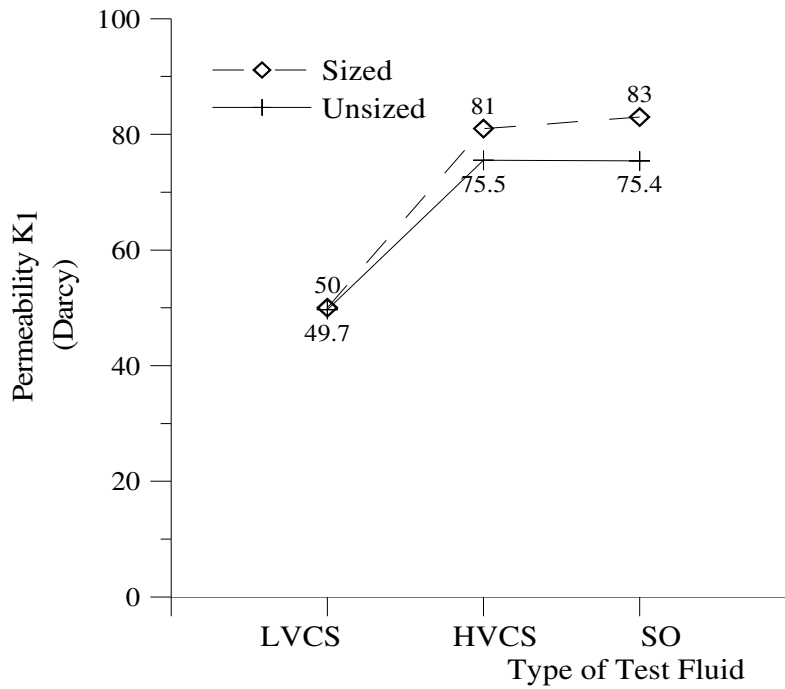


Figure 15. Permeability comparison of UD Carbon 2 (1 Darcy = $9.87 \times 10^{-13} \text{ m}^2$)

The saturated flow study done by Karbhari and Palmese [72] does not specify the FV of the fibers in the experiments. The experiments conducted by Palmese and Karbhari [73] simulate RTM experiment. Dual scale flow is noticed for various fiber types in that study. A transient regime of rapid flow followed by a gradual steadying of the flow rate is observed for dual scale flow behavior as displayed in Figure 16.

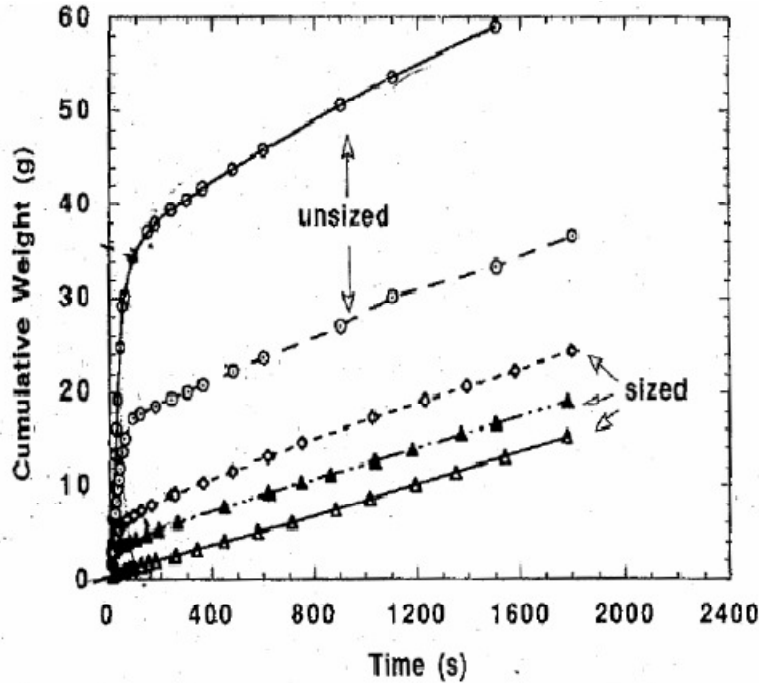


Figure 16. Saturated Flow behavior of Hercules AS 4 fibers with Vinyl Ester resin in RTM Process [72]. Reprinted with permission from John Wiley & Sons, Inc.

The dual scale flow is attributed to the large tow gaps resulting in macro flow and micro flow outside and inside the tow respectively. The saturated flow characteristics studied here for both the sized and unsized fibers at a FV of 48% for glass and 60% for carbon does not show dual scale flow behavior. The relationship between cumulative weight and time is linear indicating a homogeneous flow characteristic in the heterogeneous media. All the fibers with tow

sizes of 1.2 K, 24 K and 68 K display single scale flow behavior as opposed to dual scale behavior, thus confirming that this behavior is not subject to variations in tow sizes. The results are plotted in Figures 17 and 18 for both sized and unsized fibers.

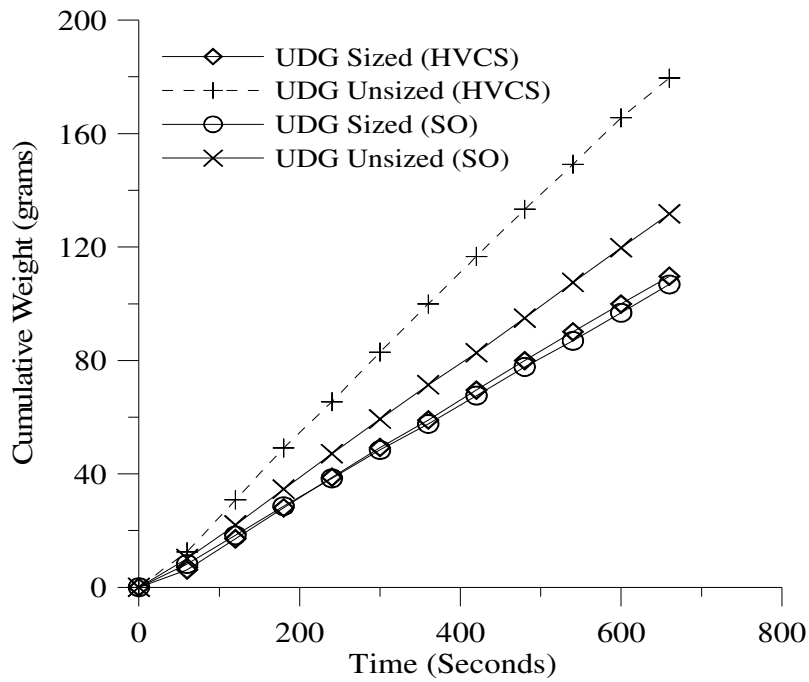


Figure 17. UD Glass Saturated flow behavior

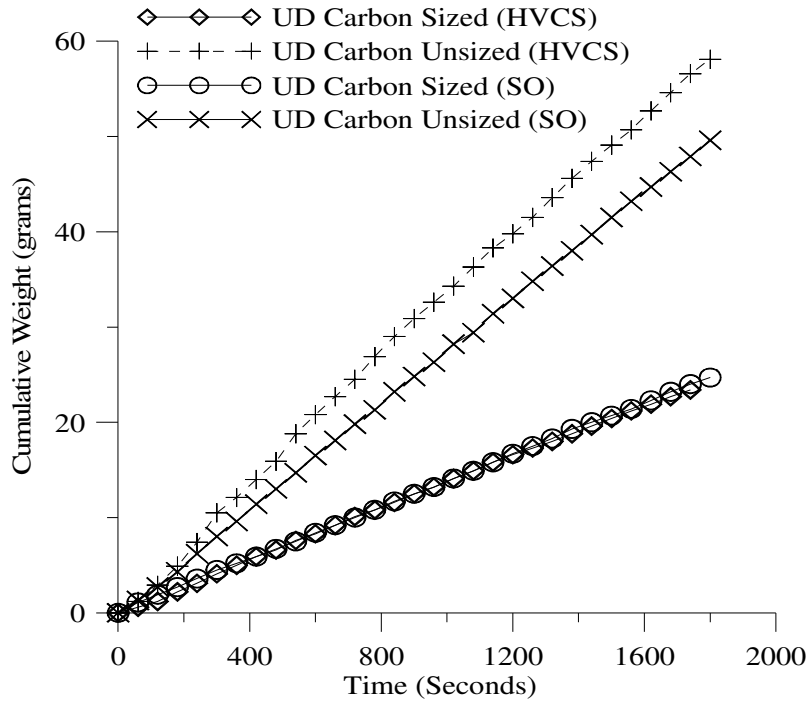


Figure 18. UD Carbon Saturated flow behavior

The primary reason for this single scale homogeneous flow behavior can be attributed to a higher FV due to the compaction of tows under vacuum pressure. The compaction of tows results in the nesting effect and hence minimizes the large tow gaps responsible for the dual scale flow behavior. This homogeneous flow behavior in VARTM process indicates that the use of sink term in the continuity equation for modeling is not warranted. However, it is important to investigate if similar homogeneous single scale flow is observed at higher FV due to compaction in RTM as well. The close unsaturated permeability values obtained either for UD glass or UD carbon by SO and HVCS is confirmed by the saturated flow behavior observed in Figures 10 and 11. The saturated flow curves for the sized glass and carbon fibers obtained by HVCS and SO are overlapping well indicating that their permeability values should be very close. The unsized

carbon and glass fibers show variations in saturated flow behavior when the fluid is changed from HVCS to SO.

3.4. Conclusions

This study details the permeability variations induced due to dissimilar fluids used in the experiments. It is found that two dissimilar fluids of the same viscosity results in the same unsaturated permeability values for four different types of fiber systems. This is especially true for fibers with sizing indicating that the variation in permeability induced is not well understood. These fiber systems have different sizing, orientations, tow sizes and architecture. Previous studies as reviewed by Abrate [74] had used fluids of differing viscosity values to identify permeability variations induced due to the nature of fluids.

It is recommended that more experiments with dissimilar fluids but same viscosity be carried out. One of the fluids should be chosen as diluted corn syrup. The corn syrup can be diluted to achieve the viscosity of the second fluid.

The saturated cumulative flow behavior of the continuous fibers under VARTM process display a different characteristic plot as compared with the RTM studies. In RTM, there is a distinct transient region governed by rapid flow through the intra tow region of the fibers. This flow reduces in time as the tow is saturated completely. But a completely linear behavior is observed for the same phenomenon in VARTM. This can be attributed to the fact that the distinction between intra tow and inter tow flow is blurred due to fiber compaction under vacuum pressure. A more exhaustive study to determine the change from dual scale flow to uniform flow as a function of FV is necessary. This may lead to a better judgment in the use of the sink term in the continuity equation for flow modeling.

CHAPTER 4

DEVELOPMENT OF AN ACOUSTIC METHODOLOGY TO DETERMINE PHYSICAL PROPERTIES OF ISOTROPIC POROUS MATERIALS

4.1 Introduction

Flow through porous medium has been extensively investigated. It is known that the flow behavior is governed by porosity, tortuosity and permeability. Various attempts at measuring permeability to predict flow behavior in composite performs are reviewed by Abrate [74]. These flow based methods have been shown to give dissimilar permeability values of the same porous medium [74]. Limitations of Darcy's law in some of the flow based methods have been reported by Pillai [75]. The dependence of wave energy dissipation in porous medium on the same physical properties brings some interesting similarities between these two disparate natural phenomena. The lack of agreement in measurement of permeability using the flow based method, this article presents a validated acoustical method to predict permeability of porous medium.

The isotropic materials chosen for measurement in this study are most commonly used in noise attenuation. They can be considered as rigid, elastic or limp depending upon the physical make up. Some examples of the isotropic porous materials are foams such as melamine (Wiltec), polyimide (Solimide), Ensolite, etc. and fiberglass. The most important acoustical properties for design and analyses in noise control are absorption coefficient, impedance ratio and Transmission Loss (TL). In this work, the acoustical properties are measured using the impedance tube. A total of thirty different types of foams and fibers are tested.

The use of Foam–X and AutoSEA2 for computational purposes is included to verify the direct measurements. As first step, it is proposed that Foam–X utilizes experimentally measured acoustical properties to perform reverse calculations. Reverse calculations are done from absorption coefficient to yield material physical properties such as flow resistivity, porosity, tortuosity, thermal and viscous characteristic lengths. The input for these calculations is the acoustical properties of the porous medium. These acoustical properties are: absorption coefficient, reflection coefficient and the impedance ratio. The output from Foam–X is physical properties which are used in conjunction with the structural properties as input in AutoSEA2 model. The AutoSEA2 model generates acoustical properties. These computed acoustical properties can be compared with the experimentally measured properties. The validation loop is used to compare measured and computed values of absorption coefficient and TL. Based upon the level of correlation a more appropriate acoustic property amongst the two is recommended for the acoustic method.

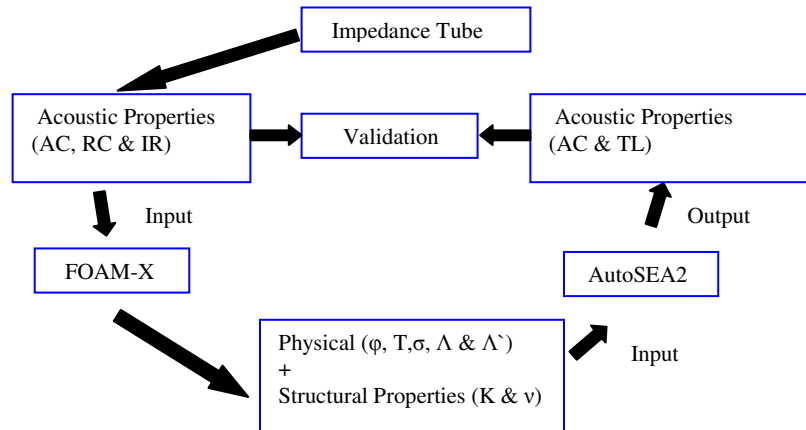


Figure 19. A closed–loop validation process

(AC: Absorption Coeff., RC: Reflection Coeff., IR: Impedance Ratio & TL: Transmission Loss)

4.2 Background and Proposed Model

4.2.1 Impedance Tube Method

In many noise control applications, the designer uses the absorption coefficient and/or transmission loss to quantify the ability of a material to reduce noise transmission. For all materials, these parameters vary as a function of frequency, and are dependent on various material physical properties such as airflow resistance, porosity, elasticity and density. Evaluating the acoustic properties of materials in terms of absorption coefficient has been explored in the literature [101-106]. Of these, several [101, 105–106] discuss the use of impedance tube method for evaluating various acoustic parameters. The impedance tube method has been widely used to evaluate the acoustic absorption coefficients of porous materials. Techniques have also been developed to evaluate the sound transmission loss characteristics of materials.

Impedance tube set up works on the principle that standing wave pattern can be created inside a tube with known diameter for a certain bandwidth. Two sizes of tubes are chosen to maximize the bandwidth covered, viz. 29 mm for range 500 Hz to 6.4 KHz and 100 mm for a range 50 Hz to 1500 Hz. The smaller tube measures higher frequency range as the smaller wavelengths are controlled in a more restricted diameter tube to enforce a standing wave pattern. If there is any wave progression in a direction other than parallel to the tube axis, then it would disturb the standing wave pattern. It is assumed that the tube walls do not aid in sound absorption. The wave progression for measurement should be normal to the sample surface and hence the measurement is termed as normal impedance. The microphones are placed in the tube at known distance from the speaker and with each other. The measured pressure levels from the

microphones can thus be correlated with their positions and acoustical properties of the porous medium be determined.

4.2.2 Proposed Model

The objective of creating a closed loop methodology is to validate all components of the acoustic property measurement/prediction system using SEA simulations. The normal incidence sound absorption coefficients are measured using the two-microphone transfer function method described in ISO 10534-2 [106] and ASTM E1050-98 [108], while the normal incidence sound transmission loss measurements are made using the B&K proprietary four-microphone transfer function method. Measurements for all materials of varying thicknesses and/or densities are made in the frequency range of 50 Hz to 6.4 kHz.

A database of the measured acoustic properties is constructed. The results obtained from direct measurements are then used with the commercially available software FOAM-X to characterize the acoustic parameters of the corresponding fibers and foams. The reverse calculation of physical properties is based upon a genetic search algorithm. These material physical properties include porosity, flow resistivity, tortuosity, as well as viscous and thermal lengths. The computed physical properties, in conjunction with the structural modulus data of foams, are used as input for AutoSEA2 to predict the absorption coefficients and transmission loss of the corresponding materials. If however, the porous material has low porosity (<80%), it is assumed to be rigid and structural modulus is not required. . Using AutoSEA2, the ASTM procedure is used to predict the acoustic properties of the corresponding materials. AutoSEA2 implements statistical energy analysis to predict the acoustic properties of materials based on the international standards [107, 108]. The output of acoustic properties from AutoSEA2 and the

results obtained from direct measurements using the impedance tube method are then compared in a plot displaying measured and computed acoustic properties in the frequency range of 50 Hz to 6.4 kHz for each individual material. The reverse calculated physical properties are validated if a close correlation between the measured and predicted acoustical properties is observed.

The schematic of an acoustic model in AutoSEA2 as per ASTM E90–02 [109] is illustrated in Figure 20. The ASTM standard specifies the use of two large rooms, one being the source room, and the other is a receiver room.

These rooms are separated by a concrete wall with an opening for sample placement. This is represented by a model consisting of two acoustic cavities of dimension $1 \times 1 \times 1 \text{ m}^3$ and a 1–mm thick steel panel. By creating area junctions between the steel panel and the adjacent acoustic cavities, the three subsystems sharing the common boundaries are connected and all of the appropriate wave fields that occur between the panel and the acoustic cavities will be accounted for in the transmission loss calculation.

The source room can be excited by applying an acoustic constraint which fixes the response of the system to a known level. A noise control treatment of known physical and elastic properties can be applied to the steel panel to predict the acoustic properties of the material. The damping between the panel and the acoustic cavities should be specified to account for the energy dissipation due to damping effects of the noise control treatment that occurs between the three subsystems.

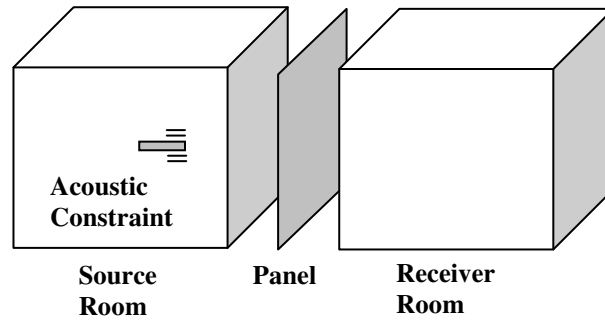


Figure 20. An acoustic model in AutoSEA2 based on ASTM E90-02

This model uses flow resistivity, porosity, tortuosity, thermal and viscous characteristic lengths as input for the noise control treatment's physical properties. If the noise control treatment is an elastic material like open cell foams, then additional mechanical properties i.e. bulk modulus and Poisson's ratio are also input in the model. These properties determine the acoustical characteristics of the porous medium. The analysis is run to get the outputs consisting of the absorption coefficient and TL as a function of frequency.

4.3 Experimental Methodology

The size and shape of test samples are critical for accurate measurements. Test sample should fit snugly into the sample holder. If the diameter of the sample exceeds the cross section of the impedance tube, the sample will bulge in the center.

This will cause the reflected wave from the uneven surface to not become a plane wave. On the other hand, if the sample is smaller than the cross section of the tube, leaks between the sample and tube walls, will affect the measured surface impedance and transmission loss. A minimum of two samples is needed so the results can be averaged to give a better estimate of the acoustic properties of the material.

4.3.1 Experimental Apparatus and Setup for Direct Measurements

The measurement system is composed of impedance tube set up, a B&K Type 2706 Power Amplifier, a Sound Level Calibrator Type 4231. The impedance tubes used in these measurements are the B&K impedance measurement tube type 4206. This 4206 system consisted of a 100–mm diameter tube, a 29–mm diameter tube, one sample holder and extension tube for each size, and two ¼–inch microphones type 4187 for acoustic absorption measurements. Impedance measurement tube type 4206T consists of two 100–mm diameter tubes, two 29–mm diameter tubes, one sample holder and extension tube for each size, and four ¼–inch microphones type 4187 for transmission loss measurements. Both tube types are assembled into two different setups: a large tube (or low frequency) setup to measure the parameters in the frequency range of 50 Hz to 1.6 kHz, and a small tube (or high frequency) setup for frequency range from 500 Hz to 6.4 kHz. The test samples used in these measurements are cut using water jet to conform to circular shapes of required diameter.

The impedance measurement tube types 4206 and 4206T setups are controlled by a personal computer and illustrated in Figures 21 and 22.

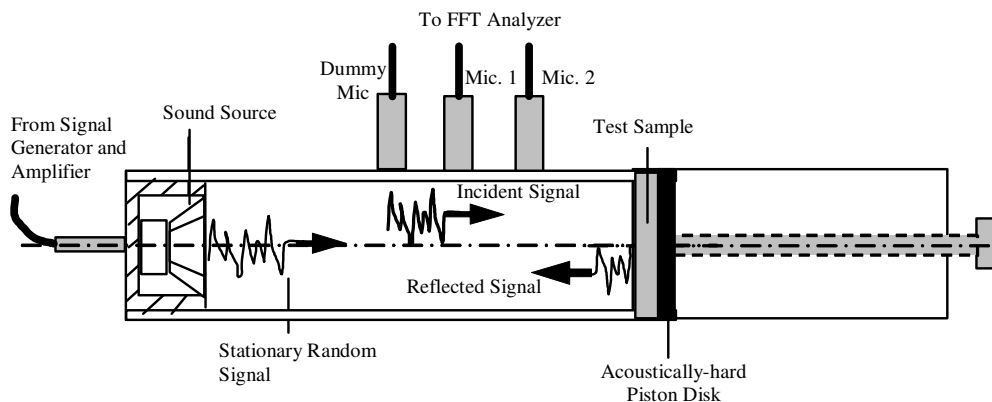


Figure 21. Setup for impedance tube for absorption coefficient measurements

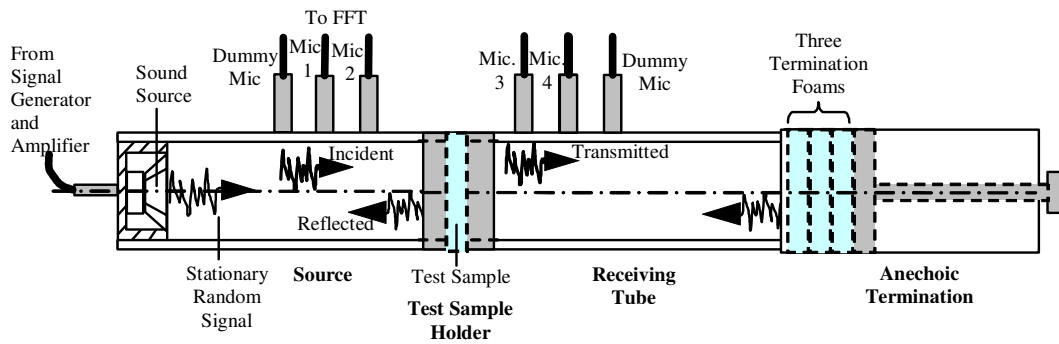


Figure 22. Setup for impedance measurement tube type 4206T for TL measurements

The front end of the multi-channel digital frequency analysis system is connected to the computer through a LAN cable. The input socket of the power amplifier is connected to the generator output of the analyzer using the BNC cable, while the output is connected to the signal input sockets of the loudspeaker on the back plate of the impedance tube. Depending on the measurement types, two or four ¼-inch microphones are placed on both sides of the test sample. The complete hardware setup for both large and small tube measurements is illustrated in Figure 23.

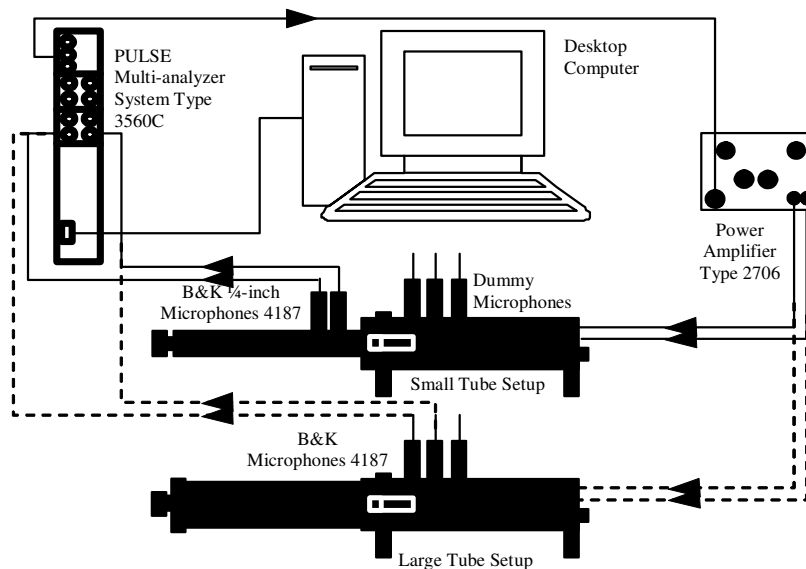


Figure 23. Schematic diagrams of large and small tube measurement systems

4.3.2 Validation Procedure

The test configuration for each material type and structural modulus data of foams are shown in Tables 5 and 6, respectively. Before making any measurements, the microphones, background noise and transfer function calibration are performed to ensure that the measurement results are not affected by phase or amplitude mismatch between the measurement channels. A random signal of varying frequencies is generated, which is then amplified before reaching the loudspeaker at one end of the impedance tube. The plane incident wave from the loudspeaker is partly reflected by the test sample, thereby creating a standing wave pattern in the tube due to the phase interference between the incident signal and the reflected signal. The analyzer measures the response of the microphones (placed on both sides of the test sample) in the frequency range of 50 Hz to 6.4 kHz.

The absorption coefficients and transmission loss are calculated based on the incident, reflected and transmitted components of the sound pressure at the microphone positions. Measurements are made for both faces of each test sample and are averaged to give a better estimate of the acoustic properties. The measured acoustic properties are then used with the commercially available software FOAM-X to compute the physical properties of each material. Based on these reverse calculated physical properties, the acoustic absorption coefficient and TL for each material are predicted using the AutoSEA2 model. The output from AutoSEA2 (the predicted acoustical properties) is compared with the measured acoustic properties from the impedance tube to validate the computed physical properties.

Table 5. Material test configuration

Material Type	Thickness (cm)	Density (Kg/m ³)	# of Small Samples for Each Configuration (29mm)	# of Large Samples for Each Configuration (100mm)
Polyimide Foam	0.635, 0.9525, 1.27, 2.54, 5.08	7.048	3	3
Melamine Foam	1.27, 2.286, 4.318	8.0097	1	1
Polyurethane Foam	4.318, 4.572, 5.08	8.0097	2	2
PVC Foam	0.635, 1.27, 2.54, 3.556	107.54	3	3
PVDF Foam	1.27	30.435	3	1
Fiberglass	0.635, .9525, 2.54	7.04, 8.009, 9.611, 19.22, 24.027	3	3

Table 6. Material elastic properties of foams

Material Type	Young's Modulus (N/m ²)		Loss Factor		Poisson's Ratio	
	Mean Value	Standard Deviation	Mean Value	Standard Deviation	Mean Value	Standard Deviation
Polyimide Foam	36378	790	0.096	0.034	0.458	0.003
Melamine Foam	91068	1668	0.078	0.024	0.430	0.005
Polyurethane Foam	51419	794	0.171	0.010	0.466	0.003
PVC Foam	535850	7148	0.517	0.004	0.425	0.029
PVDF Foam	538845	13511	0.237	0.004	0.182	0.028

The computed physical properties, in conjunction with the structural modulus data for foams are used as input for the AutoSEA2 model created as per ASTM E90–02 to predict the absorption coefficients and transmission loss of the corresponding materials. A noise control treatment of known physical and elastic properties is applied between the panel and adjacent

receiving room (see Figure 20) and the model is run twice: one having the panel with noise control treatment and the other without. The output of transmission loss in dB from the treated panel is then subtracted by the output from untreated panel to get the actual transmission loss of the material alone. Correlation between the measured and predicted results is developed by comparing the measured and computed acoustical property plots.

4.4 Discussion of Model Performance

Fiber and foam sample measurements as compared with the computed values are illustrated in Figures 24 through 27. Computed values of the physical properties for some of the fibers are displayed in Table 7.

It is to be noted here that to compute the physical properties of fibers, it is not required to measure the bulk modulus, loss factor and Poisson's ratio. This is because the fibers are considered as a limp material.

Table 7. Physical properties of fibrous materials

Material Trade Name	Thickness (in)	Density (pcf)	Porosity	Resistivity (Ns/m ⁴)	Tortuosity	Viscous Length (μ)	Thermal Length (μ)
Microlite AA (Standard)	0.375	0.42					
	1.000	0.42	0.9999	20447.83	1	42.387	84.77
	0.500	0.60					
	1.000	0.60	0.9157	50869.42	1	92.583	185.17
Microlite AA (Premium NR)	0.375	1.50	0.8287	159157.74	1	44.149	88.30
	0.375	1.20	0.7000	118751.04	1	34.927	69.85
MC-8-4591B	1.000	0.50	0.7554	63922.26	1	91.083	182.17
	0.500	5.80	0.8657	77088.26	1	28.074	56.15
			0.8209	93834.93	1	33.196	66.39

For absorption coefficient, all the fibrous and foam samples show very good correlation, as illustrated in Figures 24 and 25. However, slightly poorer correlation between the measured and computed transmission loss for both foams and fibers at low frequencies is observed, Figure 26. A close match at high frequencies is observed for fibers. For certain foam types, viz. ALC, APH & Foamex of thickness 1” or above, the correlation for TL is very poor, Figure 27.

Two reasons may have contributed to the poor correlation between the predicted and measured transmission loss. AutoSEA2 utilizes the statistical energy analysis method, which is mainly used to predict the high frequency noise and vibration response of complex structural–acoustic systems. At mid and high frequencies, each subsystem in the vibro–acoustic model is relatively large compared to the acoustic wavelength, and therefore tended to be extremely sensitive to small perturbations due to a modally dense system. Thus, the computed transmission loss compares well with the results obtained from direct measurements at mid and high frequencies.

However, at low frequencies, the subsystems in the SEA model are relatively small compared to the acoustic wavelength and contained relatively few modes per frequency band. The long wavelength behavior of such subsystems tends to be fairly insensitive to perturbations and therefore not particularly well defined by the method [110]. Hence large discrepancies are observed between the measured and predicted transmission loss at low frequencies for both foams and fibers.

The second reason for poor correlation can be attributed to the differences between B&K measurement method used for obtaining transmission loss vs. the predictive AutoSEA2 model based on ASTM E90–02 standard. The transmission loss tube setup has the test samples snugly fit into the tube, thus creating a very stiff simply supported boundary condition not necessarily

representative of the ASTM method. This boundary condition results in spurious resonances in the samples as observed in the peaks and dips occurring at low and mid frequencies in Figure 27. This is mostly noticed for the foams and much less for the fibers due to higher structural moduli of the former.

The close proximity of the sample boundary to the incident and transmitted acoustic waves in the B&K setup also exacerbates this problem. Thus, in summary, the small size of the samples, their fit and close proximity of the sample boundary to the incident and transmitted acoustic waves accounts for relatively poorer TL measurements.

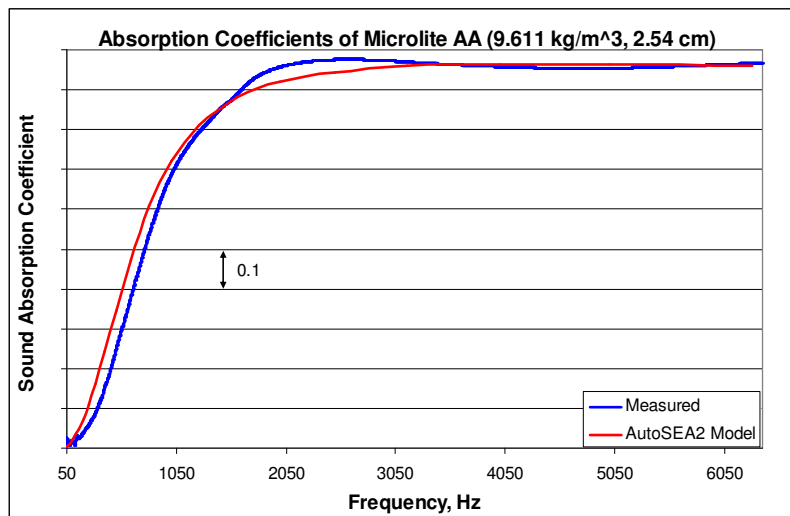


Figure 24. Comparison of predicted and measured absorption coefficients for 1–inch fiberglass

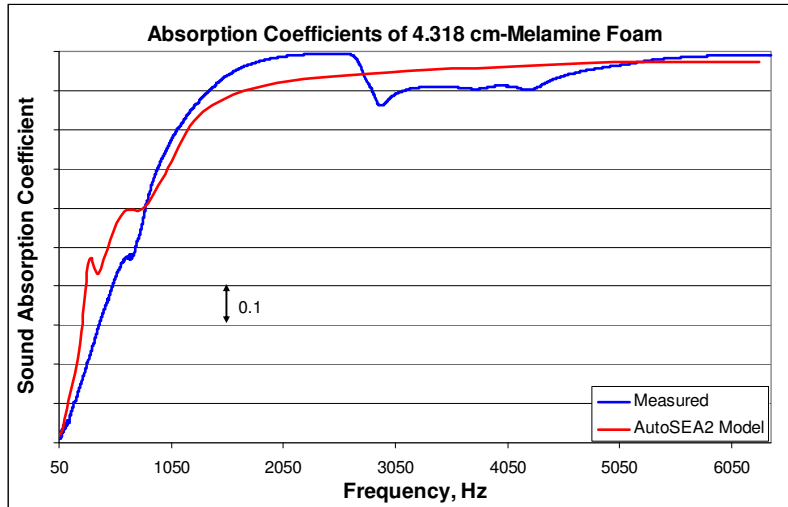


Figure 25. Comparison of predicted and measured absorption coefficients for 1.7-inch melamine foam

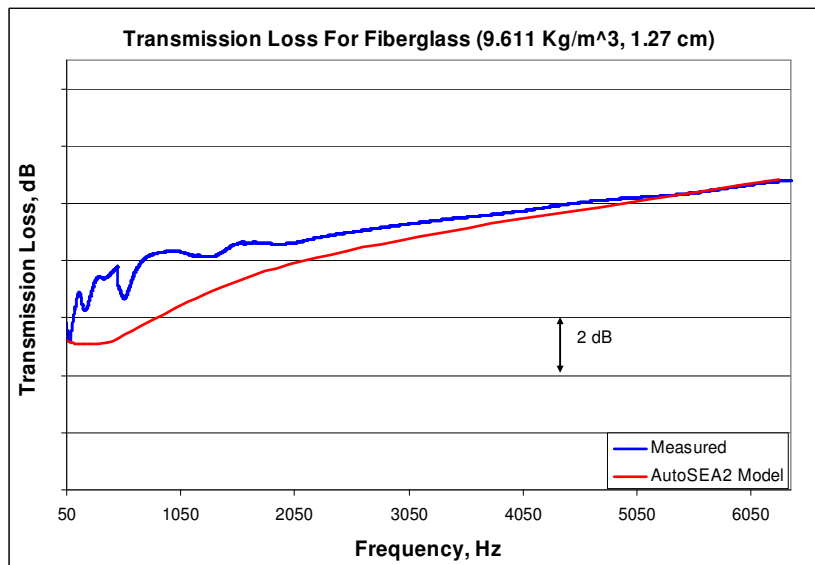


Figure 26. Comparison of predicted and measured TL for 1-inch fiberglass

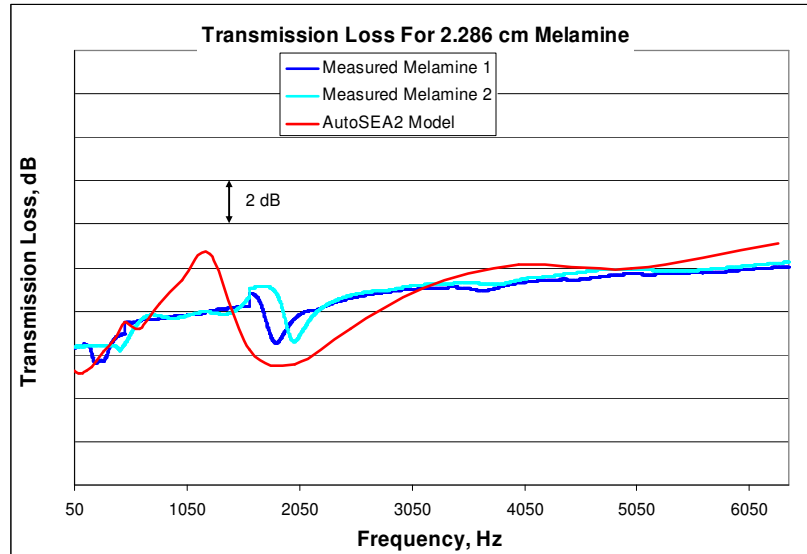


Figure 27. Comparison of predicted and measured transmission loss for 0.9–inch melamine foam

4.5 Conclusions

The objectives of this study are to propose and validate an acoustical method to determine physical properties of isotropic porous materials. Systematic measurements are conducted to determine the acoustic properties of some porous materials. A methodology to analytically validate the computed physical properties is developed. The comparisons between the computed and measured absorption coefficients of foams and fibers show very good correlation. However, when comparing the computed and measured transmission loss of each material, a close match is observed for fibers, but poor correlation is observed for most foam samples across a wide frequency range. The reverse calculation of physical properties from absorption coefficients using FOAM-X and the use of its output as input for AutoSEA2 has validated the methodology. Since the validation methodology shows excellent results for absorption coefficient

measurement, it is proposed to use this acoustical parameter for reverse calculation of material physical properties.

The analytical validation of the inversely calculated physical properties also needs to be reinforced by experimental measurement of the parameters. Of these five physical properties, porosity, tortuosity and flow resistivity can be measured if due technique is used. In order to have a complete validation of the predicted physical properties, the measured and predicted physical properties should be compared for some samples. The measured and predicted physical properties should be used in predicting the acoustical properties of interest for the tested porous samples.

CHAPTER 5
EXPERIMENTAL VALIDATION OF INVERSLY CALCULATED FLOW
RESISTIVITY

5.1 Introduction

All the physical properties affect the sound attenuation in a given medium as explained in previous chapter. The loss of sound energy occurs due to viscous losses, heat conduction losses and losses associated with molecular exchanges of energy. Depending upon the medium these losses can vary. For air at room temperature and atmospheric pressure, viscous losses are slightly more than twice that of heat conduction loss for acoustic energy dissipation. Consequently, these acoustical characteristics of a given medium can be expressed as a function of material physical properties. For a poro-elastic medium hence the characteristic impedance is a function of the physical properties given as,

$$Z_c = f(\phi, T, \sigma, \Lambda, \Lambda') \quad (45)$$

Where, Z_c is the characteristic impedance, ϕ is the porosity, T is tortuosity, σ is the flow resistivity, Λ and Λ' are the viscous and thermal characteristic lengths respectively.

In the previous chapter, measurement of impedance ratio, absorption coefficient and reflection coefficient by an impedance tube is explained. The measured impedance ratio along with absorption coefficient is utilized in reverse calculation of the physical properties. Reverse calculation of physical properties were validated analytically based on a SEA model for a reverberation and receiving room. This chapter details the experimental validation of the physical property of interest, viz. flow resistivity by the use of ASTM C 522 testing method. The experimental method of validation involves a direct correlation between the values of reverse

calculated flow resistivity and measured flow resistivity for a given sample and a comparison of the absorption coefficient based upon the measured and predicted physical properties. Since there are a total of five physical properties, measurement of as many properties helps in better prediction of the remaining ones by inverse technique. With this in mind, it is proposed to measure porosity, tortuosity and flow resistivity of five samples.

5.2 Experimental setup for Measuring Physical Properties

This section explains the methods of determining open porosity, tortuosity and effective flow resistivity. The equipment used for all 3 measurements is made by Mecanum Inc. and housed at Hawker Beechcraft Acoustics lab. The requirement of sample sizes is the same for all 3 measurements i.e. 100mm in diameter. It is desirable to have more than one sample to accurately capture the variation in measurements and hence have an average value. In this study 3 samples of each material type were measured.

5.2.1 Measurement of Porosity

Porosity is defined as the fraction of the interconnected air volume to the total volume of a porous material. In this measurement method solid phase volume of the porous material is sought to be determined.

The unit called PHI 2008 has a test chamber to place the samples, a connection for vacuum pump and a connection for compressed gas. The compressed gas used in this process is Argon which has a recommended pressure value of 88 psi. Initially the test chamber with the sample is maintained at vacuum pressure. The PHI 2008 is then fed with Argon which then supplies the gas to the test chamber. The final calculation of porosity is done by the software which takes into

account the mass of the samples in vacuum and the mass of the samples with infused Argon. Measurements are repeated for 3 samples and an average value is taken as the final result.

5.2.2 Measurement of Tortuosity

The tortuosity meter (TOR2008-1) is shown in the figure 28. It is used on all 5 material types. It consists of transmitters to transmit ultrasound pulses and receivers on the opposite side.

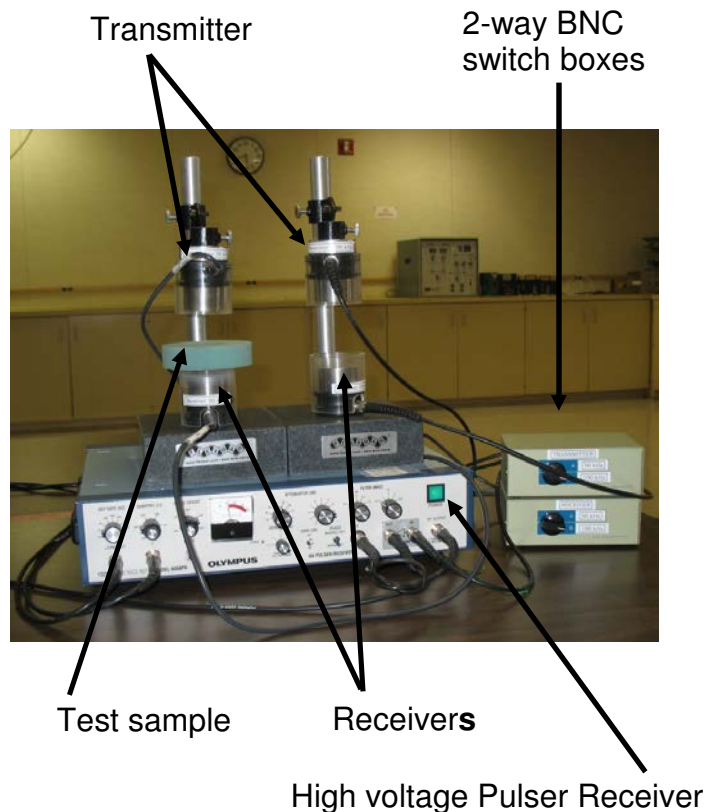


Figure 28. Tortuosity meter TOR 2008-1 (Courtesy Hawker Beechcraft Co.)

The samples are placed between the transmitter and receiver. A pair of ultrasound transducers which can measure for a frequency range up to 100 KHz each are placed at the transmitting side and receiving side. The pulser/receiver generates the ultrasound pulse of known frequency and receives the attenuated waveform. This attenuated waveform is refracted from the

sample and viewed in an oscilloscope. Since the acoustical refraction index of the material is linked to tortuosity, the readings from the Oscilloscope are processed through the software to yield the desired parameter.

5.2.3 Measurement of Flow Resistivity

The measurement of airflow resistivity requires samples to be cut in precise 100mm diameter and uniformity of the flow, boundary conditions (leaks or bulges) and the thickness of the specimen. For this reason all the samples measured for airflow resistivity are cut using water-jet. The equipment used for the measurement is the SIG2008 manufactured by Mecanum Inc. It contains a specimen holder of 100mm internal diameter, power supply and pressure regulator along with the readout displays for pressure. The unit is connected to an air compressor and the outlet takes the compressed air to the specimen holder. Measurement of volumetric flow rate and pressure drop across the test specimen gives the airflow resistivity. The sample thickness and surface area are input as known parameters in the software.

5.3 Measurement Results

Five materials chosen for the measurement are PHM and PHMUL from PTI Industries, AC550 and Soundcoat from Soundfoam Industries, and UAI Fiber Glass. These porous materials are commonly used for insulation. The first four materials chosen are open cell and are considered to have rigid frame. The 5th material fiberglass is considered limp. During measurement AC550 samples did not yield accurate results for flow resistivity due to bad surface finish of some of the samples. However the other 4 samples did not display any problems with finish or sizing. The results for the 4 material types are displayed in table 8.

Table 8. Measured physical properties (Courtesy HBC co.)

Material	Porosity	Flow Resistivity (rayls/m)	Tortuosity	Density (kg/m ³)
PTI PHM	0.96	9850	1.02	8.7
PTI PHM-UL	0.99	7390	1.01	5.7
UA1	0.99	34700	1.02	9.6
Soundcoat	0.99	34600	2.7	9.6

5.4 Comparison of measured results with analytically validated physical properties

These 5 samples measured for physical properties were also measured for absorption coefficient, impedance ratio and reflection coefficient using the impedance tube as detailed in the previous chapter. Using the acoustical properties measured by the impedance tube and the measured porosity and tortuosity, reverse calculations from FOAM-X for flow resistivity were carried out. The output from FOAM-X included flow resistivity, viscous and thermal characteristic lengths. The 2 measured and 3 predicted physical properties were then used to predict absorption coefficient as a function of frequency. Table 9 shows the comparison of measured and predicted flow resistivity.

Table 9. Comparison of measured and predicted flow resistivity values

Sample	Flow Resistivity (rayls/m)	
	Measured	Predicted
PHM	9850	9666
PHM UL1	7390	7834
UA1	34700	35505
Soundcoat	34600	31569

Figure 29 shows the close correlation between the measured and predicted flow resistivity values for these 4 materials. The accuracy of prediction is improved by input of 2 known physical properties from a total of five properties.

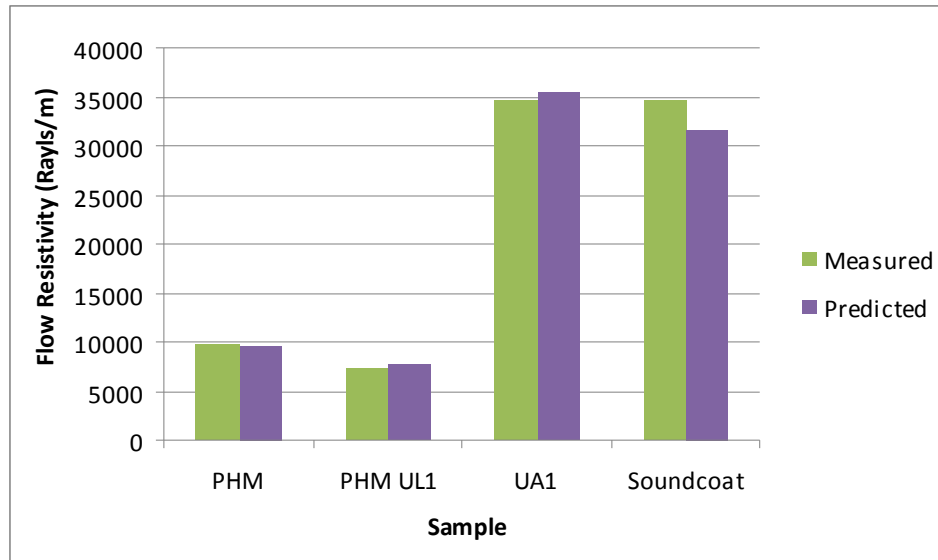


Figure 29. Bar chart of the predicted and measured flow resistivity values (ASTM C 522)

The confidence in the predicted values of airflow resistivity is increased when along with other physical properties; acoustical parameters can be reasonably predicted. The 2 measured physical properties (porosity and tortuosity) and the 3 predicted properties (airflow resistivity, thermal and viscous characteristic length) are used as input in the SEA model to predict absorption coefficient. The results of comparison between the directly measured and the predicted absorption coefficient curves of these 4 materials are displayed in figures 30-33.

It is observed that for open cell foams viz. PHM, PHM-UL and Soundcoat the predicted and measured acoustical property correlate well. However for UA1 fiberglass, the correlation is not as perfect at lower frequency range. This could be because acoustical properties of any porous material are not just dependent upon the flow resistivity but also on the viscous and thermal characteristic lengths. This leads to the conclusion that for this particular material the predicted values of viscous and thermal characteristic lengths are not very close to the actual values.

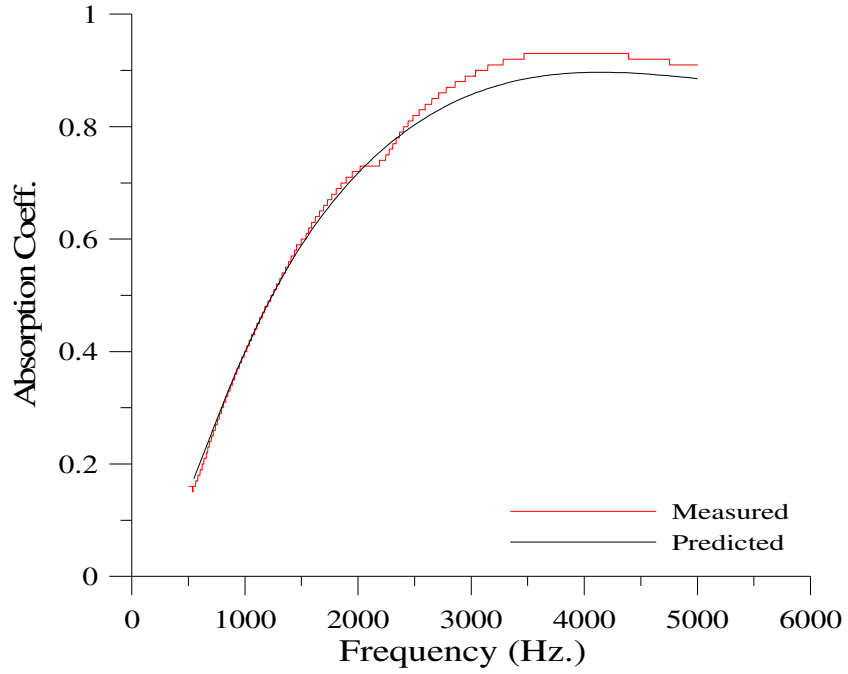


Figure 30: A comparison of measured and predicted absorption coefficient curves for PHM foam

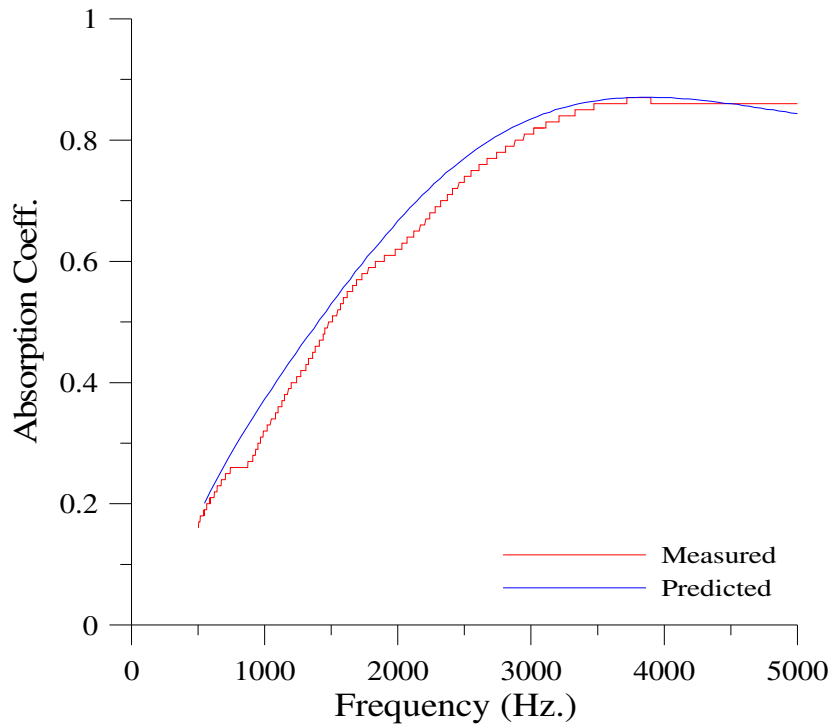


Figure 31: A comparison of measured and predicted absorption coefficient curves for PHM

ULfoam

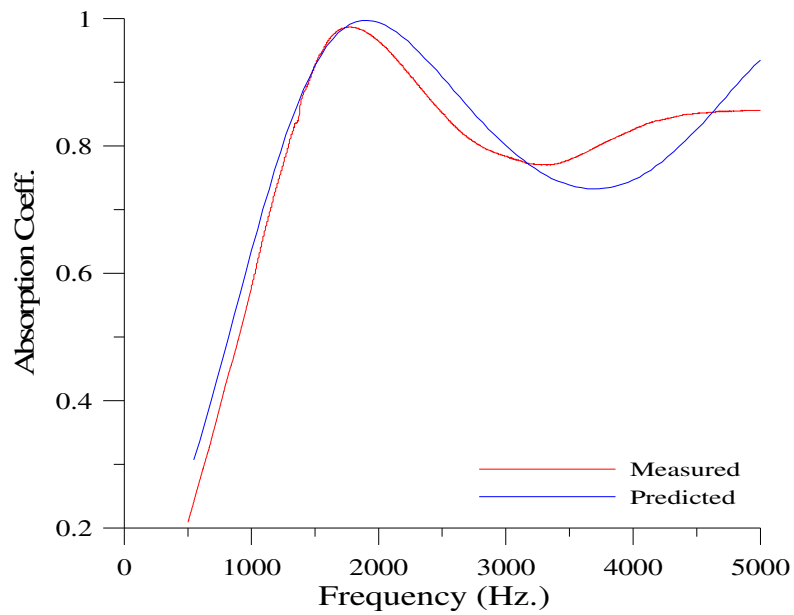


Figure 32: A comparison of measured and predicted absorption coefficient curves for Soundcoat

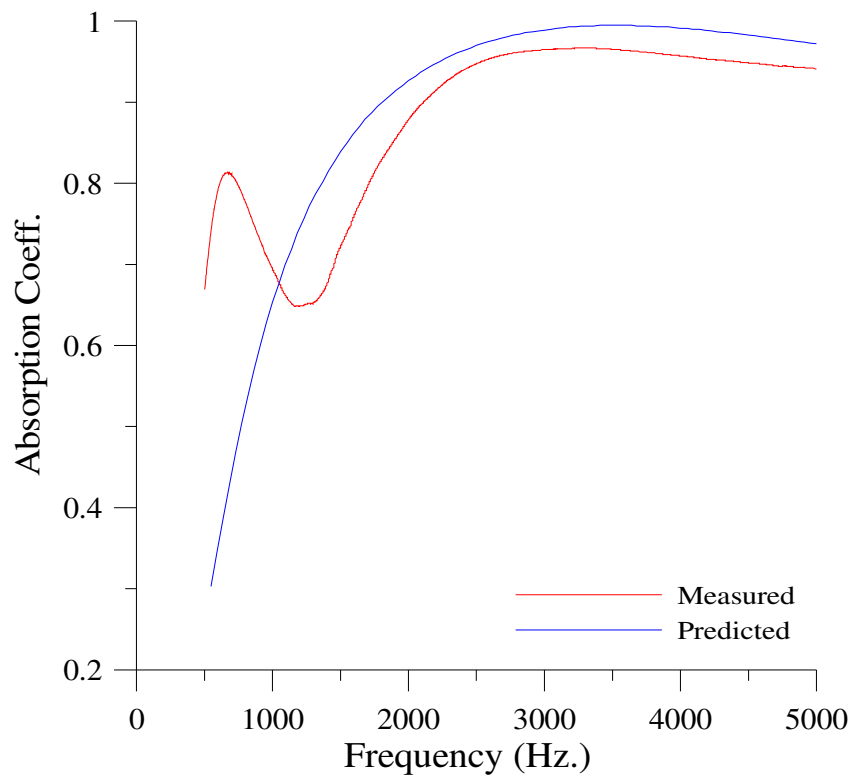


Figure 33: A comparison of measured and predicted absorption coefficient curves for UAI

CHAPTER 6

PREDICTION OF PERMEABILITY OF ORTHOTROPIC COMPOSITE FIBERS USING THE ACOUSTICAL METHOD

6.1. Introduction

The governing equations describing wave propagation in porous medium are well documented and used in many applications, Biot [111-113]. In particular the dependence of wave energy dissipation in porous medium on the same physical properties brings some interesting similarities between these two disparate natural phenomena. Johnson et al [114] relate the tortuosity and permeability as a function of high frequency of acoustic waves in fluid saturated porous media.

One of the ways to predict flow resistivity is to use characteristic impedance of a porous medium. Woodcock and Hodgson [115] compare methods of calculating effective flow resistivity from acoustical methods. Delaney-Bazely model [116] is used to predict effective flow resistivity from characteristic impedance and propagation constant of the material. Two ways of surface impedance measurement are compared with differing boundary conditions. These methods are two thickness and two cavity methods each of which requires two measurements for every sample. Estimation of characteristic impedance and wave numbers for limp and rigid frame porous materials is done using a two microphone transfer function method as detailed by Song and Bolton [117]. The approach is used to predict acoustical properties of homogeneous and isotropic porous materials. Atalla and Panneton [118] use an optimization technique to reverse calculate the material physical properties.

The inverse calculation is based upon the measured surface impedance of the porous material. A differential evolution algorithm is used for inverse characterization of the physical

properties assuming the medium to be an equivalent fluid. Sebaa et al. [119] propose an acoustic reflectivity method based upon reflected and transmitted wave pulses at very low frequency (0-100 Hz). Reflection and transmission scattering operators for porous material assumed to have rigid frame is derived for acoustic pulse. Flow resistivity is predicted from the reflection operator. For low frequency it is very difficult to determine flow resistivity and hence an inverse method based on least square error operator is utilized. The least square error function is based on the difference between experimentally observed and predicted pressure field from the reflected pulse. All the reverse calculation methods discussed above have not been validated using analytical tools.

As concluded in chapter three of this work, fiber preforms used in composites do not show a dual scale flow for VARTM process. A dual scale orthotropic medium would require intra tow and inter tow permeability distinct from each other for accurate characterization. For the same fiber preforms used in chapter three, the acoustical technique as explained below can be utilized for material characterization.

This chapter details the use of the acoustical method developed in the previous chapters to predict in-plane and out of plane permeability of orthotropic fibers. A comparison of the permeability of sized and unsized fibers for the same porosity measured using the acoustical technique is made. Results of permeability measured for sized and unsized fibers using channel flow methods are contrasted with the results from the acoustical method.

6.2.1 Experimental Constraints

Impedance tube shown in Figure 21 is used for standardized absorption coefficient measurement. Carbon and glass sample preparation is done in two ways. Orthotropic materials

need to be measured for longitudinal and transverse fiber directions. Therefore the samples are prepared with a) the fibers aligned along the axis of the tube to measure longitudinal acoustical properties and b) the fibers perpendicular to the tube axis. The number of tows of carbon fibers and glass fibers used in this study varies from 150 to 300. The tows are varied according to the desired Fiber Volume Fraction (FV) in the impedance tube. Larger number of tows would increase the FV.

In addition, two samples of glass and two samples of carbon fibers having different thickness but all other physical properties as the same are also measured. The two samples of different thicknesses measured have the same porosity, tortuosity, characteristic lengths and flow resistivity. These samples yield different absorption coefficient results when measured in the impedance tube due to their thicknesses. However these samples should result in similar reverse calculated physical properties. The purpose of two measurements of carbon fiber samples with different thickness is to ensure repeatability in reverse calculation of physical properties.

Carbon and glass samples are prepared for transverse measurement by cutting individual preform layers in a circular diameter of 29 mm. Measurement of permeability in the documented literature pertains to either carbon or glass fiber preforms. Industrial applications require a large usage of glass-carbon hybrid composite fibers. Two samples of glass and carbon hybrid preforms are also prepared in different proportions. Finally, carbon and glass samples are washed with acetone to remove the sizing. The samples are dried in the oven at 150° F for two hours. Some measurements of the unsized samples are taken to compare the permeability with the sized sample.

All the samples are cut from the fiber rolls as shown in Figure 34. The number of tows across the width of the roll is known. The desired FV is attained by rolling the fiber with known tows to make a cylindrical shape of diameter 29 mm as shown in Figure 35.



Figure 34. UD Glass fabric cut in 50.4 mm width strips to roll into samples with the desired tows.



Figure 35. UD Glass fiber strips rolled into 29 mm diameter sample for measurement in the Impedance tube

6.2.2 Proposed Comparison of Acoustical Method with the Flow Method

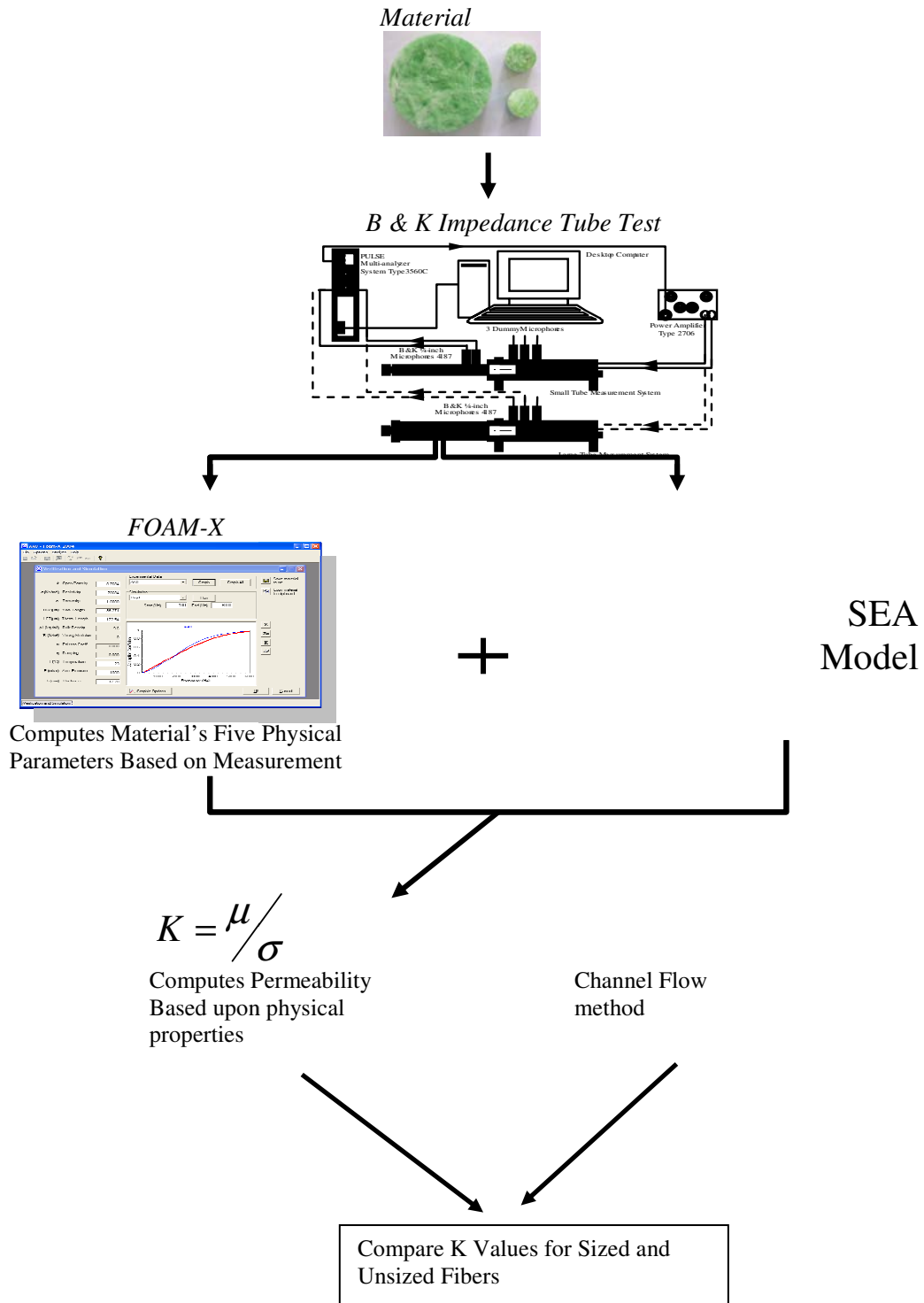


Figure 36. A comparison of acoustical method with the channel flow technique

Figure 36 displays the proposed acoustical method for permeability and its comparison with the commonly used channel flow method. The channel flow method can be substituted by radial flow or other techniques.

6.3 Validation Procedure

Before making any measurements, the microphones, background noise and transfer function calibration are performed to ensure that the measurement results are not affected by phase or amplitude mismatch between the measurement channels. A random signal of varying frequency is generated by a computer controlled noise generator, which is then amplified before reaching the loudspeaker at one end of the impedance tube. The sample is placed at the other end of the tube with a hard backing. The plane incident wave from the loudspeaker is partly reflected by the test sample, thereby creating a standing wave pattern in the tube due to the phase interference between the incident signal and the reflected signal. The analyzer measures the response of the microphones placed on both sides of the test sample in the frequency range of 500 Hz to 6.4 kHz. The absorption coefficient is calculated based on the incident and reflected components of the sound pressure at the microphone positions.

Fifteen samples of carbon, glass and hybrid (glass and carbon) lay ups of varying FV are measured for absorption coefficient. Since the reverse calculation is based on a search algorithm, if one or more of these physical properties are known a priori then confidence in the prediction is improved. For orthotropic fiber preforms that are unidirectional in nature, tortuosity is assumed to have a value of one. Porosity is calculated by the number of fiber tows inside the impedance tube of known diameter. After the reverse calculation of physical properties, sensitivity analysis is carried out to vary the physical parameters without affecting the absorption coefficient. The

final values of physical properties reported in Table 10 are based upon the completed sensitivity analysis performed using FOAM-X. There are three models of reverse calculation that can be used to predict the physical properties. The applicability of these models depends upon the nature of the porous medium. For stitch bonded or woven fibers commonly used in composite manufacturing, the frame is considered limp.

Permeability is related to flow resistivity by,

$$K = \frac{\mu}{\sigma} \quad (46)$$

Where K is the permeability, μ is the viscosity and σ is the flow resistivity of the porous medium. Determining the flow resistivity by the acoustical method and using Equation 46 yields permeability of the preform.

6.4 Acoustical Methodology Results

The objectives of this study are to propose and validate an acoustical method to determine the permeability of orthotropic fiber preforms. A methodology to validate the computed physical properties is developed. The comparisons between the computed and measured absorption coefficients of fibers show very good correlation. The reverse calculation of physical properties from absorption coefficients using FOAM-X and the use of its output as input for AutoSEA2 has validated the methodology.

The principal motivation for the development of acoustical method is the observed variability of permeability for a given fiber preform when measured using different flow methods. It is also well documented that the permeability values differ for the same fiber preform

when different fluids are used for infusion. However, permeability as a material physical property should not change with the use of different test fluids.

Since the dimensions of permeability are L^2 and it represents the cross sectional area available for flow, the presence or absence of sizing should not affect this property for a given porosity. The use of different types of fluids in the porous medium also cannot alter the available cross sectional area for flow. Results from the validated acoustical method are displayed in Table 10. It shows the longitudinal permeability values for carbon and glass fibers that are sized and unsized for a variety of FV values. For the same porosity value, the sized and unsized carbon and glass fibers display permeability values that are fairly close to each other. The maximum difference between these values is about 5%. These results are validated as displayed in Figures 37-40 by comparing their measured and predicted absorption coefficient curves. These experimental results are repeatable as they are based on standardized measurement procedures.

Transverse permeability of glass fibers is easily measured using the acoustical technique. It requires samples of fiber performs to be cut in circular discs and stacking them together to the required thickness. Transverse permeability results are reported for unidirectional Glass fibers with 8 plies as mentioned in the last row of Table 10. Glass-Carbon hybrid preform samples are measured for longitudinal permeability as displayed in Table 10. The proportion of glass fibers is increased while keeping the carbon fiber quantity as the same in this example. Some more plots comparing the measured and predicted absorption coefficient curves for different porosity values are displayed in Appendix B.

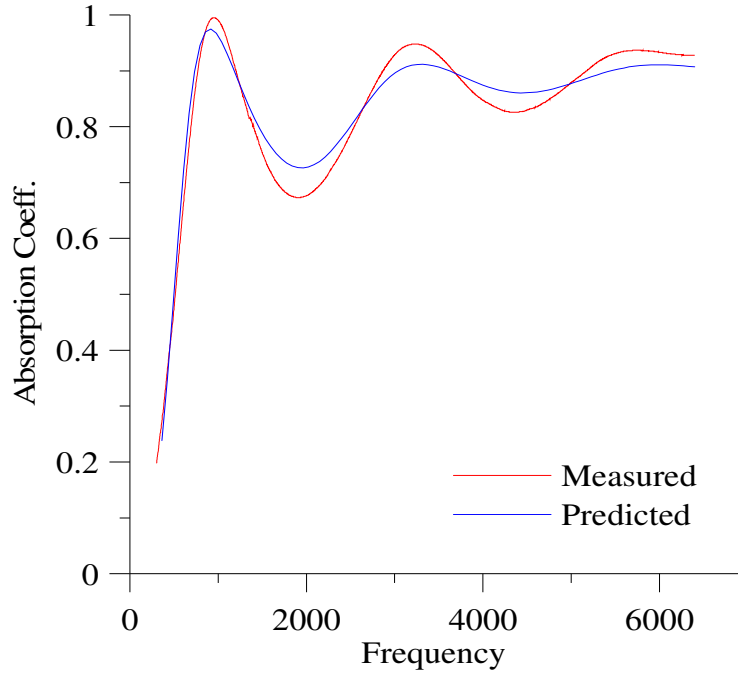


Figure 37. UD Carbon 135 tows sized- Comparison of measured and predicted absorption coefficient curves based on the computed physical properties

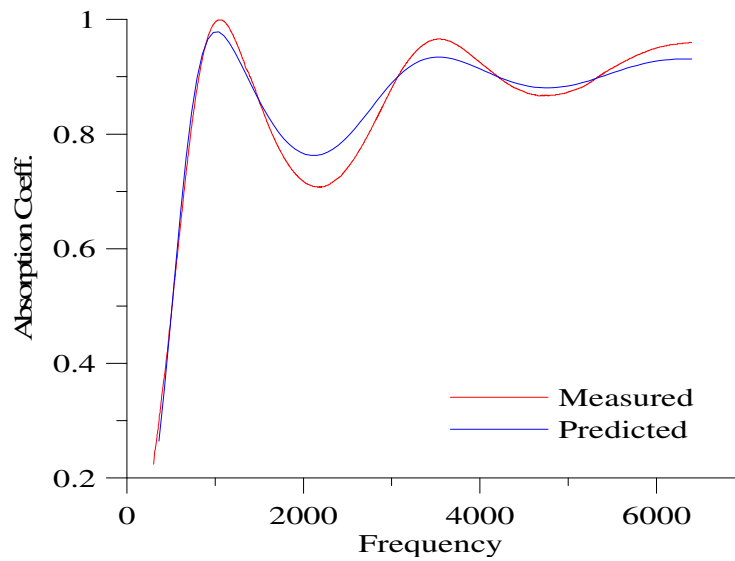


Figure 38. UD Carbon 135 tows Unsized- Comparison of measured and predicted absorption coefficient curves based on the computed physical properties

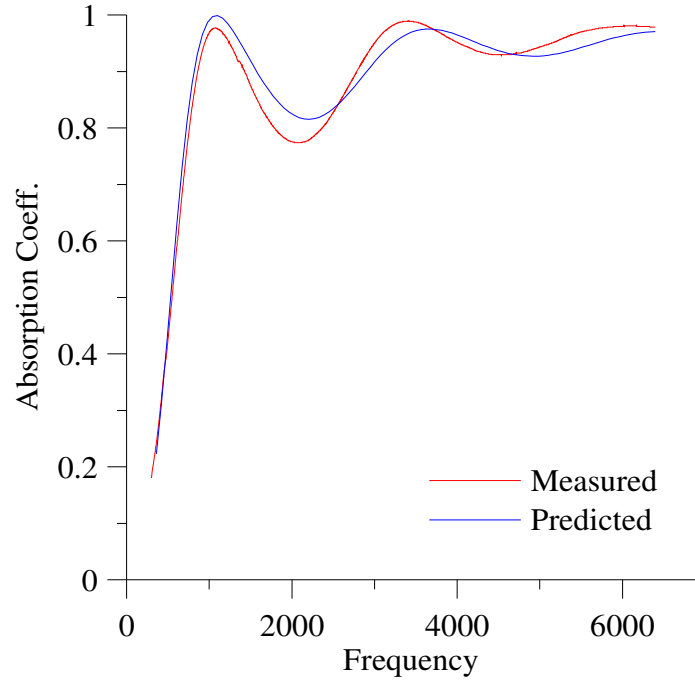


Figure 39. UD Glass 200 tows Sized- Comparison of measured and predicted absorption coefficient curves based on the computed physical properties

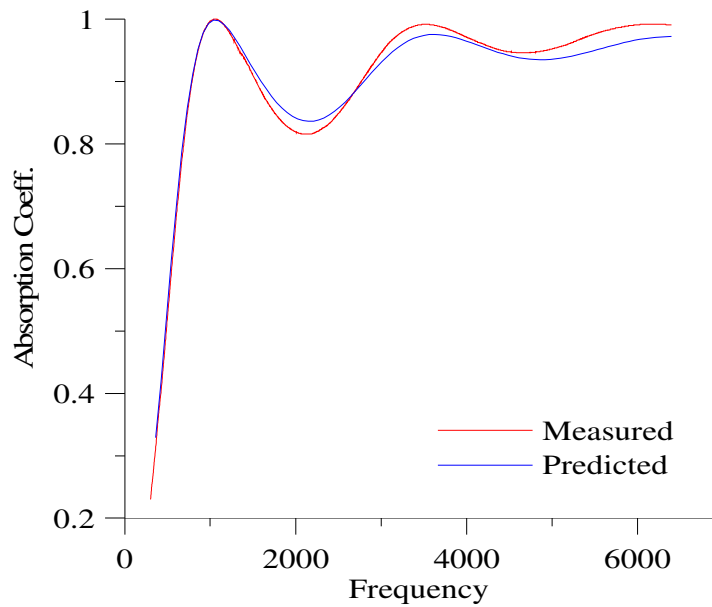


Figure 40. UD Glass 200 tows Unsized- Comparison of measured and predicted absorption coefficient curves based on the computed physical properties

The reported values for flow resistivity should be considered with a standard deviation of $\pm 5\%$. This deviation occurs as the upper and lower bound values do not show significant change in its correlation to the predicted absorption coefficient.

Table 10. Physical Properties of Orthotropic Fiber Preforms

Sample	Bulk density Kg/m³	FV %	Resistivity N s/m²	Permeability Darcy	Viscous L µm	Thermal L µm
UDC 185	465.61	0.26	154329	564.4	3	215.3
UDC160-1IN	402.69	0.22	15000	5807.3	13	256.5
UDC160- 2IN	402.69	0.22	15365	5669.4	18	265
UDC 135 W	339.77	0.19	10000	8711.0	28.6	3000
UDC135	339.77	0.19	10372	8398.6	33.9	814.8
UDG300-1IN-1	160.13	0.06	8039	10835.9	18.4	485.7
UDG300-1IN-2	160.13	0.06	8146	10693.6	18.9	487
UDG300-2IN	160.13	0.06	8129	10715.9	18	397.6
UDG250	133.44	0.05	6957	12521.2	24.4	749.1
UDG200	106.76	0.05	5980	14566.9	35.5	3000
UDG200-W	106.76	0.04	6056	14384.0	29	488.9
C50+G150	253.62	0.10	15981	5450.8	26.6	488.9
C50+G100	224.62	0.09	11754	7411.1	34.2	1172.5
UDG8PLIES- 90DEG	243.50	0.25	84342	1032.8	3	286.7

W- washed or unsized fibers, UDC 135- Unidirectional carbon 135 tows, C50+G100- Hybrid layup, Carbon 50 tows and Glass 100 tows, UDG 8 PLIES-90DEG – Unidirectional Glass 8 plies measured for transverse permeability.

6.5 A Comparison of Acoustical vs. Existing Methods

Various methods and associated models of measuring permeability have been discussed in the second chapter. Relationship between permeability and porosity based upon predictive models and observed experimental values from previous studies are shown in Figure 41 [120]. The figure shows a significant variation between various models. It is also worth noting that the measured permeability as compared with the best model differs by a factor of four to five. But of

these models, the prediction of Young’s model compares best with the observed permeability vs. porosity results. Young’s model is derived from a curve fitting equation extrapolated from the measured permeability vs. porosity plot.

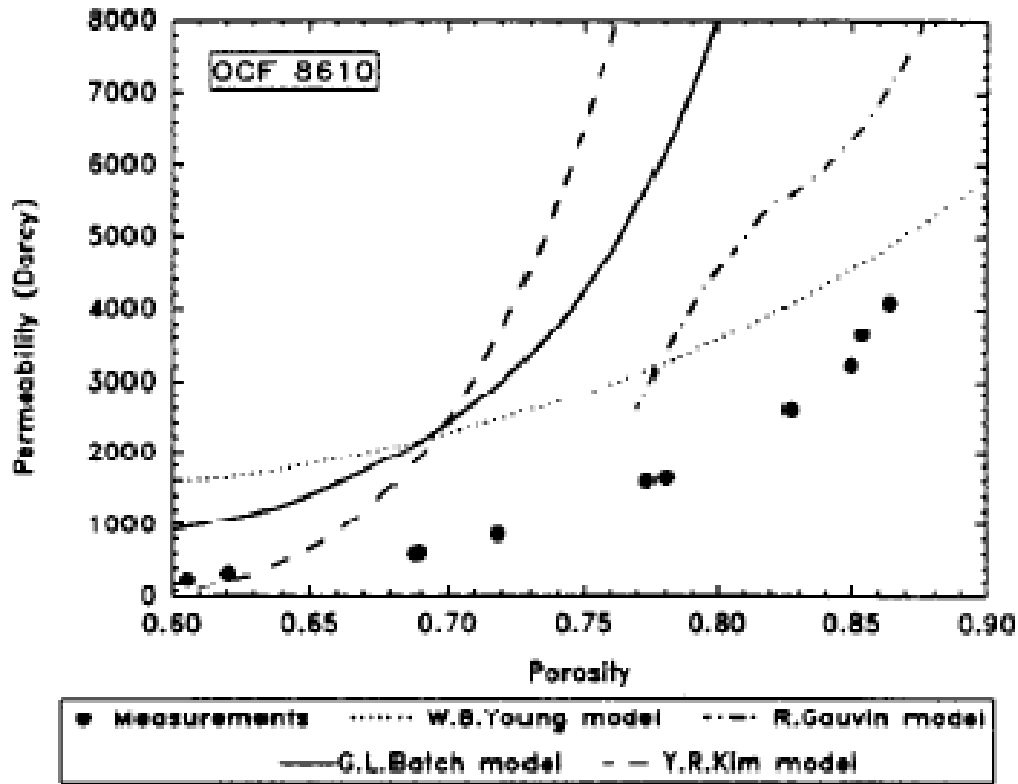


Figure 41. Various models for permeability vs. porosity relationship [120]

We consider Young’s model along with three of the most commonly used predictive models for comparison with the acoustical method. The reason for choosing this model over others is due to the observed similar trend between measured and predicted values as shown in Figure 41. The predictive models considered for comparison are the Kozeny model and Gebart model for square and hexagonal fiber arrangement. All the models considered here for comparison are discussed in section 2.1.5 of this work.

Figure 42 and 43 display the comparison of permeability vs. porosity derived from Young's model, Channel flow employed in chapter three, Kozeny model and Gebart's method. Non dimensional permeability is compared for glass fibers in Figure 42. At the porosity for which glass fibers are measured, excellent correlation with Young's model is found. At the same time, Kozeny's and Gebart's models are found to be under predictive for permeability. Since Kozeny and Gebart models are based on the assumption of a regular arrangement of fibers, they ignore the large gaps between tows that enhance permeability.

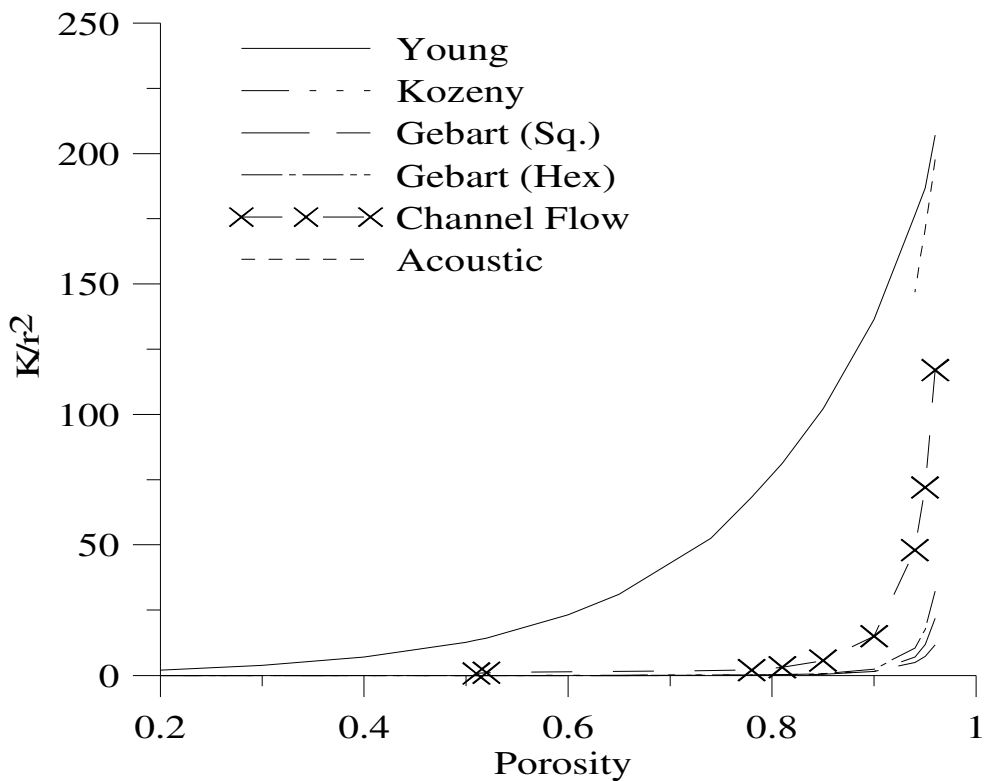


Figure 42. A comparison of permeability measured by acoustical method with existing models and methods for glass fibers (r is the fiber diameter).

Although only two values of permeability for channel flow are available, a trend based on a simple scaling factor between the Kozeny model and the channel flow results is employed to

extrapolate the trend in Figure 42. The measured values of channel flow permeability lie between the predictive models' permeability and that of the Young's model. The details of the data used in these figures are shown in Appendix C.

Figure 43 displays the permeability comparison between various methods/models for carbon fibers. For the values of porosity at which permeability is measured, a good correlation between the acoustical method and Young's model is seen. However there is a sharper drop in permeability with respect to porosity for the acoustical method.

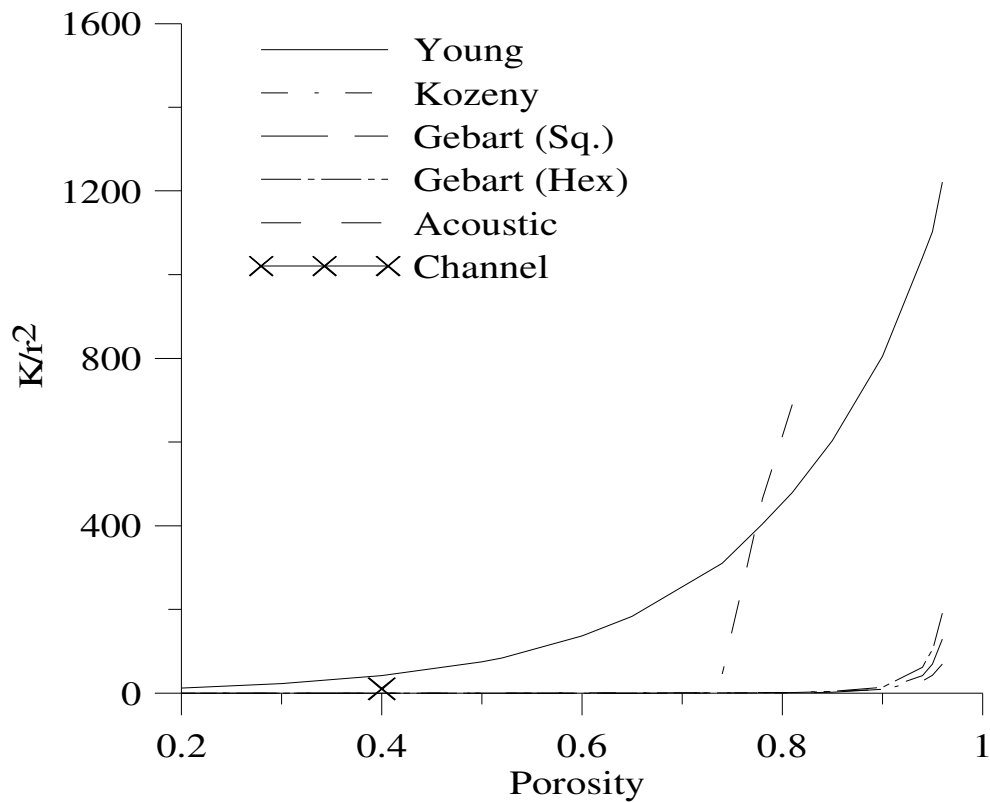


Figure 43. A comparison of permeability measured by acoustical method with existing models and methods for carbon fibers (r is the fiber diameter).

Reasons for this observed sharper drop could be due to the type of carbon fiber employed in this study. It has been observed earlier that fiber architecture could significantly impact the

permeability [70]. The carbon fibers used in this study have flatter tows that ease nesting and close the intra tow gaps. Owing to this, perhaps there is a sharper drop in permeability with a decrease in porosity.

Permeability values obtained from the channel flow method for the same sized and unsized glass and carbon fibers are shown in Figures 12-13. Significant variability in permeability values is observed when different test fluids are used. Permeability values for the same fluid fiber system changes significantly due to the presence or absence of sizing. The prevailing understanding for this variability has been explained on the basis of fluid-sizing interaction.

Palmese and Karbhari [73] have explained this variation on the basis of work of spreading the fluid on the fiber surface. A change in dynamic contact angle between the fiber and fluid is ascribed to the corresponding change in surface morphology of fibers due to the absence of sizing. Steenkamer et al. [71] observe and report permeability variations due to the different test fluids used.

6.6 Some Observations on Permeability Measurement and Modeling

From the standpoint of flow simulation using Darcy's law, variation in permeability values and/or variations in flow behavior due to different fluids pose a problem in composite manufacturing. Since Darcy's law is used to measure permeability and model flow behavior as well, a complete explanation of this observed discrepancy cannot be satisfactorily given by measurement techniques that utilize the same model. This is in contrast to the results obtained from the validated acoustical method which predicts nearly the same value of permeability for sized and unsized fibers. Interestingly however, the sized and unsized fiber samples of the same

porosity display different viscous and thermal characteristic lengths. The acoustic energy dissipation is shown to be dependent upon the five physical properties.

While the flow resistivity remains the same for sized and unsized fibers, viscous and thermal characteristic lengths change. For the glass and carbon fibers measured in this study, unsized fibers display smaller viscous characteristic lengths as compared with the sized fibers (Table 10, UDC 135W/ UDC135 and UDG 200W/UDG 200). A visual inspection of the unsized fibers show the fibers clumped together as compared with their sized counterparts.

The flow behavior in the same medium when explained using Darcy's law considers permeability as the only material parameter affecting it. The changes due to sizing and fluids cause an unexplained alteration in flow behavior based upon the existing flow equations in porous media.

Based on the comparison of acoustical and flow measurement methods of permeability, it is recommended that a more rigorous flow model that accounts for other porous material physical properties be developed in order to better characterize the observed differences in flow behavior. Darcy permeability, it is observed, includes unknown parameters that affect the flow behavior in the porous media. Darcy's empirical relationship developed for sand with random porosity and tortuosity with water as the test fluid may not be adequate to describe flow through highly ordered porous and tortuous orthotropic medium. The alterations in the thickness of viscous boundary layer due to changes between fiber surface and fluid and its subsequent impact on the effective area available for flow can perhaps be explained by the viscous characteristic length. Acoustic energy dissipation due to the interaction between fluid and structure in the micro pores is well explained on the basis of viscous characteristic length. A similar relationship

for the loss of momentum of fluid through the porous medium may provide a more complete explanation of the observed discrepancies in the flow based experiments.

As the FV in fiber preform increases, the pore sizes reduce. The reduction on pore size has a more pronounced effect on viscous characteristic length and hence the variability in permeability values measured by flow based methods increase.

It is recommended that direct measurement of viscous characteristic length of composite fiber preforms saturated by different types of fluids should be compared.

6.7 Conclusion

A validated acoustical method based on standardized measurement of absorption coefficient using impedance tube has been developed to predict longitudinal and transverse permeability of orthotropic fiber preforms. The acoustical method is easy to use and quicker than the flow based methods. Permeability values obtained for sized and unsized fibers by the acoustical method are nearly the same. However variability in the permeability values is observed when different types of fluids are used in the channel flow method. The observed variability in flow based methods in contrast to the close similarities of permeability values using the acoustical method are explained on the basis of characteristic length.

This method based on impedance tube cannot be applied to soil or rock samples as the signal to noise ratio in measurements will exceed the limit. Further, samples that are higher than 50-55% in FV will be difficult to fit inside the tube unless a method is developed to prepare the samples for such a purpose. Hence this method is limited to measuring porous samples of less than 50 % in FV.

CHAPTER 7

CONCLUSION & RECOMMENDATION

7.1 Summary of Work

The objectives of this study were to a) Survey the existing permeability measurement methods and their associated equations, b) Determine the fluid-sizing interaction resulting in variation in permeability, c) Study the dual scale flow behavior in orthotropic fibers, d) Develop an acoustical methodology of predicting material physical properties, and e) Predict permeability for orthotropic fibers using the validated methodology. The existing methods of permeability modeling and measurement are incapable of accounting for the variations induced due to: a) Type of flow i.e. channel flow vs. radial flow, b) type of sizing on the fiber, c) type of fluid used in the experiment, d) non-linear pressure profile during flow, and e) lack of agreement with predictive permeability methods. These factors have resulted in a lack of agreed upon permeability measurement method for composite fibers. As reported by Tan and Pillai [121], an estimate of measurement accuracy without knowing the absolute permeability of fibers is reported between $\pm 20\%$ to $\pm 50\%$ depending upon the type of fiber preform.

For the channel flow method, the variability in permeability is examined by changing the fluid in the experiment. Researchers in the past have shown that this permeability variation occurs due to the nature of fluid and its interaction with the fiber sizing. But to separate the effect of fluid – sizing interaction no studies had been carried out that used two fluids of the same viscosity but different chemical composition. Existing understanding of this variability based upon fluid-sizing interaction is challenged in this work. Research in the past has shown dual scale flow regime in orthotropic fibers that has necessitated the use of sink term in the continuity

equation. But the the previous studies were carried out for a FV up to 30%. This work studies the dual scale flow behavior for FV from 47% (for glass fibers) to 60% (for carbon fibers). The results from this work challenge the applicability of the dual scale flow modeling practice for the entire range of FV. Further a novel acoustical method of predicting permeability is detailed in this work that uses impedance tube for measurements. A comparison of results from the acoustical method and other established techniques agree well. The acoustical method shows promise in determining not just permeability but viscous characteristic length of the porous media that is a potential future scope for investigation.

7.2 Conclusions

A lack of accuracy and inability to determine absolute benchmark permeability values for a given preform poses questions on the adequacy of a simplified empirical equation's application to the various flow based experiments. Darcy's law shows excellent correlation for soil and rock materials from which it is derived. However, alterations in flow behavior due to changes in sizing, fluids and experimental set up are not understood on the basis of Darcy's equation as amply demonstrated by a wide range of investigations reported in the literature review. Various types of RVE's based upon the porous material architecture as modeled by Du Pleisses and Diedricks [2] have shown better results in soil and rock samples. A similar approach in composite preforms for different fiber preforms viz. unidirectional, woven, braided biaxial etc. along with surface characteristics of these preforms if included in the governing equation may perhaps narrow our understanding.

7.3 Original Contribution to Literature

7.3.1 Effects of Sizing on Permeability:

This study has investigated a previously reported behavior of permeability variation due to fluid-sizing interaction. The established theory on the observed permeability variation due to changes in fluids or sizing is explained by eq. (37). The investigations had concluded that due to an interaction between type of fluid and surface characteristics of the fiber, flow behavior and hence permeability is altered. But none of these studies were conducted by using two or more fluids with the same viscosity to sort out any fluid sizing interaction. In this work, all permeability values for various fiber preforms have been determined using two dissimilar fluids with the same viscosity. It is observed that the permeability values remain unaltered when two fluids of the same viscosity are used in the experiments. This challenges the theory of fluid sizing interaction reported by earlier investigations.

7.3.2 Dual Scale vs. Single Scale Flow for VARTM:

In the last fifteen years, dual scale flow modeling has been increasingly used to explain saturated flow behavior in composite preforms. Dual scale flow modeling is based on the observed phenomenon of two distinct regimes of flow in fiber preforms. The faster and larger flow between the tow gaps is labeled as macro flow, while the slower and smaller flow inside the tows or micro pores is referred to as micro flow. Micro flow, it has been shown by various investigations, lags behind the macro flow. Post saturation, when the fluid is collected and cumulatively weighed with respect to time, the macro and micro flow regimes are easily discerned on the basis of this plot. This cumulative weight vs. time plot shows a rapid regime followed by a transient regime and then a linear region showing the eventual slowdown of the

fluid output from the porous medium due to a delayed impregnation of the intra-tow region. This delayed impregnation and loss of the observed flow rate has been accounted for by the introduction of sink term in the continuity equation. In this work, the existing dual scale modeling practice of using a sink term in the continuity equation based upon dual scale flow is shown to be incorrect for higher FV in both glass and carbon performs. Previous studies that had proposed and introduced the sink term had conducted experiments for a FV of less than 30%. It is recommended that studies be conducted to determine the transition of flow behavior as a function of FV. These studies should be focused on finding out the threshold FV, for which the flow behavior changes from dual scale to single scale. This could lead to further improvements in the modeling practices for composites manufacturing.

7.3.3 Acoustical Method of Permeability:

Having reviewed and investigated permeability measurement techniques based on channel or radial flow method, this study has undertaken to develop an acoustical method that has well developed equations. The dissipation of acoustical waves based upon Biot's equations is dependent upon, porosity, tortuosity, flow resistivity, thermal and viscous characteristic lengths. This common dependence of energy dissipation during flow or wave propagation in porous media is utilized in determining the physical properties accurately. Since Darcy's equation does not contain parameters for the physical properties except for permeability as mentioned above, the estimation or prediction of these parameters based on flow experiments becomes difficult and ambiguous.

As acoustical properties of porous medium depend upon the physical properties, this work undertakes a reverse calculation of the same. An SEA model built upon ASTM E 90

standard uses these physical properties as input in the model to predict the acoustical properties. If the measured and predicted acoustical properties correlate well, then the physical properties are analytically validated. With this procedure in place, isotropic porous materials are measured for acoustical properties and their physical properties calculated. The predicted acoustical properties based on the physical properties show excellent correlation for absorption coefficient. After analytically validating the reverse calculation of physical properties, this investigation also included actual measurements of three physical properties viz. porosity, tortuosity and flow resistivity. The measured flow resistivities of four selected isotropic porous media are compared with the predicted values from the reverse calculation methodology. A good agreement within the bounds of experimental accuracy is found for these five samples, validating the reverse calculation experimentally as well.

A good correlation between analytically validated results and experimentally validated results for these four samples is also observed indicating that the analytically validated results can be used to predict flow resistivity of porous materials. The prediction of flow resistivity when two of the physical properties are known (porosity and tortuosity), as is the case with orthotropic porous media like fiber composites, is closer to the experimental value. Results obtained from the acoustical method are compared with Young's model and some predictive models as well. For the FV studied in the acoustics methodology, a good correlation with Young's model is observed. A similarity in the general trend of the acoustics based permeability as a function of porosity enhances confidence in this technique. Glass fibers show a better correlation as opposed to carbon fibers. This could be due to the differences in fiber architecture.

The acoustical method developed to predict permeability shows little variability when measuring sized or unsized fibers. Since the cross section area available for flow in sized and

unsized fibers remains the same, the acoustical methodology is deemed better suited for permeability measurement. However, for flow modeling purposes, the lack of differentiation in sized and unsized permeability values may not be helpful in predicting fluid flow fronts. The viscous and thermal characteristic length of the unidirectional carbon (UDC 135) and unidirectional glass (UDG 200) sized and unsized fibers are different as determined from the acoustical method. Viscous characteristic length indicates the ratio of surface area to the volume of pores available for the interaction between the viscous skin and the surrounding fluid. The presence or absence of sizing affects the thickness of the viscous skin or the viscous boundary layer. The thickness of the viscous skin and the viscous characteristic length together contribute to apparent changes in the micro pore cross section area through which the flow takes place. If the viscous skin thickness increases, it reduces the available area for flow thereby slowing down the flow rate and hence affecting the permeability value. Conversely, a reduced viscous skin thickness for the same viscous characteristic length may enhance the flow rate giving a false impression of the increase in permeability value for the medium.

The results in chapter three discussed the changes in permeability values due to the absence of sizing. It was attributed due to the observed sticking together of the tows once the sizing is removed. In light of the definition of the viscous characteristic length, the same unsized fiber tows when clumped together alter the micro pore surface to volume ratio as compared to the sized fibers. This perhaps could be a better explanation for the observed variability in permeability values. Viscous characteristic length will vary with respect to the compaction pressure and the type of fiber surface. Viscous skin thickness is dependent upon the nature of fiber surface and the saturating fluid. Knowing and evaluating these additional parameters would hopefully characterize the porous media better and aid in better modeling practices.

7.4 Recommendations for Future Work:

The vast literature devoted to characterizing permeability of fiber preforms has used myriad methods with associated models. In order to extend this research further it is recommended that a clear threshold FV for dual scale flow be carried out and established by the scientists. This threshold FV should be carried out for the most commonly used fabrics with varying fiber architecture. The threshold FV should be separately determined for VARTM and RTM processes. A visual inspection of dual scale flow in fiber preforms laid on transparent tools with high power strobe lights would also help to discern macro flow vs. micro flow. Round robin studies of channel flow and radial flow methods should be employed to characterize permeability for sized and unsized fibers by agreed upon test fluids. This would remove the experimental uncertainties introduced due to human errors.

The acoustical method of determining permeability should be extended to a wider variety of samples including woven, random mat and chopped strand mat. Fibers from chopped strand mat and random mat when used in VARTM or RTM usually do not result in higher than 25% FV. This would enable easier comparison of the preform's permeability derived from the acoustical method vs. the channel flow or radial flow method. It should be noted that this comparison cannot be taken in absolute terms as there is no benchmark permeability method for fiber preforms. At best this comparison will yield the differences in the methods and the theory employed.

As mentioned earlier, viscous characteristic length for fiber preforms should be studied in more detail as a possible explanation for the discrepancies between sized and unsized permeability. Removing the sizing, as observed in this study and others [69 & 70], results in rearranging the fibers. Effects due to the type of packing (as a result of fiber rearrangement) are

not captured in Darcy's law or other flow based models used in composites processing. Changes in viscous characteristic length due to the removal of sizing and its relation to fiber rearrangement should be investigated for clearer flow behavior prediction in fiber composite processing.

REFERENCES

LIST OF REFERENCES

- [1] Darcy, H., 1856, “The Public Fountains of the City of Dijon”, Paris.
- [2] Du Plessis, J., P. & Diedericks, P,J,G., 1997, “Pore Scale Modeling of Interstitial Transport Phenomena”, Fluid Transport in Porous Media, Advances in Fluid Mechanics, pp. 61-104.
- [3] Vazquez, J., L., 2007, “The Porous Medium Equation – Mathematical Theory”, Oxford University Press, NY.
- [4] Isakov, V., 2007, “On inverse problems in secondary oil recovery”, <http://www.math.wichita.edu/~isakov/>, Math Seminar, Wichita State University, Wichita, US. Date Retrieved: 01/10/2008.
- [5] Collines, R., E., 1976, “Flow of fluids through Porous materials”, The Petroleum Publishing Company, Tulsa.
- [6] Bear, J., 1972, “Dynamic of Fluids in Porous Media”, Dover Publications, Inc., Chapter 5, pp. 137-148.
- [7] Weitzenbock, J,R., Sheno, R,A. & Wilson, P,A., 1998, “ Measurement of Principal Permeability with the Channel Flow Experiment”, Polymer Composites, . **20** (2), pp. 321-335.
- [8] Cai, Z., 1992, “Analysis of Mold Filling in RTM Process”, Journal of Composite Materials, **26** (9), pp. 1310-1329.
- [9] Chan, A., W., Larive, D., E. and Morgan, R,J., 1993, “Anisotropic Permeability of Fiber Preforms: Constant Flow Rate Measurement”, Journal of Composite Materials, **27**(10), pp. 996-1008.
- [10]Gauvin, R., Trochu, F., Lemenn, Y., and Diallo, L., 1996,”Permeability Measurement and Flow Simulation through Fiber Reinforcement”, Polymer Composites, **17** (1), pp. 34-42.
- [11]Lai, Y-H., Khomani, B., and Kardos, J., L., 1997,”Accurate Permeability Characterization of Preforms Used in Polymer Matrix Composite Fabrication Processes”, Polymer Composites, **18** (3), pp. 368-377.
- [12]Young, W., B., and Wu, S,F., 1995, “Permeability Measurement of Bidirectional Woven Glass Fibers”, Journal of Reinforced Plastics And Composites, **14**, pp. 1108-1120.
- [13]Hammami, A., Trochu, F., Gauvin, R., and Wirth, S., 1996,”Directional Permeability Measurement of Deformed Reinforcement”, Journal of Reinforced Plastics And Composites, **15**, pp. 552-562.

- [14] Han, K., K., Lee, C., W. and Rice, B.P., 2000, "Measurements of the permeability of Fiber Preforms and Applications", *Composites Science and Technology*, **60**, pp. 2435-2441.
- [15] Liu, Q., Parnas, R., S. and Giffard, H., S., 2007, "New Set-up for In-Plane Permeability Measurement", *Composites: Part A*, **38**, pp. 954-962.
- [16] A. S. Verheus and J. H. A. Peeters, 1993, "The role of reinforcement permeability in resin transfer molding", *Composites Manufacturing*, **4** (1), pp. 33-38.
- [17] Lee, Y., J., Wu, J., H., Hsu, Y. and Chung, C., H., 2006, "A Prediction Method on In-Plane Permeability of Mat/Roving Fibers Laminates in Vacuum Assisted Resin Transfer Molding", *Polymer Composites*, **27**(6), pp. 665-670.
- [18] R. Gauvin, A. Kerachni, and B. Fisa, 1994, "Variation of Mat Surface Density and Its Effect on Permeability Evaluation for RTM Modelling", *J. of Reinforced Plastic Composites*, **13** (4), pp. 371-383.
- [19] Sharma, S., Siginer, D.A., Dukkipati, R.K., and Soschinske, K.A., 2009, "Effect of Fiber Sizing Test Fluid Interaction on the Unsaturated and Saturated Flow in the VARTM Process", *Journal of Composite Materials*, **43**(15), pp. 1589-1601.
- [20] Soschinske, Kurt A. "Cellular automata simulation of resin flow through a fiber reinforcement," Ph.D. Dissertation, Department of Mechanical Engineering, Wichita State University, Wichita, KS, 1997.
- [21] Demaria, C., Ruiz, E. and Trochu, F., 2007, "In-plane Anisotropic Permeability Characterization of Deformed Woven Fabrics by Unidirectional Injection. Part I: Experimental Results", *Polymer Composites*, **28** (6), pp. 797-811.
- [22] Diallo, M.L., Gauvin, R., and Trochu, F., 1998, "Experimental Analysis and Simulation of Flow Through Multi-Layer Fiber Reinforcements in Liquid Composite Molding", *Polymer Composites*, **19** (3), pp. 246-256.
- [23] Sun, X., Li, S. and Lee, L., J., 1998, "Mold filling analysis in vacuum assisted resin transfer molding. Part1: SCRIMP based on a High Permeable Medium", *Polymer Composites*, **19**(6), pp. 807-817.
- [24] Gebart, B., R. and Lidstrom, P., 1996, "Measurement of in-plane permeability of anisotropic fiber reinforcements", *Polymer Composites*, **17**(1), pp. 43-51.
- [25] Bechtold, G. and Lin, Y., 2003, "Influence of fiber distribution on the transverse flow permeability in fiber bundles", *Composites Science and Technology*, **63**, pp. 2069-2079.
- [26] Rodriguez, E., Giacomelli, F. and Vazquez, A., 2004, "Permeability-Porosity Relationship in RTM for Different Fiberglass and Natural Reinforcements", *Journal of Composite Materials*, **38**(3), pp. 259-268.

- [27] Ding, L., Shih, C., Zhiyong, Zhang, C. and Wang, B., 2003, “ In situ measurement and monitoring of whole-field permeability profile of fiber preform for liquid composite molding processes”, *Composites: Part A* **34**, pp. 779-789.
- [28] Um, M., K., Daniel, I., M., and Childs, B,W., 2001, “A gas Flow Method for Determination of In-Plane Permeability of Fiber Preforms”, *Polymer Composites*, **22** (1), pp. 47-56.
- [29] Cairns, Douglas, S., 2004, “Fluid flow modeling of resin transfer modeling for composite material wind turbine blade structures,” SAND 2004-0076.
- [30] Bear, Jacob, 1972, “Dynamic of Fluids in Porous Media”, Dover Publications, Inc., Chapter 5, pp. 128-129.
- [31] Weitzenbock, J., R., Sheno, R., A. and Wilson, P., A., 2002, “A Unified Approach to Determine Principal Permeability of Fibrous Media,” *Polymer Composites*, **23** (6), pp. 1132-1150.
- [32] Seong, D., G., Chung, K., Kang, T., J. and Youn, J., R., 2002, “A Study on Resin Flow through a Multilayered Preform in Resin Transfer Molding”, *Polymers & Polymer Composites*, **10** (7), pp. 493-508.
- [33] Heardmen, E., Lekakou, C. and Bader, M., G., 2004, “Flow monitoring and permeability measurement under constant and transient flow conditions”, *Composites Science and Technology*, **64**, pp. 1239-1249.
- [34] Simacek, P. and Advani, S., G., 2003, “A numerical model to predict fiber tow saturation during liquid composite molding”, *Composites Science and Technology*, **63**, pp. 1725-1736.
- [35] Mathur, R., Heider, D., Hoffmann, C., Gillespie Jr., J., W., Advani, S., G. and Fink, B, K., 2001, “Flow Front Measurements and Model Validation in the Vacuum Assisted Resin Transfer Molding Process,” *Polymer Composites*, **22** (4), pp 477-490.
- [36] Belov, B.E., Lomov, S.V., Verpoest, I., Peters, T., Roose, D., Parnas, R.S., Hoes, K. and Sol, H., 2004, “Modelling of permeability of textile reinforcements: Lattice Boltzmann method,” *Composites Science and Technology*, **64**, pp1069-1080.
- [37] Kearsley, A.J., Cowsar, L.C., Glowanski, R., Wheeler, M.F., Yotov, I., 2001, “New optimization approach to multiphase flow,” *Journal of Optimization Theory and Applications*, **111** (3), pp 473-488.
- [38] Grujicic, M., Chittajallu, K.M. and Walsh, S., 2003, “Optimization of the VARTM process for enhancement of the degree of devolatilization of polymerization by-products and solvents”, *Journal of Materials Science*, **38**, pp 3729-3739.
- [39] Bailleul, J.-L., Sobotka, V., Delaunay, D., Jarny, Y., 2003, “Inverse algorithm for optimal processing of composite materials”, *Composites: Part A* **34**, pp 695-708.

- [40] Bickerton, S., Abdullah, M.Z., 2003, "Modeling and evaluation of the filling stage of injection/compression molding", *Composites Science and technology*, **63**, pp1359-1375.
- [41] Mastbergen Daniel B. and Cairns Douglas S., 2006, "Process modeling and validation of resin infusion type manufacturing of composite wind turbine blades," *Collection of Technical Papers - 44th AIAA Aerospace Sciences Meeting*, **19**, pp. 14594-14603
- [42] Parnas, R., S. and Phelan, F., R., Jr., 1991, "The Effect of Heterogeneous Porous Media on Mold Filling in resin Transfer Molding", *SAMPE Quarterly*, **22**(2), pp 53-60.
- [43] Slade, J., Pillai, K., M. and Advani, S., G., 2001, "Investigation of Unsaturated Flow in Woven, Braided and Stitched Fiber Mats during Mold-Filling in Resin Transfer Molding", *Polymer Composites*, **22**(4), pp. 491-505.
- [44] Siginer, D., A. and Bakhtiyarov, S., I., 2001, "Flow in Porous Media of Variable Permeability and Novel Effects", *Journal of Applied Mechanics*, **68**, pp. 312-319.
- [45] Buntain, M., J. and Bickerton, S., 2003, "Compression Flow Permeability Measurement: A Continuous Technique", *Composites: Part A*, **34**, pp. 445-457.
- [46] Stadtfeld, H., C., Erninger, M., Bickerton, S. and Advani, S., G., 2002, "An Experimental Method to Continuously Measure Permeability of Fiber Preforms as a Function Fiber Volume Fraction," *Journal of Reinforced Plastics And Composites*, **21**(10), pp. 879-899.
- [47] Pomeroy, R., Grove, S., Summerscales, J., Wang, Y. and Harper, A., 2007, "Measurement of Permeability of Continuous Filament Mat Glass-Fibre Reinforcements by Saturated Radial Airflow", *Composites: Part A*, **38**, pp. 1439-1443.
- [48] Feser, J., P., Prasad, A., K. and Advani, S., G., 2006, "Experimental Characterization of In-Plane Permeability of Gas Diffusion Layers", *Journal of Power Sources*, **162**, pp. 1226-1231.
- [49] Petterson, P., Lundstrom, T., S. and Wikstrom, T., 2006, "A Method To Measure The Permeability Of Dry Fiber Mats", *Wood and Fiber Science*, **38**(3), pp. 417-426.
- [50] Chappell, N., A., and Lancaster, J., W., 2007, "Comparison of Methodological Uncertainties within Permeability Measurements", *Hydrological Processes*, **21**, pp. 2504-2514.
- [51] Brusckke, M., V. and Advani, S., G., 1993, "Flow of generalized Newtonian Fluids across a periodic array of cylinders", *Journal of Rheology*, **37**.
- [52] Gebart, B., R., 1992, "Permeability of unidirectional reinforcements for RTM", *Journal of Composite Materials*, **26** (8), pp.1100-1133.
- [53] Sharma, S., 2004, "A VARTM Process for the Fabrication of Hybrid Laminated Wind Blades," *Master's Thesis, Wichita State University, Wichita*.

- [54] Young, W., B., 1996, "Consolidation and cure simulations for laminated composites", *Polymer Composites*, **17**(1), pp. 142-148.
- [55] Cai, Z., and Berdichevsky, A., L., 1993, "An improved self consistent method for estimating the permeability of a fiber assembly", *Polymer Composites*, **14**(4), pp. 314-323.
- [56] Hakanson, J., M., Toll, S., and Lundstrom, S., T., 2005, "Liquid Permeability of an Anisotropic Fiber Web," *Textile Research Journal*, **75**(4), pp. 304-311.
- [57] Yu, B. and Lee, J., L., 2000, "A Simplified In-Plane Permeability Model for Textile Fabrics", *Polymer Composites*, **21** (5), pp. 660-685.
- [58] Yu, B. and Lee, J., 2002, "A Fractal In-Plane Permeability Model for Fabrics", *Polymer Composites*, **23**(4), pp. 201-221.
- [59] Parnas, R.S., Howard, J.G., Luce, T.L., and Advani, S.G., 1995, "Permeability Characterization. Part 1: A Proposed Standard Reference Fabric for Permeability", *Polymer Composites*, **16**(6), pp. 429-445.
- [60] Luce, T., L. and Advani, S.G., Howard, J.G., and Parnas, R.S., 1995, "Permeability Characterization. Part 2: Flow Behavior in Multiple Layer Preforms", *Polymer Composites*, **16**(6), pp. 446-458.
- [61] Dunkers, J., P., Phelan, F., R., Zimba, C., G., Flynn, K., M., Sanders, D.P., Peterson, R., P. and Parnas, R.S., 2001, "The Prediction of Permeability for an Epoxy/E-Glass Composite Using Optical Coherence Tomographic Images", **22** (6), pp. 803-814.
- [62] Maloney, D., 2003, "X-Ray Imaging Technique Simplifies and Improves Reservoir-Condition Unsteady State Relative Permeability Measurements", *Petrophysics*, **44** (4), pp. 271-278.
- [63] Schembre, J., M. and Kovscek, A.R., 2003, "A Technique for Measuring Two Phase Relative Permeability in Porous Media via X-Ray CT Measurements", *Journal of Petroleum Science and Engineering*, **39**, pp. 159-174.
- [64] Weitzenbock, J., R., Shenoi, R., A. and Wilson, P., A., 1998, "Measurement of Three Dimensional Permeability", *Composites: Part A*, **29A**, pp. 159-169.
- [65] Kim, S., K. and Daniel, Isaac, M., 2003, "Determination of three-dimensional permeability of fiber preforms by the inverse parameter estimation technique", *Composites: Part A* **34**, pp. 421-429.
- [66] Scholz, S., Gillespie Jr., J., W. and Heider, D., 2007, "Measurement of Transverse Permeability using Gaseous and Liquid Flow", *Composites: Part A*, **38**, pp. 2034-2040.
- [67] Wu, X., Li, J. and Shenoi, R., A., 2007, "A New Method to Determine Fiber Transverse Permeability", *Journal of Composite Materials*, **41**(6), pp. 747-756.

- [68] Stoven, T., Weyrauch, P., Mitschahng, P. and Neitzel, M., 2003, "Continuous monitoring of three-dimensional resin flow through a fiber preform", *Composites: Part A* **34**, 475-480.
- [69] Steenkamer, D.A., Wilkins, D.J. and Karbhari, V.M., 1993, "Influence of test fluid on fabric permeability measurements and implications for processing of liquid molded composites", *Journal of Materials Science*, **12**(13), pp. 971-973.
- [70] Chih-Hsin, S. and James, L., L., 1998, "Effect of fiber architecture on permeability in liquid composite molding", *Polymer Composites*, **19**(5), pp. 626-639.
- [71] Steenkamer, D.A., McKnight, S.H., Wilkins, D.J. and Karbhari, V.M., 1995, "Experimental characterization of permeability and fiber wetting for liquid molding", *Journal of Materials Science*, **30**(12), pp. 3207-3215.
- [72] Karbhari, V.M. and Palmese, G.R., 1997, "Sizing related kinetic and flow considerations in the resin infusion composites", *Journal of Materials Science*, **32** (21), pp. 5761-5774.
- [73] Palmese, G.R. and Karbhari, V.M., 1995, "Effects of Sizing on Microscopic Flow in Resin Transfer Molding", *Polymer Composites*, **16**(4), pp. 313-318.
- [74] Abrate, S., 2002, "Resin flow in fiber preforms," *Applied Mechanics Review*, **55** (6).
- [75] Pillai, K., M., 2004, "Modeling the Unsaturated flow in Liquid Composite Molding Process: A review and Some Thoughts", *Journal of Composite Materials*, **38** (23).
- [76] Breard, J., Saouab, A. and Bouquet, G., 2003, "Numerical simulation of void formation in LCM", *Composites: Part A*, **34**, pp. 517-523.
- [77] Schoelkopf, J., Gane, P., A., C. and Ridgway, C., J., 2004, "Observed Non-linearity of Darcy-permeability in Compacted Fine Pigment Structures", *Colloids and Surfaces A: Physicochemical and Engineering Aspects*, **236**(1), pp111-120.
- [78] Kaynak, C. and Kas, Y., O., 2006, "Effects of Injection Pressure in Resin Transfer Moulding (RTM) of Woven Carbon Fibre/Epoxy Composites", *Polymers and Polymer Composites*, **14**(1), pp. 55-64.
- [79] Kim, S., K. and Daniel, I., M., 2007, "Observation of Permeability Dependence on Flow Rate and Implications for Liquid Composite Molding", *Journal of Composite Materials*, **41**(7), pp. 837-849.
- [80] Bickerton, S., Buntain, M., J. and Somasekhar, A., A., 2003, "The Viscoelastic Compression Behavior of Liquid Composite Molding Preforms", *Composites: Part A*, **34**, pp. 431-444.
- [81] Prasad, M., 2003, "Velocity-Permeability Relations within Hydraulic Units", **68** (1), pp 108-117.

- [82] Johnson, D., L., Koplik, J. and Schwartz, L.M., 1986, "New Pore Size Parameter Characterizing Transport in Porous Media", *Physical Review Letters*, **57**(20), pp. 2564-2567.
- [83] Tomadakis, M., M. and Robertson, T., J., 2005, "Viscous Permeability of Random Fiber Structures: Comparison of Electrical and Diffusional Estimates with Experimental and Analytical Results", *Journal of Composite Materials*, **39**(2), pp. 163-188.
- [84] Benson, P., M., Meredith, P.G. and Platzman, E.S., 2003, "Relating pore fabric geometry to acoustic and permeability anisotropy in Crab Orchard Sandstone: A Laboratory study using magnetic ferrofluid", *Geophysical Research Letters*, **30**(19).
- [85] Lafhaj, Z., Goueygou, M., Djerbi, A. and Kaczmarek, M., 2006, "Correlation between porosity, permeability and ultrasonic parameters of mortar with variable water/cement ratio and water content", *Cement and Concrete Research*, **36**, pp. 625-633.
- [86] Bear, Jacob, 1972, "Dynamic of Fluids in Porous Media", Dover Publications, Inc., Chapter 4, pp. 106-112.
- [87] Allard, J., F., 1993, "Propagation of Sound in Porous Media: Modelling Sound Absorbing Materials", Elsevier Science Publishers Ltd., Chapter 6, pp. 118-139.
- [88] Gauvin, R. and Chibani, M., 1986, "The Modeling of Mold Filling in Resin Transfer Molding", *International Polymer Processing* (1), pp. 43-46.
- [89] Astroem, B., T., Pipes, R., B. and Advani, S., G., 1992, "On flow through aligned fiber beds and its application to composites processing,," *Journal of Composite Materials*, **26**(9), pp. 1351-1373.
- [90] Van der Westhuizen, J. and Prieur du Plessis, J., 1996, "An attempt to quantify fiber bed permeability utilizing the phase average Navier-Stokes Equation", *Composites: Part A*, **27A**, pp. 135-141.
- [91] Ferland, P., Guittard, D. and Trochu, F., 1996," Concurrent Methods for Permeability Measurement in Resin Transfer Molding", *Polymer Composites*, **17**(1), pp. 149-158.
- [92] Um, M., K. and Lee, W.I., 1997, "A study on Permeability of Unidirectional Fiber Beds", *Journal of Reinforced Plastics And Composites*, **16**(17),pp. 1575-1590.
- [93] Bielelfield, M., 1994, "Fabrication of braided RTM driveshaft tubes for the RAH-66 Comanche", Annual Forum Proceedings, American Helicopter Society.
- [94] Choi, M., A., Lee, M., H., Chang, J. and Lee, S., J., 1998, "Permeability modeling of fibrous media in composite processing", *Journal of Non-Newtonian Fluid Mechanics*, **79** (2), pp. 585-598.
- [95] Wang, T. James, Wu, C.H. and James, L, L.(1994). In-plane permeability measurement and analysis in liquid composite molding. *Polymer Composites*, **15** (4), 278-288.

- [96] Correia, N.C., Robitaille, F., Long, A.C., Rudd, C.D., Simacek, P. and Advani, S.G. (2004). Use of resin transfer molding simulation to predict flow, saturation, and compaction in the VARTM process. *J. Fluids Engineering, Trans. ASME*, **126** (2), 210-215.
- [97] Shojaei, A., Trochu, F., Ghaffarian, S.R., Karimian, S.M.H. and Lessard, L. (2004). An experimental study of saturated and unsaturated permeabilities in resin transfer molding based on unidirectional flow measurements. *J. Reinforced Plastics Composites*, **23** (14), 1515-36.
- [98] Saraswat, M., Heider D. and Song Y.. (2006). Ultrasonic monitoring of the void formation during VARTM infusion. Research Reviews, Center for Composite Materials, Delaware.
- [99] Bender, D., Schuster J. and Heider, D. (2006). Flow rate control during vacuum-assisted resin transfer molding (VARTM) processing. *Composites Science Technology*, **66** (13), 2265-71.
- [100] National Institute of Standards and Technology data base on selection of test fluids for permeability measurements. www.nist.org.
- [101] J. F. Allard and B. Sieben, "Measurements of Acoustic Impedance in a Free Field with Two Microphones and a Spectrum Analyzer," *Journal of the Acoustical Society of America*, Vol. 77, Issue 4, pp. 1617–1618, 1985.
- [102] J. Klos, J. H. Robinson and R. D. Buehrle, "Sound Transmission Through a Curved Honeycomb Composite Panel," *AIAA Conference Paper*, # AIAA–2003–3157, 2003.
- [103] K. K. Ahuja, R. J. Gaeta, Jr. and M. D'Agostino, "Acoustic Absorption Characteristics of an Orifice with a Mean Bias Flow," *NASA Report*, NASA/CR–2000–210636, Virginia, 2000.
- [104] F. Simón, R. M. Rodríguez and J. Pfretzschner, "On the Absorption Coefficient of Porous Corrugated Surfaces," *Journal of Vibration and Acoustics*, Vol. 124, pp. 329–332, 2002.
- [105] C. A. Mills and C. E. Spiekermann, "Evaluating Acoustic Absorption Coefficients by Comparative Analysis – Experimental Part," *Journal of the Acoustical Society of America*, Vol. 91, No. 2, pp. 704 – 712, 1992.
- [106] C. Malmay and S. Cárbonne, "Acoustic Impedance Measurement with Grazing Flow," *AIAA Conference Paper*, # AIAA–2001–2193, 2001.
- [107] *ISO/DIS Standard 10534*, "Acoustics – Determination of Sound Absorption Coefficient and Impedance or Admittance by the Impedance Tube Method," International Standard Organization, Case Postale 56, CH 1211, Geneva, Switzerland, 1994.
- [108] *ASTM Standard E1050–98*, "Standard Test Method for Impedance and Absorption of Acoustical Materials Using a Tube, Two Microphones and a Digital Frequency Analysis System," American Society for Testing and Materials, Philadelphia, 1998.

- [109] *ASTM Standard E90-02*, “Standard Test Method for Laboratory Measurement of Airborne Sound Transmission Loss of Building Partitions and Elements,” American Society for Testing and Materials, Philadelphia, 2002.
- [110] P. J. Shorter, and B. K. Gardner, “Statistical Approaches to Structural Acoustics,” *AIAA Conference Paper*, # AIAA-2004-1749, 2004.
- [111] Biot, M.A., 1956, “Theory of propagation of elastic waves in a fluid-saturated porous solid. I. Low frequency range”, *Journal of Acoustic Society of America*, **28**, pp 168-178.
- [112] Biot, M.A., 1956, “Theory of propagation of elastic waves in a fluid-saturated porous solid. I. Higher frequency range”, *Journal of Acoustic Society of America*, **28**, pp 179-191.
- [113] Biot, M.A., 1962, “Generalized theory of acoustic propagation in porous dissipative media”, *Journal of Acoustic Society of America*, **34**, pp 1254-1264.
- [114] Johnson, D., L., Koplik, J. and Dashen, R., 1987, “Theory of dynamic permeability and tortuosity in fluid-saturated porous media”, *Journal of Fluid Mechanics*, **176**, pp 379-402.
- [115] Woodcock, R., Hodgson, M. (1992). Acoustic methods for determining the effective flow resistivity of fibrous materials. *Journal of Sound and Vibration*, **153** (1), 186-191.
- [116] Delany, M.E., Bazeley, E.N., (1970). Acoustical properties of fibrous absorbent materials. *Applied Acoustics*, **3**, 105-116.
- [117] Song, B.H., Bolton, S.J. (2000). A transfer-matrix approach for estimating the characteristic impedance and wave numbers of limp and rigid porous materials. *Journal of Acoustic Society of America*, **107** (3), 1131-1152.
- [118] Atalla, Y., Panneton, R. (2005). Inverse Acoustical Characterization of Open Cell Porous Media using Impedance Tube Measurements. *Canadian Acoustics*, **33** (1), 11-24.
- [119] Sebaa, N., Fellah, Z.E.A, Fellah, M., Lauriks, W. and Depollier, C. (2005). Measuring Flow Resistivity of Porous Material via Acoustic Reflected Waves. *Journal of Applied Physics*, **98** (8), 84901-10.
- [120] Gauvin, R., Kerachni, A, and Fisa, B. (1994). Variation of Mat Surface Density and Its Effect on Permeability Evaluation for RTM Modelling. *Journal of Reinforced Plastics and Composites*, **13**, 371-383.
- [121] Tan, H. and Pillai, K. (2009). A method to Estimate the Accuracy of Radial-Flow based Permeability Measuring Devices, *Journal of Composite Materials* (Online first, March 2009).

APPENDICES

Appendix A: Fiber Constituents

<p>Saertex style number: S32CU970-00520-1270-264000</p> <p>15 oz/yd² Unidirectional Carbon Fabric</p> <ul style="list-style-type: none"> • 0° carbon fibers (24,000 tows) of nominal areal weight 502 g/m² (14.81 oz/yd²) • 90° PES fibers of nominal weight 4 g/m² (8 tex) • +60° E-glass fibers of nominal areal weight 6 g/m² (68 tex) • -60° E-glass fibers of nominal areal weight 6 g/m² (68 tex) <p>The four layers are stitch bonded with nominal 6 g/m² PES fibers.</p>
<p>Saertex style number: S35EU990-00210-1270-464018</p> <p>6 oz/yd² Unidirectional Glass Fabric</p> <ul style="list-style-type: none"> • 0° E-glass fibers of nominal areal weight 213 g/m² (6.28 oz/yd²) • Random mat E-glass fibers of nominal weight 35 g/m² (0.94 oz/yd²) <p>The two layers are stitch bonded with nominal 12 g/m² PES fibers.</p>
<p>Saertex style number: S15EU910-00580-1200-100000</p> <p>16 oz/yd² Unidirectional Glass Fabric</p> <ul style="list-style-type: none"> • 0° E-glass fibers(1,200 tows) of nominal areal weight 528 g/m² (15.57 oz/yd²) • 90° E-glass fibers(68 tows) of nominal weight 35 g/m² (1.59 oz/yd²) <p>The two layers are stitch bonded with nominal 18 g/m² PES fibers.</p>
<p>Saertex style number: U32EX010-00400-1270-264000</p> <p>12 oz/yd² Double Bias (±45°) Glass Fabric</p> <ul style="list-style-type: none"> • +45° E-glass fibers of nominal areal weight 200 g/m² (5.90 oz/yd²) • -45° E-glass fibers of nominal areal weight 200 g/m² (5.90 oz/yd²) <p>The two layers are stitch bonded with nominal 6 g/m² PES fibers.</p>
<p>Saertex style number: U32EX010-01291-1270-264000</p> <p>38 oz/yd² Double Bias (±45°) Glass Fabric</p> <ul style="list-style-type: none"> • +45° E-glass fibers of nominal areal weight 643 g/m² (18.96 oz/yd²) • -45° E-glass fibers of nominal areal weight 643 g/m² (18.96 oz/yd²) <p>The two layers are stitch bonded with nominal 6 g/m² PES fibers.</p>

**APPENDIX B: Comparison of Predicted and Measured Absorption Coefficient Values
for Orthotropic Fibers**

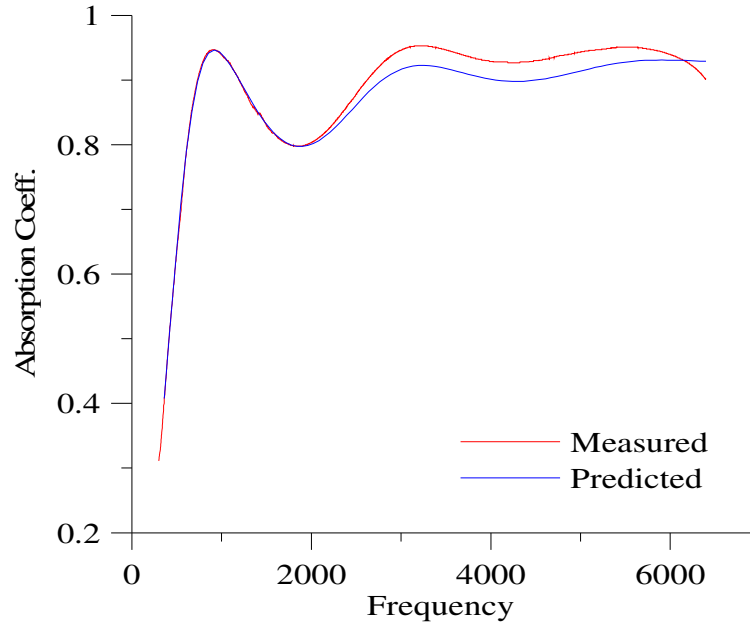


Figure B-1. UDC50+UDG150 Unsized hybrid fibers

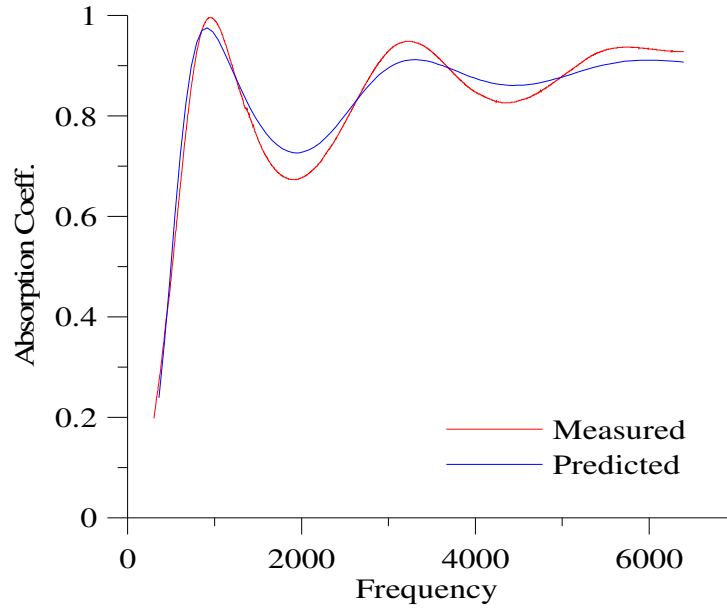


Figure B-2. UDC 135- 2 inch thickness- Sized

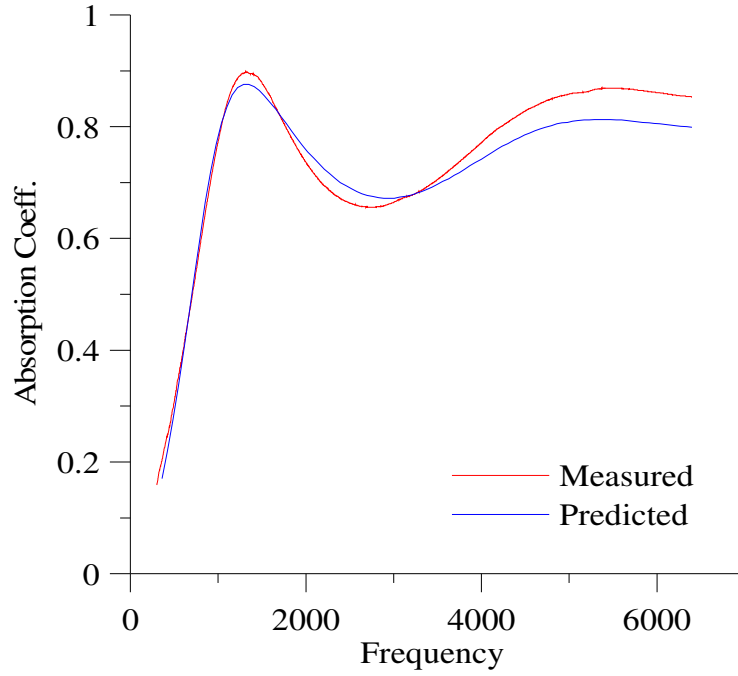


Figure B-3. UDC 160- 1 inch thickness- sized

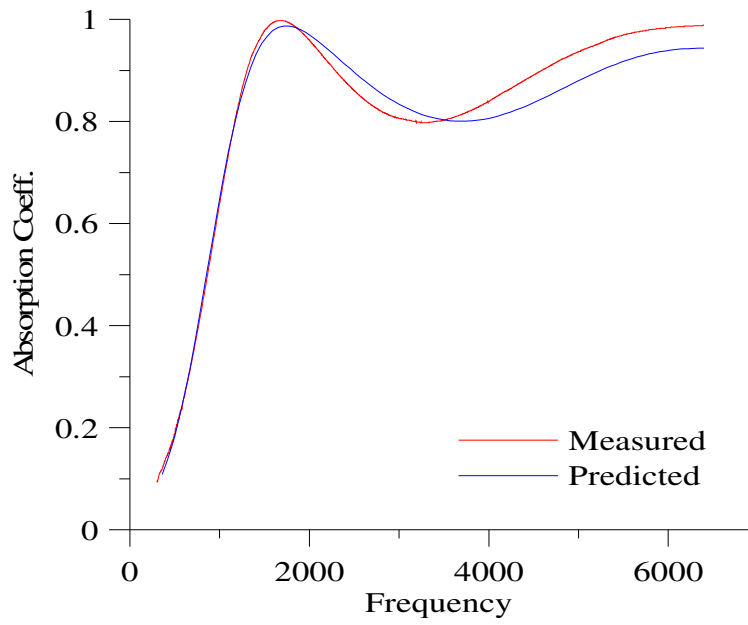


Figure B-4. UDG 300 – 1 inch thickness sized

Appendix C: Data for Figures 42 and 43.

Porosity	K young	K Kozeny	K Gebart sq.	K Gebart Hex.	K flow	K Acoustic
0.96	207.07	11.71931	21.874046	32.392256	117	197.74
0.95	186.90	7.26840	11.759277	17.575162	72	171.05
0.94	176.54	4.88978	6.989583	10.547993	48	146.81
0.9	136.46	1.54503	1.479467	2.332740	15	
0.85	102.23	0.57847	0.362136	0.612412	5.7	
0.81	81.20	0.31200	0.138968	0.253006	3.1	
0.78	68.36	0.20780	0.070270	0.137296	2	
0.74	52.53	0.12704	0.028241	0.062536		
0.65	31.10	0.04751	0.002477	0.009837		
0.6	23.24	0.02861	0.000259	0.002793		
0.52	14.26	0.01293	0.000259	0.000076	1.05	
0.51	13.44	0.01171	0.000259	0.000028	0.7	
0.5	12.68	0.01060	0.000259	0.000006		
0.4	7.00	0.00377	0.000259	0.000006		
0.3	3.80	0.00117	0.000259	0.000006		
0.2	1.97	0.00026	0.000259	0.000006		

Data for Glass fibers

Porosity	K young	K Kozeny	K Gebart sq.	K Gebart Hex	K Acoustic
0.96	1221.304	69.12	129.01223	191.048205	
0.95	1102.324	42.86875	69.355736	103.6575877	
0.94	1041.216	28.83972	41.2242735	62.21163492	
0.9	804.8481	9.1125	8.72583506	13.75840606	
0.85	602.9214	3.411806	2.13586535	3.611983177	
0.81	478.9397	1.84017	0.81962786	1.492219	689.208
0.78	403.2032	1.225599	0.41444828	0.809767915	462.31886
0.74	309.8393	0.749305	0.16656353	0.368832501	45.442286
0.65	183.3992	0.28023	0.01460743	0.058019162	
0.6	137.0827	0.16875	0.00152614	0.016475526	
0.52	84.10674	0.076285	0.00152614	0.0004472	
0.51	79.29675	0.06906	0.00152614	0.000164451	
0.5	74.75858	0.0625	0.00152614	3.32542E-05	
0.4	41.29551	0.022222	0.00152614	3.32542E-05	
0.3	22.41986	0.006888	0.00152614	3.32542E-05	
0.2	11.61426	0.001563	0.00152614	3.32542E-05	

Data for Carbon fibers